CHALMERS

Application of CFRP Cables in Super Long Span Cable Supported Bridges

- A feasibility study

Master of Science Thesis in the Master's Programme Structural Engineering and Building Technology

FILIPH BANCK & OSKAR ROSÉN ALMBERG

Department of Civil and Environmental Engineering
Division of Structural Engineering
Steel and Timber Structures
CHALMERS UNIVERSITY OF TECHNOLOGY
Göteborg, Sweden 2014

Master's Thesis 2014:138

MASTER'S THESIS 2014:138

Application of CFRP Cables in Super Long Span Cable Supported Bridges

- A feasibility study

Master of Science Thesis in the Master's Programme Structural Engineering and Building Technology

FILIPH BANCK & OSKAR ROSÉN ALMBERG

Department of Civil and Environmental Engineering
Division of Structural Engineering
Steel and Timber Structures
CHALMERS UNIVERSITY OF TECHNOLOGY

Göteborg, Sweden 2014

Application of CFRP Cables in Super Long Span Cable Supported Bridges
A feasibility study

Master of Science Thesis in the Master's Programme Structural Engineering and Building Technology

FILIPH BANCK & OSKAR ROSÉN ALMBERG

Examensarbete / Institutionen för bygg- och miljöteknik,
Chalmers tekniska högskola 2014:138

Department of Civil and Environmental Engineering
Division of Structural Engineering
Chalmers University of Technology
SE-412 96 Göteborg
Sweden
Telephone: + 46 (0)31-772 1000

Cover: Picture of The Akashi Kaikyo Bridge, Japan, with a main span of 1 990 meters (yokogawa-bridge.co.jp, 2014)

Chalmers reproservice / Department of Civil and Environmental Engineering
Göteborg, Sweden 2014

Application of CFRP Cables in Super Long Span Cable Supported Bridges
A feasibility study

Master of Science Thesis in the Master's Programme Structural Engineering and Building Technology

FILIPH BANCK & OSKAR ROSÉN ALMBERG
Department of Civil and Environmental Engineering
Division of Structural Engineering
Steel and Timber Structures
Chalmers University of Technology

ABSTRACT

Although engineers have designed bridges with main spans of almost 2 000 meters, there is still a desire of overbridging longer crossings. The cable supported bridges has the highest potential in terms of span lengths, but the use of conventional steel cables are impeding further development. The self-weight of the steel cables ultimately becomes the governing factor, why research in lightweight cable materials is essential for reaching longer spans.

Carbon fibre reinforced polymers (CFRP) are the most promising alternative for substituting steel in the cables, and the application of CFRP cables in super long span bridges[1] is analysed in this thesis. The static and dynamic performance of CFRP cables are reviewed and compared with steel cables, both for cable-stayed and suspension bridges. Numerical analyses are, however, only performed for the application in suspension bridges. The aerodynamic analysis is based on a semi-empirical model for evaluating the critical flutter velocity, which has been proved to give a good indication of the aerodynamic behaviour[2].

The results from the static analysis show that the performance of CFRP cables is superior to steel cables, both in cable-stayed and suspension bridges. The aerodynamic analysis indicates that the aerodynamic performance of CFRP and steel cables are quite similar, perhaps with a slightly higher critical wind speed for CFRP cables. The conclusion from these results is that CFRP cables have a higher potential than steel cables for the application in super long span bridges. However, problems related to the low shear capacity and transverse weakness of the cables may arise in structures with such dimensions, and these problems have to be solved before the implementation of CFRP cables in super long span bridges is technically feasible.

Key words: super long spans, long spans, Carbon fibre reinforced polymers, CFRP, lightweight cable material, aerodynamics, cable supported bridges, suspension bridges, cable-stayed bridges.

[1] In this thesis, super long span bridges refer to bridges with main spans longer than the longest bridge spans up to date. That is spans > 2 000 meters for suspension bridges and spans > 1 100 meters for cable-stayed bridges.

[2] Allan Larsen (Chief Specialist, Aero and Structural Dynamics, Cowi Lyngby), from a meeting with the authors on the 26th of Mars 2014 in Lyngby, Denmark.

Contents

Preface

In this study the feasibility and applicability of CFRP cables in cable supported bridges have been investigated using analytical and semi-empirical methods. The work was carried out in collaboration with the Norwegian Public Roads Administration (Statens Vegvesen), at the Department of Structural Engineering, Steel and Timber Structures, Chalmers University of Technology, Sweden. The study was conducted between January and June 2014.

We would like to thank our supervisors at the department Steel and Timber Structures, Associate Professor Mohammad Al-Emrani, Assistant Professor Reza Haghani and Senior Lecturer Mario Plos for their assistance and guidance throughout the project. We would also like to thank our supervisor Mathias Kjerstad from *Statens Vegvesen* for the support and involvement during the project. Finally, we would like to thank Chief Specialist Allan Larsen, Cowi Lyngby, for the essential assistance with the aerodynamic analysis.

Göteborg August 2014

Filiph Banck

Oskar Rosén Almberg

1 Introduction

The following introduction gives the reader a background of the studied subject, aim and objectives, method, and scope and limitations. The background briefly clarifies the need for further investigation in the subject, the state of the art in the field, and existing gaps of research. The aim and objectives define the purpose of the study and necessary sub targets. The method shortly describes the approach of the work, and the scope and limitations finally explains the main choices of direction for the thesis.

1.1 Background

The bridge with the longest span today is the Akashi Kaikyo Bridge in Japan, finished in 1998, with a main span of almost 2 000 meters. Longer spans have not been built ever since, even though there is an increasing demand of overbridging longer crossings. An example is the Strait of Messina, separating Sicily and the Italian mainland, where a single span suspension bridge of 3 300 meters was investigated for the crossing. Another well-known and hypothetical project that involves super long span bridges is the crossing of the Strait of Gibraltar, where bridge designs with spans exceeding 5 000 meters has been proposed for linking the continents of Europe and Africa together. However, since today's structural materials in bridge applications are unable to meet the requirements of these drastically increased span lengths, none of the projects above have yet been realized. Further research in the field of new structural materials is therefore necessary, especially for the cable systems.

The main restriction for increasing the span lengths of cable supported bridges is related to their structural dead load, with the cables comprising a major part of it. For this reason, mechanical properties such as high stiffness and strength in relation to density become increasingly important for the materials in the cables in super long span bridges. In Norway, the Norwegian Public Roads Administration (Statens Vegvesen) investigates the possibilities of crossing Sognefjorden, and one alternative is to build a single span suspension bridge of 3 700 meters. Due to the limitations in terms of mechanical properties of the conventional cable material HS steel, the Norwegian Public Roads Administration announced a desire of investigating the possibilities of implementing other structural materials for use as cables. This thesis is a part of that investigation, and the crossing over Sognefjorden will therefore be used as a reference throughout the calculations. However, the purpose of this thesis is not to investigate Sognefjorden in particular, but super long span bridges (as Sognefjorden) in general.

The most prominent material for the substitution of HS steel in the cable systems is the Carbon Fibre Reinforced Polymers (CFRP), mainly due to its superior mechanical properties in terms of low density and high tensile strength. The density of CFRP is only one fifth compared to the density of HS steel, and the ultimate tensile strength is about twice as high (Zhang & Ying, 2006). Researchers have concluded that the potential in static performance of cable supported bridges would be enhanced radically with the use of CFRP cables (Meier, 2012) (Liu, LV, Mei, & Zang, 2007) (Wang & Wu, 2010).

Another significant advantage of CFRP cables is their excellent fatigue behaviour and corrosion resistance compared to HS steel (Adanur et al., 2011). The maintenance of HS steel cables due to fatigue and corrosion related problems comprise a major cost,

especially for bridges that are exerted to high traffic volumes or located in corrosive environments.

However, despite the many desirable features of CFRP, the actual applications are scarce. The limited use of CFRP in actual designs can be deduced to high manufacturing costs and a lack of research on solutions to possibly related problems, especially for super long span suspension bridges. A main problem with CFRP is the poor shear capacity, which leads to difficulties in the anchorage design and the fixation of the cables to the pylon tops.

In addition to the problems related to the poor shear capacity of CFRP, the dawning possibility of significantly increased span lengths might generate problems related to the aerodynamic stability. The aerodynamic stability is already a critical aspect in longer cable supported bridges, and might become the governing factor when the structures become even longer and lighter. This problem is clearly related to the increased span lengths, but the lighter and slenderer structures with CFRP cables will influence the aerodynamic behaviour in one way or another as well. However, even though plenty of research has proved the potential of the static performance of CFRP cables in super long span bridges, there is a lack of research in the field of the aerodynamic behaviour. Research has been done on the aerodynamic behaviour of cable supported bridges with CFRP cables up to span lengths of 1 500 meters, and CFRP showed an aerodynamic behaviour in the same range as HS steel for these span lengths (Zhang & Ying, 2006). Nevertheless, more analyses on the aerodynamic behaviour for longer spans are necessary in order to tell if CFRP is a feasible cable material in super long span bridges.

1.2 Aim and limitations

The aim of this master thesis is to, from a structural point of view, investigate the feasibility of increasing current span lengths of cable supported bridges with the implementation of CFRP cables in the cable system. The objectives are the following:

- Address the limitations of conventional structural cable materials.
- Evaluate the advantages and disadvantages related to the mechanical properties of CFRP with respect to the implementation in cables for bridge applications.
- Evaluate and compare the static performance of CFRP cables and HS steel cables in super long span cable supported bridge.
- Evaluate and compare the aerodynamic performance of CFRP cables and HS steel cables in super long span cable supported bridge.

1.3 Method

This is a feasibility study that contains both literature reviews and analytical calculations. The initial phase of the thesis is dedicated to a broad literature review of the structural behaviour of cable supported bridges, with objective of addressing the governing factors for increasing span lengths. This is followed up by a general review of CFRP as a material and a state of the art review of CFRP cables in cable supported bridges. From these parts, the problems and potentials of implementing CFRP cables

in cable supported bridges are evaluated, and the gaps of research in the field are identified. The identification of gaps in the research is the basis for the calculations and analyses in the thesis.

The conducted calculations and analyses are related to the static performance, the dynamic performance, and problems due to low shear capacity and transverse weakness of the cables. The calculations are based on the future suspension bridge over Sognefjorden (3 700 meters), with objective of evaluating the feasibility of CFRP cables in super long span bridges. The literature review and the results from the analyses are then the basis for the final discussion and conclusion.

1.4 Scope and limitations

This thesis is limited to the feasibility of implementing CFRP cables in super long span bridges from a technical point of view. The economic aspects are mentioned briefly, but not analysed in detail. The economics is clearly a key for the implementation of CFRP cables in bridge applications, but is beyond the scope of this thesis.

Concerning the materials of the cables, CFRP is the only material to be analysed besides the conventional HS steel. There exists other lightweight fibre reinforced polymers (FRP) that are economically more beneficial, but CFRP has the highest structural potential in bridge applications, and is therefore studied. If CFRP proves to be feasible in cables for super long span bridges, analyses of other FRPs would be interesting from an economical point of view, but this is beyond the scope of this thesis.

Regarding the types of cable supported bridges, both suspension and cable-stayed bridges are covered in the literature review. However, the calculations are exclusively conducted for suspension bridges, for two main reasons. First of all, the design of a suspension bridge is the most suitable for crossing Sognefjorden, and the models in the analyses are based on the conditions at the site of this future crossing. Secondly, there are more gaps of research in the field for suspension bridges, and these analyses are therefore more relevant.

2 Cable Supported Bridges

Cable supported bridges are primarily distinguished by two features; their capability of overbridging long spans and their main structural element, the cable system. Generally, cable supported bridges are sub-divided with respect to the cable system into two main categories, suspension and cable-stayed bridges. Although a differentiation is made with respect to the different cable systems, the structural system is to a large extent similar for the two different bridge types, and in both cases the structural system consists of the following main structural elements:

- Bridge deck (stiffening girder)
- Cable system (supporting the bridge deck, consisting of either main cables and hangers, or inclined stays)
- Pylons (supporting the cable system)
- Anchorage device (anchoring the tensile forces, either an earth-anchored or a self-anchored system)

The main structural elements, in typical design, for both suspension and cable-stayed bridges are shown in Figure 1 and Figure 2, respectively.

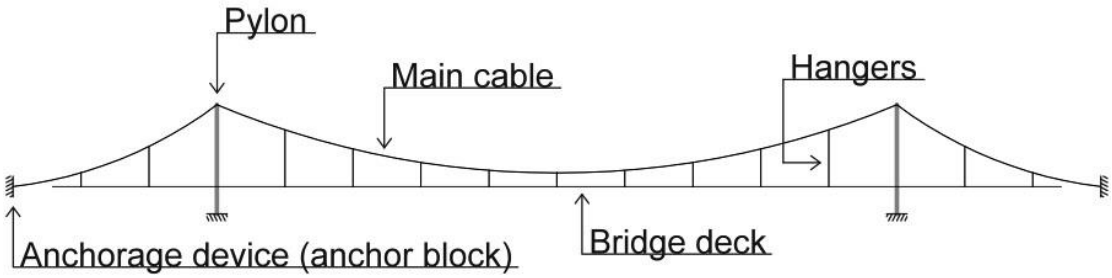

Figure 1. Typical design of a suspension bridge and its main structural elements.

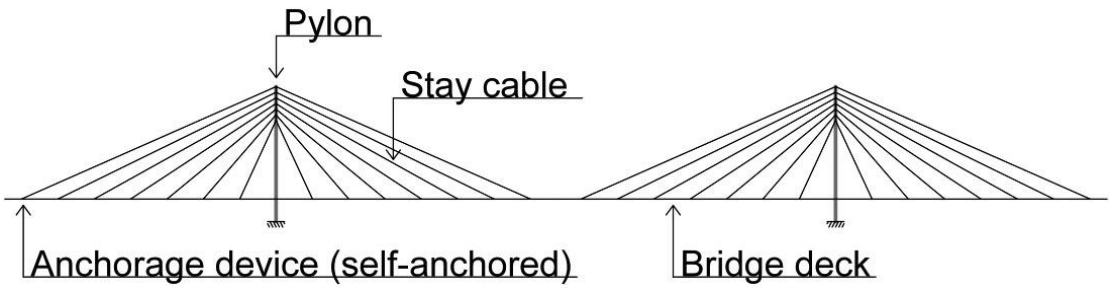

Figure 2. Typical design of a cable-stayed bridge and its main structural elements.

In the following chapter, suspension and cable-stayed bridges are treated separately. The aim of this chapter is to provide fundamental understanding of the structural behaviour and identify the governing factors with respect to ultimate span lengths. Main focus lies on the structural system, particularly the cable system, due to its large influence on the overall structural behaviour.

2.1 Suspension bridges

Modern suspension bridges originates from the 18th century along with the development of full-scale iron production, and in the 19th century a rapid increase in span length was made possible with the invention of mass-produced steel (Chen & Duan, 2000). The end of the last century represented a milestone for long span suspension bridges with the erection of the Akashi Kaikyo Bridge (1 990 meters) in Japan, Figure 3, and the Great Belt Bridge (1 624 meters) in Denmark, with main spans approaching 2 000 meters. Today, suspension bridges comprise about 20 of the longest bridge spans in the world.

Figure 3. The Akashi Kaikyo Bridge, Japan, with the longest span in the world of 1 990 meters *(yokogawa-bridge.co.jp, 2014)*.

2.1.1 Structural system

The cable system of a suspension bridge is characterized by the parabolic-shaped main cables that support the deck via hangers (suspenders), see Figure 1. In a conventional design, the main cables are supported at four nodes; on top of each pylon and externally anchored in anchor blocks at each side, see Figure 1. The structural purpose of the main cables is to transmit the live load and the self-weight of the suspended structure to the supports.

The main cables are, as mentioned above, normally anchored in external anchor blocks at each side (henceforth referred to as an earth-anchored system). An alternative to this system is the self-anchored system, where the main cables are anchored in the stiffening girder instead of externally. Structurally, these two systems behave differently since the self-anchored system gives rise to axial forces in the deck, whereas the horizontal forces in an earth-anchored system are transferred into the anchor blocks. Thus, for long span bridges, the earth-anchored system is structurally more preferable and it is also the most common design. Henceforth, when referring to suspension bridges, an earth-anchored system is destined.

Since no axial forces are induced in the deck of a conventional earth anchored system, the system allows for the design of slender bridge decks. Except for transferring the load to the hangers, the structural purpose of the bridge deck is merely to provide sufficient horizontal and torsional rigidity. The torsional rigidity becomes especially important in long span suspension bridges, due to the increasing problems related to

aerodynamic instability with increasing span lengths. Nevertheless, the bridge decks may still have a low (vertical) flexural stiffness, and the global flexural stiffness of the bridge will therefore, to a large extent, depend on the stiffness of the cable system. Since the weight of the main cables comprise a great part of the total self-weight of the suspended structure, the relation between stiffness and density becomes increasingly important, especially in long span bridges. As the main cables carry the load in tension, it is their axial stiffness that mainly determines the global flexural stiffness of the bridge. This axial stiffness-to-density ratio will henceforth be referred to as the specific stiffness.

As the span length of a suspension bridge increase, the weight of the main cables will increase in relation to the total weight of the suspended structure, and a higher percentage of the cable stress will therefore be related to the self-weight of the cables themselves. Since the cables primarily work in tension (see Figure 4), their axial strength-to-density ratio (henceforth referred to as the specific strength) ultimately limits the potential span length. An interesting point is where the stress, induced by the cable weight alone, exceeds the allowable stress in the cables. This point is henceforth referred to as the theoretical span limit, and is further pursued under Section 4.1, where an expression of the theoretical span limit as a function of the ratio between the total weight of the suspended structure (except cables) and the self-weight of the cables is presented.

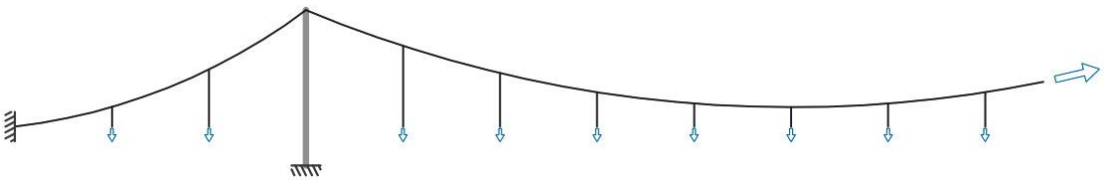

Figure 4. Structural behaviour of the cable system in a suspension bridge. Both main cables and hangers work in tension.

From the description of the structural system above, it is apparent that the specific stiffness and strength are governing factors for the theoretical span limits. However, the theoretical span limit is based on the static performance of the bridge solely, and for the evaluation of applicable span lengths, the dynamic performance has to be analysed as well. The dynamic stability is a critical aspect in long span suspension bridges, and might be the factor that governs the ultimate span lengths of super long span suspension bridges. The dynamic performance is of a more complex nature than the static, and the subject is treated more thoroughly under Chapter 5.

2.1.2 Flexibility in design

Another distinguishing feature of suspension bridges is their flexibility in terms of geometrical configuration. The possibilities in configuration of the main-to-side span ratio and the rise-to-main span ratio are here presented briefly. These aspects are of great importance for both the aesthetical appearance and the structural behaviour of the bridge. In the following section these aspects are, however, mainly discussed with respect to their influence on the structural behaviour. Although the parameters in this section are not directly dependent on the choice of cable material, they are still important for the optimization of ultimate span lengths and therefore covered here.

Main-to-side span ratio

In addition to the different alternatives in cable system configurations, the suspension bridges offer many alternatives in terms of geometrical disposition. Usually, suspension bridges are symmetrical structures consisting of one main span and two smaller side spans. However, the suspension bridge may be designed with almost any main-to-side span ratio, enabling a very flexible design, see Figure 5. For short side spans (<30% of the main span), favourable deformational characteristics are achieved due to decreased sag in the side spans, resulting in increased axial stiffness (Gimsing & Georgakis, 2012). In the extreme case, the side spans are eliminated, and the bridge consists of the main span only. The Fatih Sultan Mehmet Bridge (also known as the Second Bosporus Bridge) in Turkey is an example of a bridge with one main span only, see Figure 6. The proposed suspension bridge over Sognefjorden in Norway, which is analysed in more detail under Section 5.2, is another example of this design.

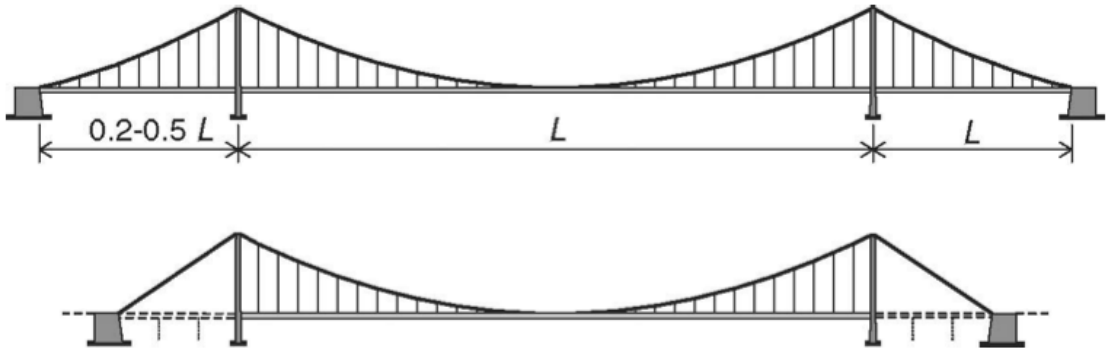

Figure 5. Symmetrical three span suspension bridge (top) and suspension bridge with main span only (bottom) (Gimsing & Georgakis, 2012).

Figure 6. The Fatih Sultan Mehmet Bridge in Istanbul, Turkey (bestbridge.net, 2011).

Rise-to-main span ratio

The rise-to-main span ratio refers to the ratio between the sag of the cable and the length of the main span. Gimsing & Georgakis (2012) analysed how this ratio affects the quantity of material used in the cables, see Figure 7. The smallest quantity of cable material was achived for a ratio corresponding to 0.35, and this is therefore the optimum value for ultimate span lengths. However, since this optimization only takes the quantity of cable material into account, this ratio is not the optimal in actual applications. Instead, if taking the pylon material into account as well, a lower ratio becomes more material efficient. Typical values of the rise-to-main span ratios lies within the range of 0.08 - 0.12 (Gimsing & Georgakis, 2012), and a ratio of 0.1 will be assumed throughout the calculations in this thesis.

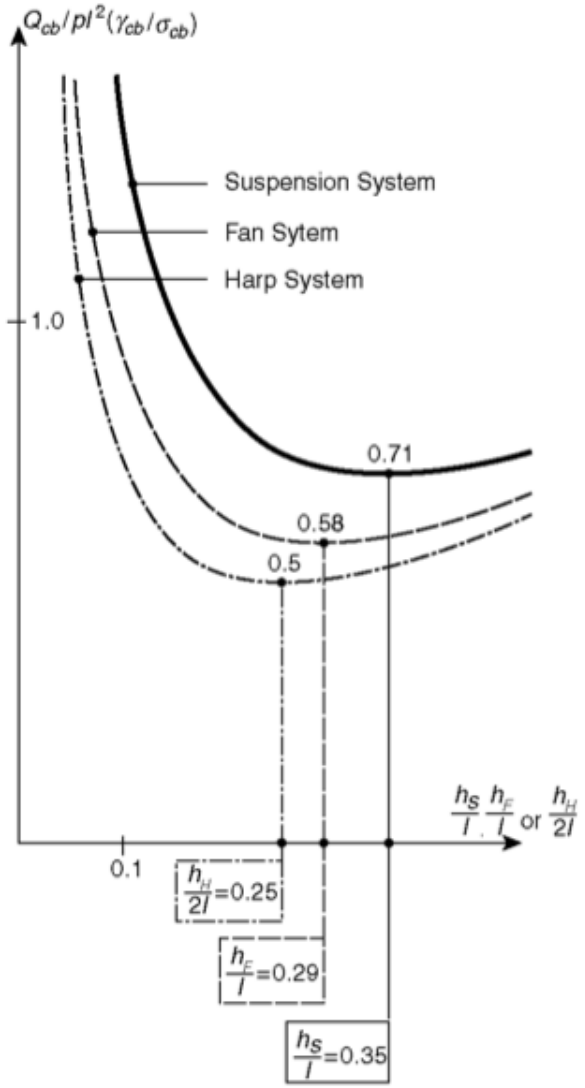

Figure 7. The quantity of cable material as a function of the rise-to-main span ratio for suspension, fan, and harp system (Gimsing & Georgakis, 2012).

2.2 Cable-stayed bridges

Even though suspension bridges have been superior in overbridging large spans throughout history, cable-stayed bridges have over the last few decades gained recognition as potential super long span bridges due to their higher overall stiffness and aerodynamic stability (Gimsing & Georgakis, 2012). The cable-stayed bridges reached a milestone at the beginning of the 21st century when the Russky Bridge (1 104 meters) in Russia, see Figure 8, the Sutong Bridge (1 088 meters) in China, and the Stonecutters Bridge (1 018 meters) in Hong Kong broke new ground as the first cable-stayed bridges with main spans exceeding 1 000 meter.

Figure 8. The world's longest cable-stayed bridge, Russky Bridge (1 104 meters), Russia (news.com.au, 2014).

2.2.1 Structural System

The structural system of a cable-stayed bridge can be seen as several overlapping triangles (or quadrangles), each consisting of one stay cable and a part of the pylon and the deck, see Figure 9. In each of these sub-systems, the stay cable is axially loaded in tension and both the deck and the pylon are axially loaded in compression. The fact that the deck is compressed can be understood by analysing the free body diagram of the isolated part shown in Figure 10, consisting of one stay cable and the connecting part of the deck. As the additional force in the deck, induced by a single stay cable, is of the same magnitude as the horizontal force component in the cable, horizontal equilibrium can be expressed as

$$N + H_i = N + dN \;\rightarrow\; H_i = dN \qquad (2.1)$$

where N is the axial force in the deck to the left of the stay cable, dN is the additional axial force in the deck induced by the stay cable, and H_i is the horizontal component of the axial force in the stay cable. Since each stay cable contributes to the induced axial force in the deck, the forces will increase towards the pylons and reach its maximum in a section adjacent to the pylons. Thus, to achieve a more efficient structure, the dimensions of the cross-section can be varied. The induced axial forces in the deck are one of the most important differences between the structural behaviour of cable-stayed bridges and suspension bridges.

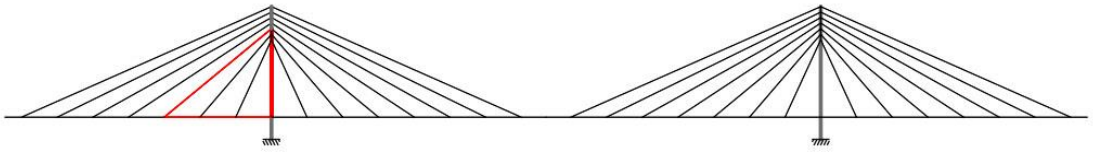

Figure 9. Structurally, the cable-stayed bridge can be seen as several overlapping triangles (or quadrangles). One triangle is here marked in red, consisting of one stay cable and a part of the pylon and the deck.

As for the main cables in the suspension bridge, the specific strength of the stay cables in a cable-stayed bridge is an important factor for the theoretical span limit. However, in long span cable-stayed bridges, the self-weight of the cable system will not be as dominant as in a suspension bridge, due to a heavier deck. Since the dimensions of the deck have to be increased in order to accommodate for the induced axial forces, the dead load of the deck increases. This will, in turn, require larger dimensions of the cables, and even higher axial forces will be induced in the deck. This effect is important for super long spans, and might impose restrictions on the ultimate span lengths of cable-stayed bridges.

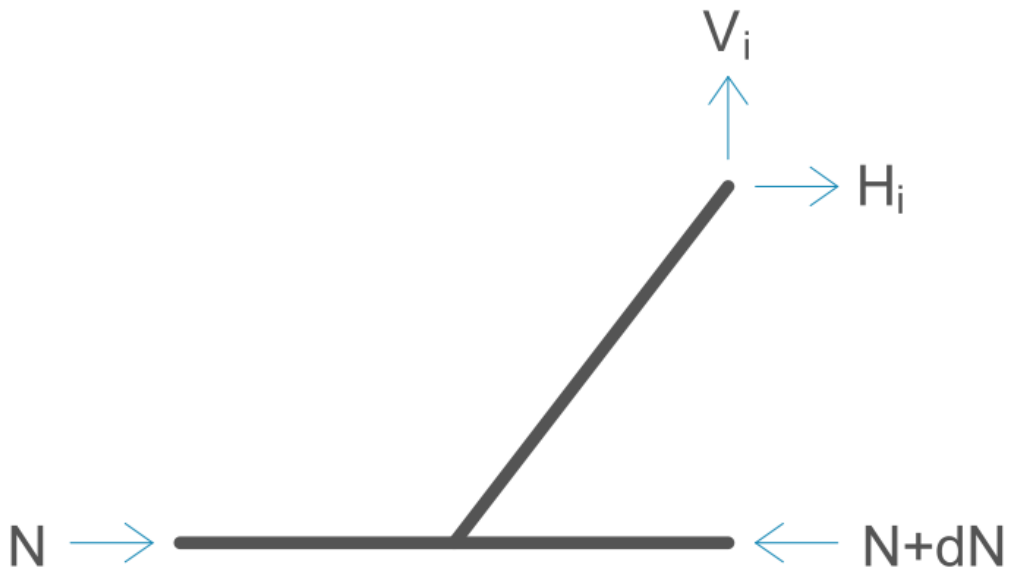

Figure 10. Free body diagram for a part of the deck connected to a stay cable.

Although the increased deck dimensions result in a stiffer bridge deck and consequently an increased contribution to the overall stiffness, the vertical stiffness of the bridge is ultimately governed by the cable system. However, when calculating the stiffness of the stay cables, their non-linear load-deformation response due to sag has to be taken into account. The sag-effect origins from the misalignment between the gravitational field and the tension direction of the cables, and is therefore inevitable in practical applications. For this reason an equivalent modulus, depending on the specific stiffness, applied cable stress and the horizontal length of the cable, determines the actual stiffness rather than the initial modulus, E_0. The equivalent modulus is defined as

$$E_{tan} = \frac{1}{\frac{1}{E_0} + \frac{(\rho l_c)^2}{12\sigma_2^3}} \qquad (2.2)$$

where ρ is the density of the cable, l_c is the cable length, and σ_2 is the design stress. From this expression it becomes apparent that the equivalent modulus decreases with increasing span lengths as well as with increasing density of the cable material. This particular relation is the most influential aspect (besides the problem of large induced axial forces in the deck for super long spans) when analysing applicable span lengths with respect to static performance. The relation between applicable span lengths and the equivalent modulus is further reviewed under Section 4.2.

2.2.2 Flexibility in design

As for suspension bridges, the flexibility in design of cable-stayed bridges is discussed. Focus is on the geometrical configuration of the cable system, which is of great importance both aesthetically and structurally. Although this configuration is not directly dependent on the choice of cable material, it is still important for optimal designs with respect to ultimate span lengths, and is therefore discussed briefly.

Geometrical configuration of cable system

The geometrical configuration of the cable system is here referred to as the different possibilities of anchorage design for the cables to the pylons. In principal, there are two different configurations, where the most commonly adopted in applications is the fan-system, due to its structural efficiency and possibility of geometrical adaption.

In a pure fan-system, all the cables are attached to the pylon top, see Figure 11. The pure fan-system is especially advantageous in long span cable supported bridges where the accumulated axial forces in the deck, induced by the inclined cables, may become the governing factor. The decreased horizontal force, due to the increased cable slope, can explain the advantage of the fan-system. However, a fan-system may turn out to be impractical in real applications due to problematic anchorage detailing, when all cables are anchored at the pylon top. The most common application of the fan-system is therefore the semi-fan system, where anchoring of the cable stays are spread out over a sufficient distance over the pylon top to ensure proper anchoring of each cable stay, see Figure 11. In the most common case where the height over which all cables are anchored is kept at a minimum, yet sufficient to ensure proper anchoring of each cable, the structural behaviour and desirable features of the pure-fan system is retained with the use of the semi fan-system (Gimsing & Georgakis, 2012).

In addition to the above described fan system, the harp system is another common solution in cable-stayed bridges. The harp system consists of parallel inclined stay cables equidistantly anchored both at the pylon and the bridge deck, see Figure 11. The harp system is often considered an aesthetically appealing design due to the symmetry of the main-to-side span ratio, as well as for the appearance of the parallel-aligned stay cables. The side-to-main span ratio for a bridge with the harp system will be very close to 0.5 (Gimsing & Georgakis, 2012).

The fan system is less restricted compared to the harp system, but the self-balancing nature of cable-stayed bridges still imposes more limitations on the geometry compared to suspension bridges. Concerning the crossing of Sognefjorden, the only option is to cross the fjord in one single span due to its underwater geometry (depths up to 1 250 meters), why the design of a suspension bridge is more preferable. Since the cable-stayed bridges have to be designed with side spans, this design would not be structurally efficient for Sognefjorden.

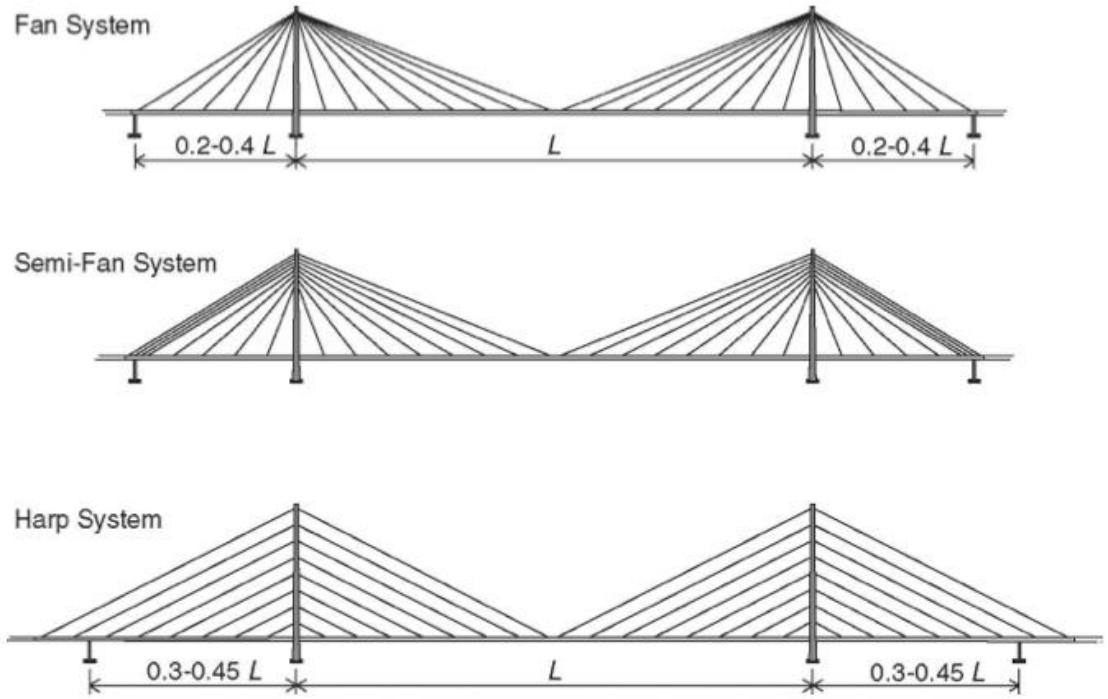

Figure 11. Cable system configurations of cable-stayed bridges (Gimsing & Georgakis, 2012)

2.3 Governing factors

In order to emphasize the most essential outcomes of this chapter, the governing factors with respect to ultimate span limits is briefly recaptured below.

Aside from the geometrical configuration and stiffness of the deck, the static performance of cable supported bridges is essentially governed by the axial mechanical properties of the cables. Features such as high specific stiffness and strength become especially important in long span bridge applications, due to increasing cable weight in proportion to the total load of the suspended structure. For this reason, new lightweight materials such as CFRP, with superior mechanical axial properties in relation to density, are particularly interesting in future super long span bridge applications. The characteristics of CFRP are further discussed in Chapter 3 and the static performance of cable supported bridges with both CFRP and steel cables is analysed in Chapter 4.

3 Mechanical Characteristics of CFRP Cables

Fibre reinforced polymers are composite materials composed of at least two constituent materials, tailor-made to create a material with superior mechanical properties. The final structure of a composite material generally consists of a fibrous material (reinforcement) inside a cohesive bulk resin (matrix) (Zoghi, 2014). The relative volume percentage of the two constituents determines the axial mechanical properties of the composite (Meier, 2012).

In a CFRP composite, carbon chains form the reinforcement and the matrix is normally a polymer resin. The carbon atoms have high bond energy (due to low diffuse of their outer shell, atomic number 6) and therefore high ability to catenate (form long chains). The long chains are built up of strong and stable covalent bonds, enabling the extraordinary axial mechanical properties, which distinguish the carbon fibre reinforced composites from conventional structural materials. In addition to the materials high stiffness and strength the covalent bonds also make the material chemically stable, and thus less prone to interact with other elements or compounds.

Despite the rugged characteristics of carbon, pure carbon compounds do not constitute adequate structural materials due to their brittle behaviour. A small notch on the surface or a defect within the bulk of a homogenous carbon material may be enough to generate a sudden rupture (Meier, 2012). However, in the form of carbon fibre reinforced polymers, where carbon fibres are separated into a large number of fibres, a fracture cannot propagate as suddenly as within a solid material. Moreover, the fibres are embedded within a matrix (epoxy resin) and a damaged fibre can therefore once again take the full load at a certain distance from the point of fracture (Meier & Mehdi, 1996). For this reason, CFRP wires exhibit considerably increased toughness compared to pure carbon and relatively low scatter in tensile strength.

The following chapter is divided into three parts, which treats the manufacturing process of CFRP wires, their properties, and the properties of commercial CFRP cables.

3.1 Manufacturing process of CFRP wires

The manufacturing process of CFRP wires starts with the process of carbonization of organic polymers into carbon fibres, where the precursor (organic polymer) is drawn into long strands and heated without coming in contact with oxygen, removing the non-carbon atoms from the polymers.

In the next step, the carbon fibre yarns are drawn through an epoxy-resin bath and a forming die that matches the desired number of filaments in the wire, followed by final curing of the wire. The pattern in which the precursor is drawn is predetermined and the fibres will have a unidirectional orientation.

The main objective is hereby to produce a feasible structural material with sufficient ductility, while still maintaining the desirable features of carbon. This is achieved through the use of high carbon content in the mix together with a sufficient amount of epoxy-resin, generating a strong and stiff material.

3.2 Mechanical properties of CFRP wires

In a homogenous isotropic structural material, properties are constant and independent of location and orientation. Fibre reinforced composites, on the other hand, are inhomogeneous materials with orthotropic structure (uni-axial, or bi-axial fibre alignment inside a matrix), where the properties depend on location as well as orientation. However, in contrast to the full 3-dimensional orthotropic structure with unequal properties in all orthogonal directions, the unidirectional CFRP wire only exhibits differences between the properties in the transverse and the longitudinal direction, whereas the properties in the two transverse directions are equal. This type of structure is referred to as a transversal isotropic material. The transverse isotropy of a fibre reinforced composite is shown in Figure 12.

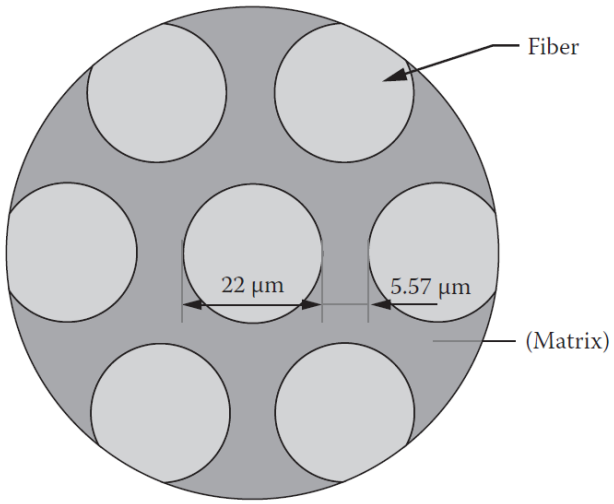

Figure 12. Transverse isotropic microstructure of FRP (Zoghi, 2014).

To better understand and analyse the response, fibre reinforced composites are studied both at the micro- and macromechanical level. Micromechanics involve assumptions regarding the interaction between the two constituents, and is useful when describing the different failure modes of fibre reinforced composites. Micromechanics is also used when determining the mechanical properties of a single wire, where assumptions regarding interaction between fibre and matrix are required. Macromechanics, on the other, regards the structural response of the complete structural material in which the material is considered homogenous, but with orthotropic properties. However, in the case of CFRP cables, where the structural material consist of parallel CFRP wires, the axial mechanical properties can be deduced directly using micromechanics, and macromechanics is therefore not treated further in this thesis.

In the following, some basic expressions of the mechanical properties of the single CFRP wire are deduced, utilizing a number of highly idealized assumptions to describe the fibre-matrix interaction. Emphasis is given to the tensile axial response of the wires, as this is the predominant state of stress in both stay cables and main cables. However, despite the relative simplicity in terms of required mechanical properties of stay cables and main cables, transversal forces and shear forces cannot be completely precluded in applications. Therefore, some basic concepts for evaluating the strength with respect to transversal compressive loading and shear are also included.

The structural mechanical response of the CFRP wire is here derived based on the simplified mechanics of material approach, as presented by Mallick (2007). The basic assumptions of the simplified approach are as follows:

- Full interaction between fibre and matrix (no bond slip)
- Linear elastic behaviour of both fibre and matrix
- Uniform distribution of fibres within the matrix
- No stresses are present before loading (no residual stresses in the fibres or matrix)
- Homogenous matrix free of voids and other impurities
- All fibres are assumed to have equal strength, and exceeding of the ultimate fibre stress, σ_{fu}, leads to the final rupture of the material.

Based on this, the fibre-matrix response in axial tensile loading and non-uniaxial state of stress is treated.

3.2.1 Axial tensile loading

By assuming the aforementioned idealized conditions, the longitudinal elastic modulus and the axial strength, of a single wire, can be derived in the following simple manner.

Modulus of elasticity of a single wire

As the applied axial force is carried by both the fibres and matrix, equilibrium implies

$$P_{CFRP} = P_F + P_M \tag{3.1}$$

where P_{CFRP} is the applied load and P_F and P_M are the forces carried by the fibres and matrix, respectively. Equation 3.1 can be expressed in terms of stress times area, according to

$$\sigma_{CFRP}A_{CFRP} = \sigma_F A_F + \sigma_M A_M \tag{3.2}$$

where σ denotes the axial stresses, and the sub-notations F, M and $CFRP$ denotes the corresponding material; fibre, matrix and composite. Since both fibres and matrix behave elastically, the equilibrium condition can be written as

$$E_{CFRP}\varepsilon_{CFRP}A_{CFRP} = E_F\varepsilon_F A_F + E_M\varepsilon_M A_M \tag{3.3}$$

where are E denotes the modulus of elasticity and ε the strain. Divided by A_{CFRP}, Equation 3.3 can be expressed in the form of volume fractions as

$$E_{CFRP}\varepsilon_{CFRP} = E_F\varepsilon_F v_F + E_M\varepsilon_M v_M \tag{3.4}$$

where v_F and v_M are the fibre and matrix volume fractions, respectively. As the assumption of full interaction implies that $\varepsilon_{CFRP} = \varepsilon_F = \varepsilon_M$, and $v_M + v_F = 1 \rightarrow v_M = 1 - v_F$, the longitudinal modulus can be expressed as

$$E_{CFRP}\varepsilon_{CFRP} = E_F\varepsilon_F v_F + E_M\varepsilon_M v_M = E_F v_F + E_M v_M = E_F v_F + E_M(1 - v_F) \tag{3.5}$$

Equation 3.5 is referred to as the rule of mixture, as the modulus of elasticity is directly related to the volume fractions of the constituents in the composite.

Axial tensile strength of a single wire

When evaluating the ultimate tensile stress of fibre reinforced composites, it is generally assumed that the final rupture of the material is caused by tensile failure of the fibres, even though the ultimate tensile strain of the matrix normally exceeds the ultimate tensile strain of the fibres. This assumption is valid except for very low fibre contents. In the case of CFRP wires where the carbon content used in applications today generally ranges from 65 - 72 % (Meier, 2012), the assumption is valid and longitudinal strength of the wire can be calculated as

$$\sigma_{Ltu} = \sigma_{Fu} v_F + \sigma_M'(1 - v_F) \qquad (3.6)$$

where σ_{Ltu} is the ultimate longitudinal tensile strength of the CFRP wire, and σ_M' is the stress in the matrix corresponding to the ultimate tensile strain of the fibre, ε_{Fu}.

Microfailure modes under tensile loading

It should be emphasized that although Equation 3.6 accurately predicts the strength of fibre reinforced composites, the assumption it was based upon, of simultaneous breakage of the fibres leading to the final rupture of the material, is not a rightful delineation of the actual failure mechanisms in fibre reinforced composites (Mallick, 2007). Instead, failure of fibre reinforced composites generally involves a number of different micro failure mechanisms, instigated by stress concentrations due to premature rupture of some of the weaker fibres. Fibre breakage will generally commence already for relative low values of applied stresses due to the natural scatter in strength. At the breakage of a fibre, the stresses in the vicinity of the broken end must increase as the stress in the broken end tends to zero. Thus, breakage of a single fibre leads to an increase in shear stress between the matrix and fibre in the vicinity of the broken end, increase of the normal force in adjacent fibres, and consequently also a stress concentration at the void generated by the rupture (Mallick, 2007), see Figure 13.

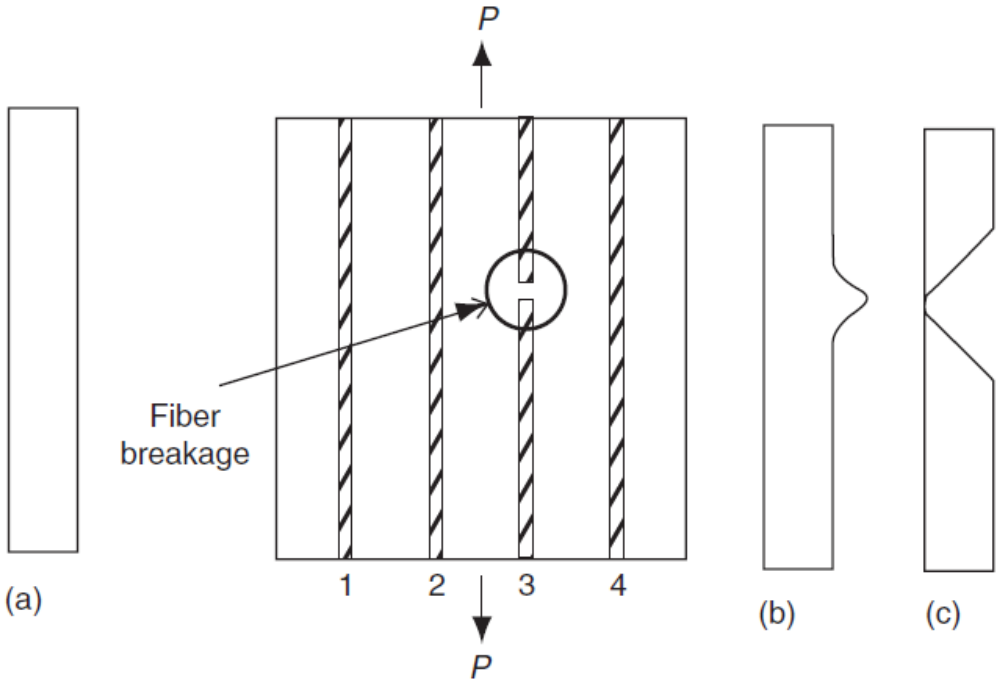

Figure 13. Longitudinal stress distribution in a unidirectional fibre composite; a) stress distribution in all fibres before breakage, b) stress distribution in adjacent fibres after breakage, c) stress distribution in broken fibre (Mallick, 2007).

Several micromechanical failure modes are related to the stress increments in the vicinity of the broken ends of the fibres. Some of the most common failure modes are, (1) debonding of the fibre due to high interfacial shear stresses between fibre and matrix, (2) cracking of the matrix due to the local stress raising effects of the void, and (3) breakage of adjacent fibres (Mallick, 2007), see Figure 14. The final rupture of the material in tensile loading is a result of continuous fibre breakages at various locations under increasing load, and the fracture toughness is consequently the sum of energy dissipated in the development of micro failures.

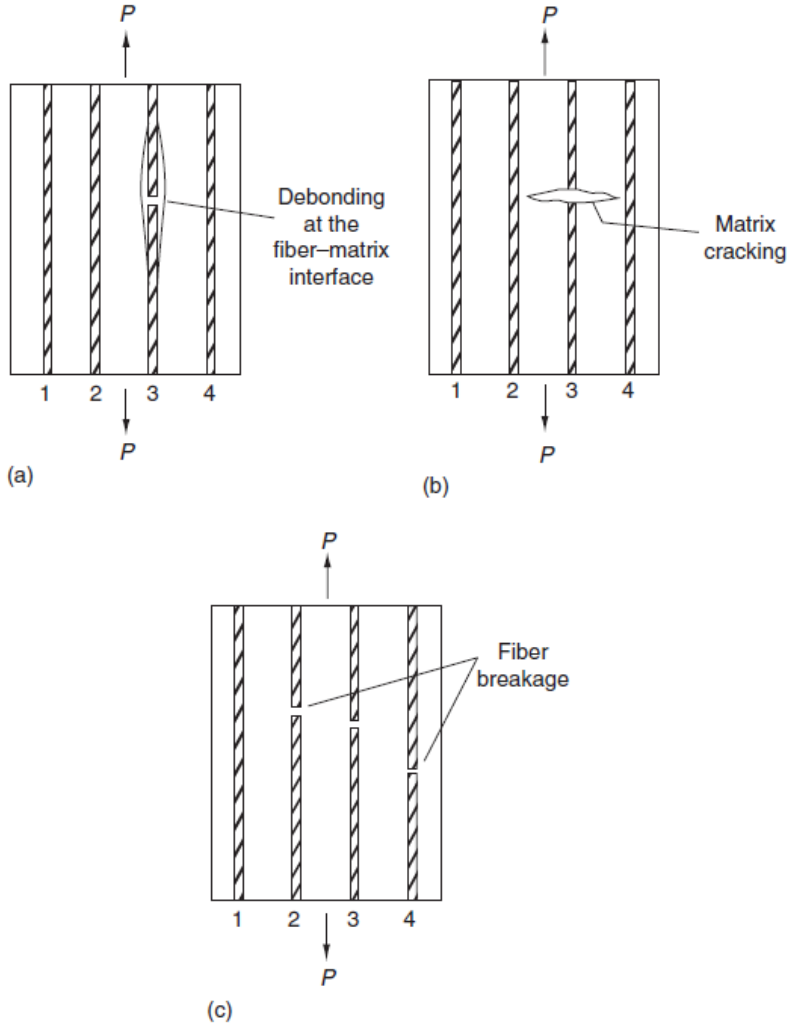

Figure 14. Possible microfailure modes resulting from fibre breakage (Mallick, 2007).

3.2.2 Non-uniaxial states of stress

Although, the transverse isotropy of fibre reinforced polymers enables superior axial mechanical properties, it also constitutes a problem as the materials consequently have relatively poor lateral properties, including in-plane shear (Meier & Mehdi, 1996). In the following, typical values of the mechanical properties for the two most critical loading conditions in applications of CFRP cables in suspended structures are given, along with brief descriptions of their corresponding failure modes.

Transverse compressive strength

The most common failure mode under transverse compressive loading is shear failure within the matrix (Zoghi, 2014). This type of failure is often instigated by debonding of the fibres, and appears as inclined shear cracks parallel to the fibre direction (Mallick, 2007), see Figure 15.

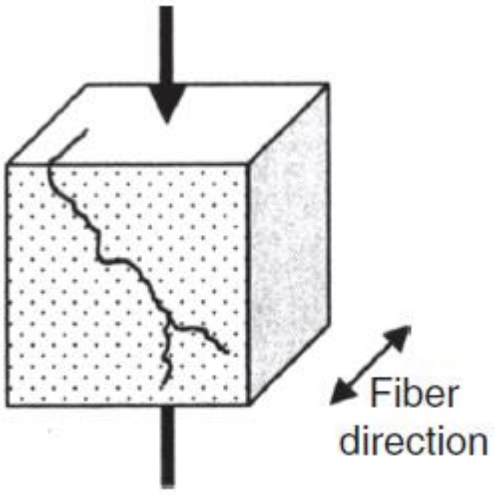

Figure 15. Shear failure under transverse compression (Mallick, 2007)

Several empirically fitted expressions have been proposed for evaluating the transverse strength, based on the properties and the volume fractions of the constituents. None of these have, however, been found to give accurate results when compared to empirically obtained data. In design it is therefore recommended to either determine the strength experimentally, or use the following conservative estimation (Zoghi, 2014)

$$\sigma_{2cu} = \sigma_{mcu} \tag{3.7}$$

where σ_{2cu} is the transverse strength of the composite and σ_{mcu} the transverse strength of the matrix. Setting the transverse strength equal to strength of the matrix is, however, in general a very conservative estimation.

Shear strength

The in plane shear strength τ_{12u}, is also governed by shear failure of the matrix and possible debonding of the fibres. Similar to the transverse compressive strength, empirical expressions of the in-plane shear capacity are afflicted with large uncertainties, and in design it is therefore recommended to use experimentally obtained values, or set the shear strength equal to the shear strength of the matrix according to (Zoghi, 2014)

$$\tau_{12u} = \tau_{mu} \tag{3.8}$$

In Table 1, the transverse and in-plane shear strength of a CFRP wire is shown, using both the conservative estimations (Equation 3.7 and 3.8) and empirically obtained data. The transverse strength of HS steel is also included for comparison.

Table 1. Example of a CFRP wires transverse compression- and in-plane shear strength compared to HS steel. The values in the table are based on the study from Schmidt et al. (2012).

Material	Fibre content	Transverse strength (σ_{2cu})	In-plane shear (τ_{12u})
CFRP $\sigma_{2cu} = \sigma_{mcu}$ / $\tau_{12u} = \tau_{mu}$	-	102 MPa	34 MPa
CFRP (empirical)	0.65	228 MPa	71 MPa
HS steel	-	1 770 MPa	-

From Table 1 it becomes apparent that the anisotropic structure of CFRP wires is coupled with poor capacity with respect to transverse compressive loading and in-plane shear.

3.3 Properties of commercial CFRP cables

CFRP cables consist of parallel wire bundles of CFRP wires. Similar to the manufacturing of CFRP wires, the objective is to produce a durable structural element with minimum loss of stiffness and strength compared to the single wires (Meier & Mehdi, 1996). The specific stiffness and strength of the cable depends on the weight ratio between the CFRP-wires and the non-structural material. The only non-structural materials in the cables are those used for protection against deteriorating UV-light and wind-erosion. No corrosive inhibiting compound or grout needs to be added, due to the inherent corrosive resistance of the CFRP itself (Meier & Mehdi, 1996). With the use of polyethylene (PE) or polypropylene (PP) covers, adequate for shielding against the deteriorative environmental processes (Noisternig, 2000), very low strength- and stiffness-to-weight loss is feasible. Hence, the mechanical properties of the CFRP cables are very similar to the properties of the single wires. Figure 16 shows the CFRP cable used in the Stork Bridge (case study that is further discussed under Chapter 7), consisting of 241 parallel CFRP wires.

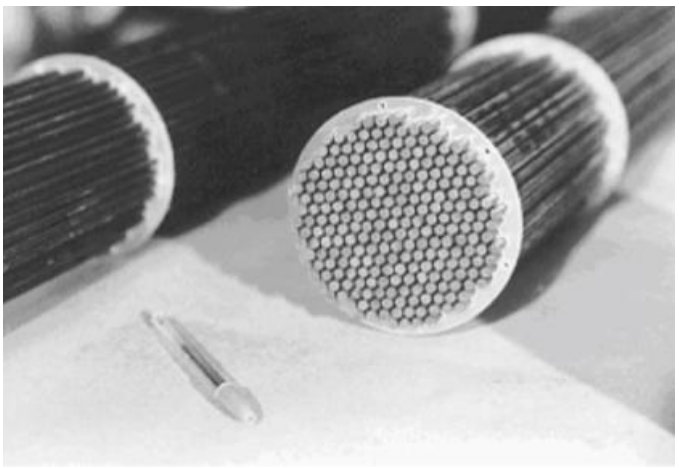

Figure 16. CFRP cable consisting of 241 wires (Meier, 2012).

Properties of commercial CFRP wires

The properties of carbon fibre vary considerably, depending on the manufacturing process. The strength of commercial carbon fibres ranges from 3 500 to 7 000 MPa, and the elastic moduli from 200 to 650 GPa (Meier & Mehdi, 1996). The most commonly used carbon fibre in civil applications is the Torayca T 700S, with strength of 4 900 MPa and an elastic modulus of 230 GPa (Meier, 2012). The density for this type of carbon fibre is 1.8 g/m^3 and the elongation at failure 2.1 %. The mechanical properties of the epoxy resin are however only in magnitude of a couple GPa in terms of modulus of elasticity, and generally below 100 MPa for the ultimate tensile strength. Therefore, it becomes apparent that the fibre volume percentage and the mechanical properties of the carbon fibre almost exclusively govern the axial properties of the CFRP wires, see Equation 3.5 and 3.6. However, as previously mentioned, in load cases where the stress deviates from the axial direction, the mechanical properties of the matrix become highly important.

The development of CFRP wires for applications in cables of suspended structures dates back to 1980 when EMPA and BBR Ltd. in Switzerland started their development of CFRP cables (Meier, 2012). The first application of CFRP cables in a road bridge were in early 1996, during the erection of the Stork Bridge in Winterthur, where two out of 24 stays were made out of CFRP. Each cable consists of 241 CFRP wires, with a diameter of 5 mm, and has a total load-carrying capacity of 12 MN. The wires used in the applications were produced by EMPA and BBR Ltd., and their mechanical properties are to be found in Table 2.

Besides the Swiss developers, there are several other manufacturers producing CFRP wires. Two important producers are the Tokyo Rope Manufacturing Company and the Mitsubishi Chemical Company. Tokyo Rope produces the Carbon Fibre Composite Cables (CFCC) and Mitsubishi Chemical produces the Leadline bars, and mechanical properties of these wires are presented in Table 2 as well.

Table 2. Mechanical properties of CFRP wires. The values for the CFCC wire are based on a diameter of 12.5 mm, and the values for the Leadline on a diameter of 8 mm (Meier, 2012) (Mahmoud, 1997).

	Stork Bridge wire (EMPA and BBR Ltd.)	**CFCC wire** (Tokyo Rope)	**Leadline wire** (Mitsubishi Chemicals)
Tensile strength (longitudinal)	3 300 MPa	2 100 MPa	1 970 MPa
Elastic modulus (longitudinal)	165 GPa	137 GPa	147 GPa
Density	1.56 g/cm^3	2.0 g/cm^3	1.6 g/cm^3
Fibre content	68 Vol. %	64 Vol. %	65 Vol. %
Thermal expansion (longitudinal)	$0.2 * 10^{-6}$ °C	$0.6 * 10^{-6}$ °C	$0.68 * 10^{-6}$ °C
Elongation at failure	2.1 %	1.57 %	1.3 %

4 Static Span Limits

In this chapter, the static span limits are evaluated for both suspension and cable-stayed bridges. Due to their differences in structural behaviour, a different evaluation method has been adopted for each bridge type. For suspension bridges, a simplified expression, relating the span length to the weight of the suspended structure and the static strength of the cable, is derived from vertical equilibrium of a small cable segment.

For cable-stayed bridges, on the other hand, a similar approach is not applicable for the evaluation of span limits. Instead, a more apt evaluation method is based on the stiffness efficiency of the material, which decreases sharply in long stay cables and limits the applicable cable lengths. The stiffness efficiency is related to the applied level of stress, horizontal cable length, and the density of the cable material. The stiffness efficiency is, therefore, determined by the static material characteristics of the cable material and the adopted safety factor. However, it has to be noticed that the applicable cable lengths for cable-stayed bridges should not be directly interpreted as half the applicable span length. The induced axial forces in the deck, explained under Section 2.2, might govern the span lengths before the limit of the cables. An evaluation of the required dimensions of the deck is therefore necessary for each specific project in order to find the applicable span lengths. However, since these axial forces are irrelevant for the comparison of the cable materials, they are not treated here.

4.1 Suspension bridges

The following sub-chapter contains calculations performed by the authors. The theory behind the calculations is first presented, followed by calculations and results. In the last part of the sub-chapter, the results are compared with previous studies in the field.

4.1.1 Theory

During the latter part of the nineteenth century and the beginning of the twentieth century, analytical models such as the elastic theory and the deflection theory were developed (Clemente, Nicolosi, & Raitel, 2000). The progressions in the analytical field led to great improvements in the predictions of the structural behaviour of long span suspension bridges, and resulted in the construction of bridges such as the George Washington Bridge, with a main span of about 1 000 meters, and the Golden gate bridge with a span of 1 240 meters (Clemente, Nicolosi, & Raitel, 2000).

The most prominent analytical method developed at the time was the deflection theory. The deflection theory is, as opposed to the elastic theory, a non-linear analysis that accounts for the second order effects under the action of live loads. Although the analytical solutions of the deflection method are rarely used today, numerical solutions of the governing differential equation can still be used for basic understanding of the static behaviour of suspension bridges (Cobo del Arco & Aparicio, 2001). However, a full-scale non-linear numerical analysis, required to solve the governing differential equations of the deflection theory, is not performed in this thesis. Instead, a simplified relation between the theoretical span limit and the ratio between weight of the suspended structure, except cables, and the self-weight of

the cables is given, based on the first governing differential equation of the deflection theory. The first governing differential equation is defined as

$$H\frac{d^2w}{dx^2} = q_0 \qquad (4.1)$$

where H represents the horizontal component of the axial force in the cable, $\frac{d^2w}{dx^2}$ is the change of slope over the cable segment, and q_0 is the total dead load acting on the cable segment. The first governing differential equation can be deduced from vertical equilibrium of a small cable segment exerted to distributed dead loads only, see Figure 17. From the figure it can be seen that horizontal equilibrium requires the two horizontal components of the axial cable forces to be equal. Thus, vertical equilibrium implies that the change in slope, $\frac{d^2w}{dx^2}$, times the horizontal force, H, equals the total dead load acting on the cable segment.

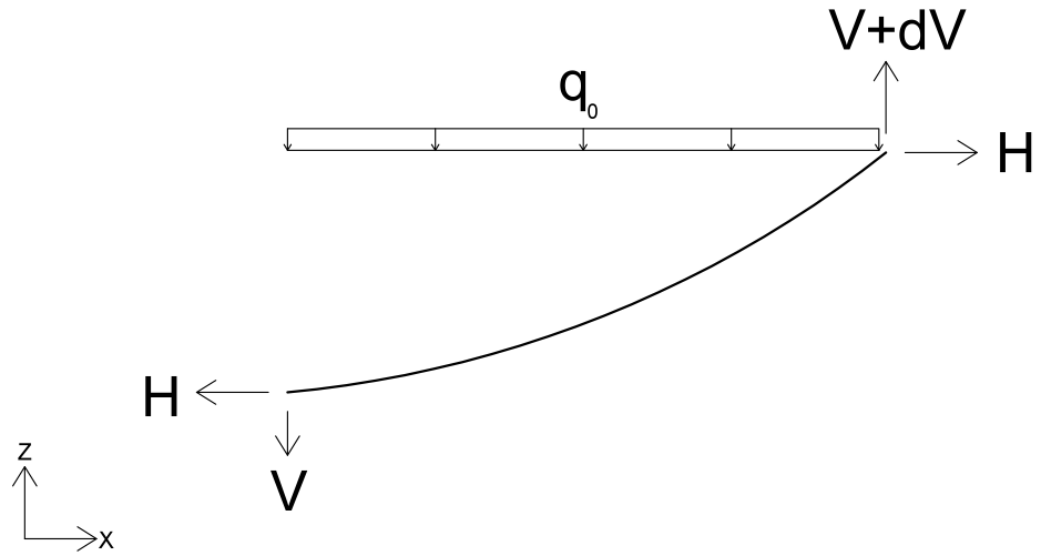

Figure 17. Free body diagram of a small cable segment that is exerted to distributed dead loads only.

In addition, the expression may, with good approximation, be simplified by approximating the shape of the cable segment with the shape of a parabola (Thylén, 2009). Hence, the equilibrium equation can be expressed according to

$$\frac{q_0\, l_m^2}{8d} = H \qquad (4.2)$$

where l_m represents the main span length and d is the cable sag in main span.

When evaluating the theoretical span limit with respect to static strength, it is helpful to start by looking at a free hanging main cable, i.e. a main cable exerted only to its self-weight. Although this is a highly unrealistic load case, it is of interest when analysing applicable span lengths since a high percentage of the cable stress will be induced from the self-weight of the cables. The expression can also easily be extended to include other uniformly distributed loads.

The theoretical span length can be deduced from the equilibrium condition in Equation 4.2 for the small cable segment exerted to the highest stress. By setting the axial force in this cable segment equal to the product of the allowable stress,

$\sigma_{allowable}$, and the cross-sectional area, A_c, the theoretical span limit can be evaluated. Moreover, for usual values of the sag ratio, $\frac{d}{l_m} \approxeq 0.10$, the self-weight of the cables can be approximated as uniformly distributed along the span length (Clemente, Nicolosi, & Raitel, 2000). Thus, vertical equilibrium for the cable segment exerted to the highest stress can be expressed as

$$H = A_c * \sigma_{allowable} * \cos\alpha_m = \frac{g * \rho_c * A_c * \frac{l_{mc}}{l_m} * l_m^2}{8d} \qquad (4.3)$$

where α_m is the maximum slope of the cable (adjacent to the pylon top), ρ_c is the cable density, and l_{mc} is the cable length in main span. With the assumption of a parabolic-shaped main cable, the cable length and the maximum angle (adjacent to the pylon) can be expressed as

$$l_{mc} = l_m * \left(1 + \frac{8}{3}\left(\frac{d}{l_m}\right)^2\right) \qquad (4.4)$$

$$\alpha = \arctan\left(\frac{4d}{l_m}\right) \qquad (4.5)$$

which gives the following expression for theoretical span limit of a free hanging main cable

$$l_m = \left(\frac{\cos\left(\arctan\left(\frac{4d}{l_m}\right)\right) * 8d * \sigma_{allowable}}{g * \rho_c * l_m * \left(1 + \frac{8}{3}\left(\frac{d}{l_m}\right)^2\right)}\right) \qquad (4.6)$$

From Equation 4.6 it becomes apparent that the theoretical span length is independent of the sectional cable area, and solely determined by the geometrical configuration and the material parameter $\frac{\sigma_{allowable}}{\rho_c}$.

The expression for the theoretical span limit will now be extended to include all types of distributed loads. However, in contrast to the deflection theory, the live loads are included without respect to their induced second order effects and instead all distributed loads, irrespective of load duration, are treated as dead loads. With this approach it is straightforward to extend the expression and include additional distributed loads, such as dead load from the deck and uniformly distributed live loads. The additional loads are simply accounted for by introducing a load factor, β, representing the relation between the additional loads and the cable weight

$$\beta = \frac{sum\ of\ all\ additional\ loads}{self - weight\ of\ cable} = \frac{w_{add}}{\frac{g\rho_c l_{mc}}{l_m} A_c} \qquad (4.7)$$

where w_{add} is the sum of all distributed loads, except for the cable. The theoretical span length can now be determined for any given β- value according to

$$l_m = \left(\frac{\cos\left(\arctan\left(\frac{4d}{l_m}\right)\right) * 8d * \sigma_{allowable}}{g * \rho_c * l_m * \left(1 + \frac{8}{3}\left(\frac{d}{l_m}\right)^2\right)(1+\beta)}\right) \qquad (4.8)$$

Just as for the case when the theoretical span limit was evaluated based solely on the self-weight of the cables, it can be seen that in addition to the load factor β, the theoretical span limit is exclusively governed by the geometrical configuration of the bridge and the specific strength of the cable material.

4.1.2 Calculations and results

To evaluate the effect of the cable material on the limiting span with respect to static tensile strength, calculations were conducted for both HS steel and CFRP cables. The theoretical span limit, shown in Figure 18, was calculated utilizing Equation 4.8 above, and the results are presented as a function of the β- value. In the calculations both the conventional rise-to-main span ratio, $\frac{d}{l_m} = 0.10$, and the optimum value with respect to performance, $\frac{d}{l_m} = 0.35$, were used. Other input parameters were set according to Table 3. The calculations were performed in MATLAB, and the entire code is to be found in Appendix B.

Table 3. Mechanical properties and safety factors of the CFRP and steel used in the calculations.

Mechanical properties and safety factors	**CFRP**	**HS steel**
Density (ρ)	1 600 $\frac{kg}{m^3}$	7 850 $\frac{kg}{m^3}$
Tensile strength ($\sigma_{ultimate}$)	3 300 MPa	1 770 MPa
Safety factor	4.4	1.8
β- value (Sognefjorden)	6.81	1.08

It should be commented that the adopted safety factor for CFRP in the calculation is based on the discussion of safety factors from Section 5.2.3. The adopted value is an interpolation of the safety factor based on tensile strength (lower limit), and the one based on equivalent stiffness (upper limit). It should also be clarified that the marked out β-values in the plot (same values as in Table 3) corresponds to the β-values of the single span suspension bridge over Sognefjorden with HS steel/CFRP cables. The values are based on the preliminary sizing performed in Section 5.2.3.1, which is described in more detial in Appendix A. Other input parameters, such as density, tensile strength and geometrical parameters, are all set in accordance with the values used throughout the thesis.

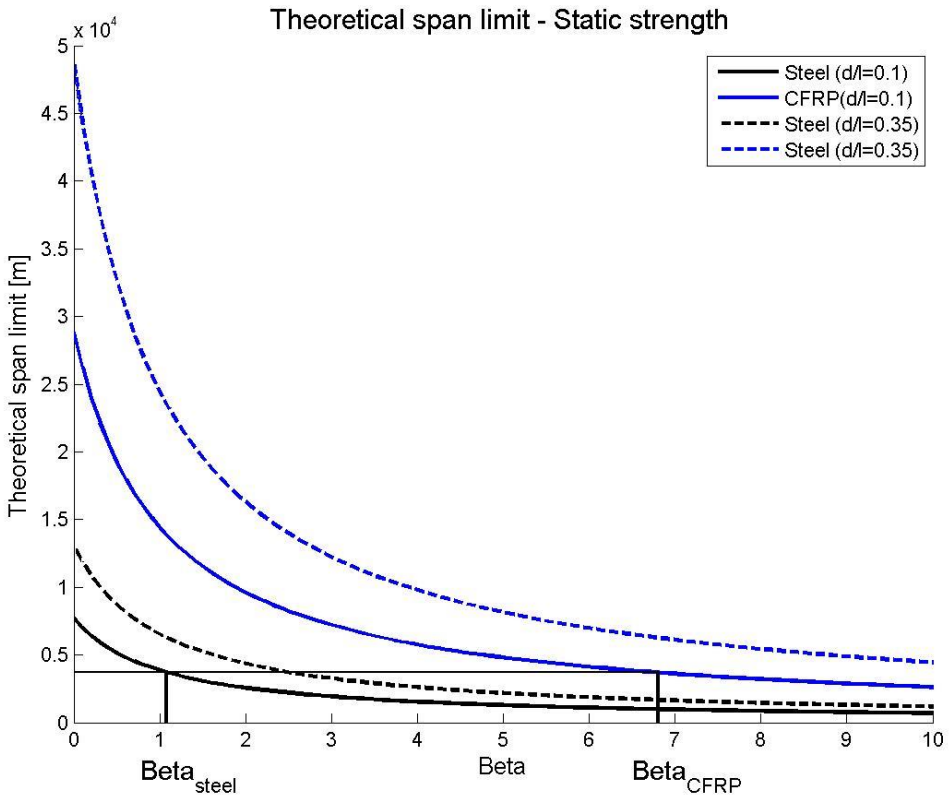

Figure 18. Theoretical span limit as a function of the ratio between additional loads and the cable weight. The graphs of the span limit for CFRP is represented by the blue lines and the span limits of steel is represented by the black lines. The span limits of both materials are evaluated for the rise-to-main span ratios 0.1 and 0.35, shown in solid and dashed lines, respectively.

The most important outcome of the calculations, shown in Figure 18, regards the relation between the theoretical span limit and the β-value. From the figure it can be seen that the β-value of Sognefjorden with HS steel cables corresponds to a cable weight of half the total load of the suspended structure, whereas the weight of the CFRP cables comprise less than $\frac{1}{8}$ of the total load. This surely indicates that HS steel is approaching the upper practical span limit with respect to static strength, as an even further increase in span length would increase the cable weight in relation to other loads even more. CFRP on the other hand is far from its static limit with respect to static tensile strength, which is indicated by its high β-value. Thus, the general conclusion from this simplified analysis is that CFRP cables, from a static and strength point of view, is far superior compared to steel and highly feasible in super long span suspension bridges.

4.1.3 State of the art

Research on the static performance, with respect to span limits, of CFRP cables has already been conducted with quite similar approaches, as adopted by the authors of this thesis. Both Meier (2012) and Jiang & Jia (2012) have compared CFRP and steel cables in suspension bridges with respect to theoretical span limits, and their results supports the results, presented in previous section.

When evaluating the theoretical span limit, Meier (2012) introduced a specific design load parameter, defined as the dead load of the superstructure divided by the dead load of the deck and the live loads. The densities used in the calculation were 7 800

$kg/m^3$for steel and 1 600 kg/m^3 for CFRP. The values for the allowable stresses were set to 1 000 MPa for both materials and the rise-to-main span ratio was chosen as $\frac{d}{l_m} = 0.10$. The results from the calculations are demonstrated in Figure 19, where it can be seen that the theoretical limiting span is approximately 7 700 meters for steel and 37 500 meters for CFRP. Taking the input data into account, it can be verified that the values obtained from the author's model correspond well with those presented by Meier (2012).

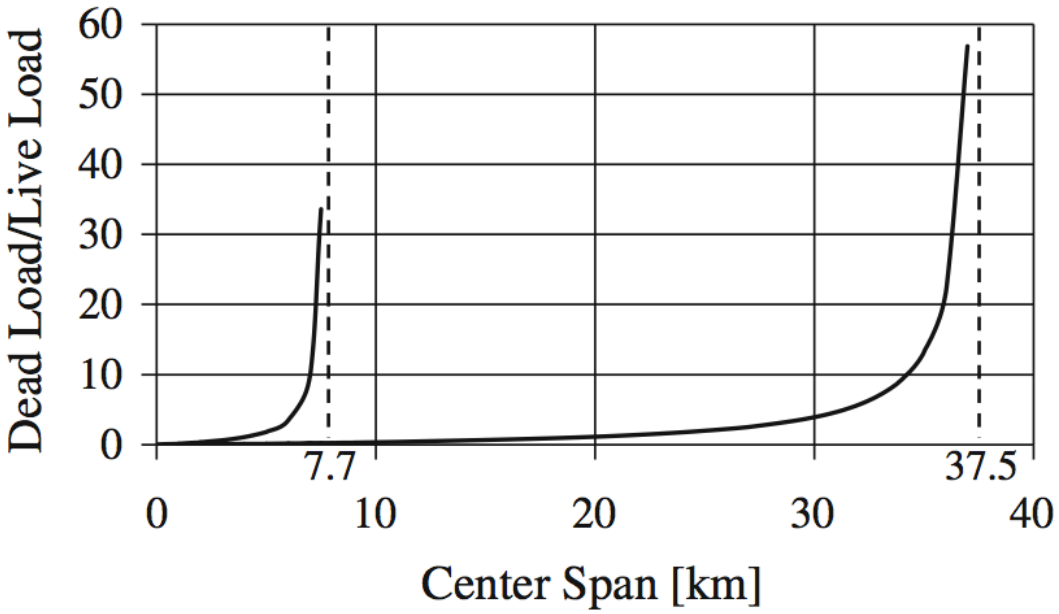

Figure 19. Specific loads over different span lengths of a fictitious suspension bridge for both steel and CFRP in the cables. Steel has a limitation of 7.7 km and CFRP of 37.5 km (Meier, 2012).

Since the theoretical limiting span of a free hanging cable in the calculations corresponds to the span length for which the specific load approaches infinity, more realistic span lengths are found for lower specific loads. In Table 4, the specific loads for the already existing bridge Verrazano Narrows and the two possibly future bridges over the Strait of Messina and the Strait of Gibraltar are listed. The specific loads are given for both steel and CFRP, and the results emphasize the great potential of using CFRP instead of steel as cable material in super long span suspension bridges.

Table 4. Comparison of specific design load for three different bridges with both steel and CFRP cables (Meier, 2012).

Bridge	Center span, ℓ (m)	Specific design load, g/p	
		Steel	CFRP
Verrazano narrows	1,300	0.5	0.04
Messina	3,000	2.0	0.06
Gibraltar	8,400	∞	0.29

In the calculation conducted by Jiang & Jia (2012), the assumption of a free-hanging main cable with the form of a parabola was assumed as well. The calculation was performed for five different rise-to-main span ratios, S, ranging from 1/12 to 1/8. High strength steel with a tensile strength of 1 670 *MPa* and a safety factor of 2.5 was adopted in the calculation. For the CFRP cables, the density was set to 2 000 kg/m^3 but no tensile strength was defined. The results are presented in Figure 20, were the results for the steel cables are located on the left hand side of the figure and the results

for CFRP cables on the right hand side. Jiang & Jia (2012) only presented results of spans up to 20 000 meters, but it still highlights the potential of CFRP compared to steel in terms of applied stress.

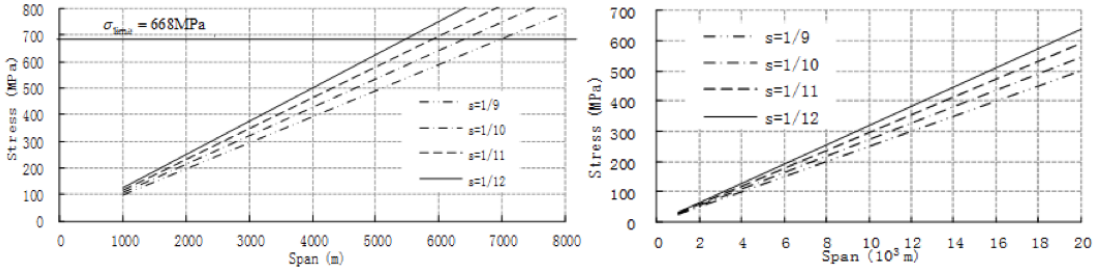

Figure 20. Span length vs. applied stress for suspension bridge exerted to the self-weight of main cables solely. The calculation with steel cables is shown to the left and the calculation with CFRP cables to the right (Jiang & Jia, 2012).

4.2 Cable-stayed bridges

As mentioned in the introductory text of this chapter, it is not possible to derive an expression for the ultimate span length of cable-stayed bridges purely based on the static strength of the cables. Instead, the coupling effect between the horizontal forces in the deck and the total load of the suspended structure might be the governing factor, and preliminary sizing of the bridge deck is required prior to any estimates of applicable span lengths. However, since previous studies have shown that the static performance of cable-stayed bridges essentially is governed by the equivalent modulus and stiffness of the cables (Wang & Wu, 2010), it is still valuable to analyse and compare the isolated response of the cables for different cable materials and cable lengths. Therefore, in the first part of this sub-chapter, the characteristics of HS steel and CFRP, in terms of equivalent modulus and stiffness, are studied with respect to adopted safety factors. In the second part, these relations are used together with estimates of the lowest applicable safety factors, in order to evaluate applicable cable lengths of the two materials.

4.2.1 Theory

In practical applications, stay cables suffer from a reduction in stiffness in long and super long span bridges, due their pronounced sag-effect. To alleviate the deficiency in material stiffness under increasing span lengths, the cable area must increase to maintain the equivalent stiffness of the stay cables. However, as the equivalent modulus of the stay cables is dependent not only on the initial modulus and density of the cable material but also on the applied level of stress, the relation between the sectional area and equivalent stiffness ($E_{eq}A$) is nonlinear. This nonlinearity in equivalent modulus and equivalent stiffness, as a function of cable area, is fundamental when analysing applicable cable lengths. Hence, in the following, the characteristics of these two parameters are investigated, with respect to adopted safety factors.

Equivalent modulus and equivalent stiffness

In practical applications, all stay cables exhibits a nonlinear load-deformation response, due to the sag-effect. This sag-effect, caused by the misalignment between the gravitational field and the tension direction of the cables, is generally not obvious for span lengths within 1 000 meters (Wang & Wu, 2010). However, with further

increase in span length, and natural growth in cable length, the sag-effect of steel cables becomes evident and will significantly influence the stiffness efficiency of the material. Therefore, when analysing the static response of cable-stayed bridges, an equivalent modulus, rather than initial linear elastic modulus, is utilized to model the nonlinear static response of the cable-stayed bridges.

To account for the nonlinear load-deformation response of stay cables, the tangent modulus, showed in Equation 2.2, is generally used due to its simplicity. However, it has been shown in previous studies that the tangent modulus may generate considerable errors when used to model the mechanical behaviour of stay cables exceeding 500 meters (Wang & Wu, 2010). The inaccuracy of the tangent modulus is essentially caused by two approximations; the sagging stay cable is represented by the parabolic equation instead of the accurate catenary equation, and the stress variation in service state is constant. Therefore, since the behaviour of cables in super long span bridge applications is considered in this study, the secant modulus, which accounts for the stress variations in service state, will be utilized to model the response of the stay cables. The secant modulus is defined as

$$E_{sec} = \frac{1}{\frac{1}{E_0} + \frac{(\rho l_c)^2}{24}\left(\frac{\sigma_1 + \sigma_2}{{\sigma_1}^2 {\sigma_2}^2}\right)} \qquad (4.9)$$

where E_0 is the initial modulus, ρ is the density of cable, l_c is the horizontal length of the cable, σ_2 is the lower limit of design stress and σ_1 is the design stress. In addition to the mechanical properties in terms of specific stiffness and specific strength, it is obvious that also the magnitude and range of stress affects the equivalent modulus. The equivalent modulus is therefore also affected by the relation between cross-sectional area and applied force, i.e. the adopted safety factor. From a mechanical viewpoint, it is desirable to adopt a low safety factor. A decreased safety factor will, in fact, increase the materials efficiency due to a decreased sag-effect under increasing levels of stress. However, a low safety factor is only viable in materials with very stable mechanical properties, good long-term performance, and high stiffness (Wang & Wu, 2010).

In conventional cable-stayed bridges, within 1 000 meters, the lowest applicable safety factor is essentially determined by the long-term performance of the material (Wang & Wu, 2010). Based on the material characteristics of steel, the safety factors employed in conventional cable-stayed bridges, of current span lengths, lies in the range of 2.2 - 2.5, depending on national standards (Wang & Wu, 2010). However, in super long span bridge applications, it is not straightforward to determine appropriate safety factors, neither for HS steel nor CFRP. The HS steel stay cables exhibit a sharply decrease in equivalent modulus for cable lengths exceeding ≈ 500 meters, and the applications of CFRP cables are scarce and their material characteristics are essentially different from HS steel.

Based on the evaluation criteria of steel, very low safety factors are permissible for CFRP, due to its excellent fatigue behaviour. However, several previously conducted studies of CFRP stay cables in cable-stayed bridges, at the 1 000 meter scale, utilized a safety factor of 3.0 to account for the uncertainties regarding the use of new materials and the brittleness of carbon (Wang & Wu, 2010). It has also been suggested in other studies that even a safety factor of 3.0 might be insufficient, when taking the stiffness criterion into consideration (Wang & Wu, 2010). From this reasoning, it can be concluded that an absolute lower limit of applicable safety factors

corresponds 2.2 - 2.5 of steel and 3.0 – 5.0 for CFRP, where the latter value for CFRP is determined by the stiffness equivalence principle. However, the discussion of appropriate safety factors will not be pursued further in this sub-section, but the topic is extended in the last part of this section in the context of applicable cable lengths. The remainder of this sub-section is instead devoted to investigating the relation between the equivalent modulus and the corresponding equivalent stiffness, as a function of the adopted safety factors.

In Figure 21 and Figure 22, the equivalent modulus and equivalent stiffness of steel and CFRP are shown as functions of the adopted safety factors, for the horizontal cable lengths of 500 – 5 000 meters. The material properties of the CFRP cable is chosen in accordance with the material properties presented for the EMPA-wire, listed in Table 2, and the stress variation is set within the narrow range of $0.8\sigma_2$ - σ_2, as the stress variations are assumed to be limited in super long span bridges. The MATLAB-code for the calculations is found in Appendix C.

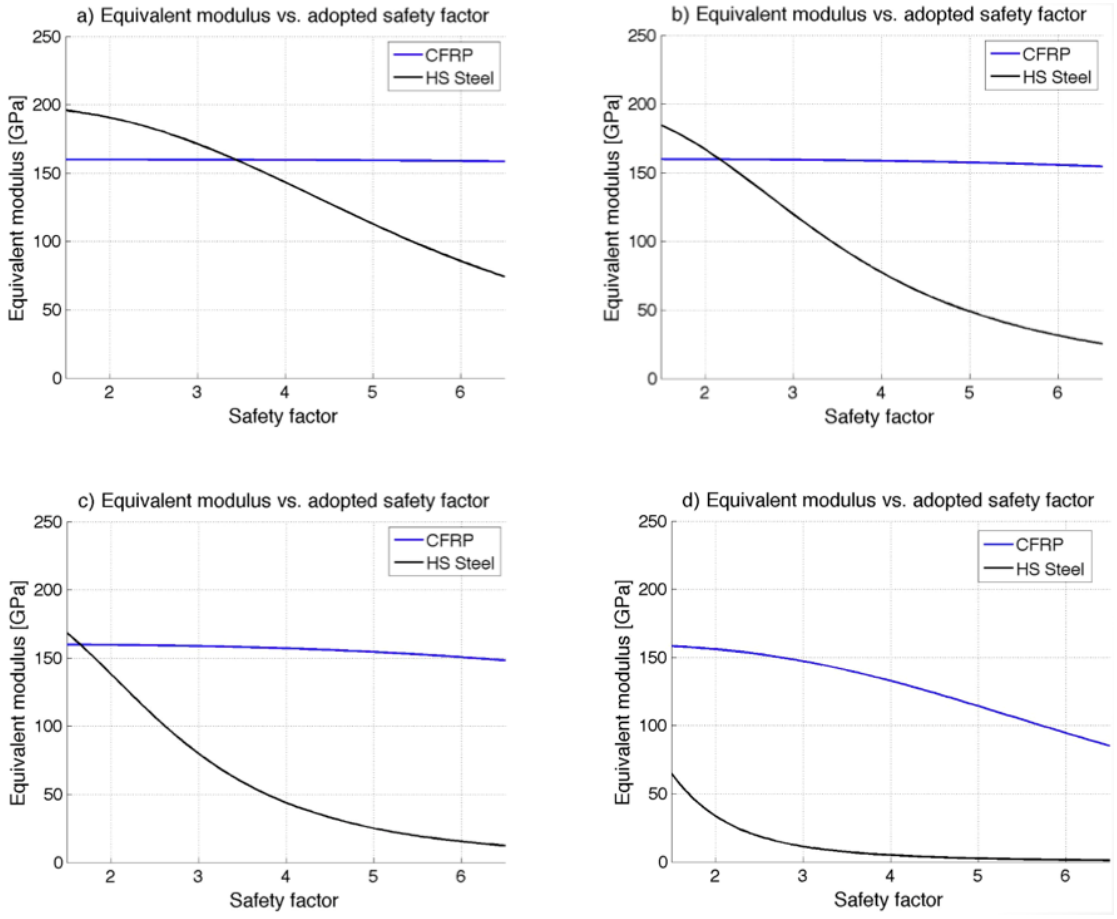

Figure 21. Relation between equivalent modulus and safety factors for a) 500 meters, b) 1 000 meters, c) 1 500 meters and d) 5 000 meters.

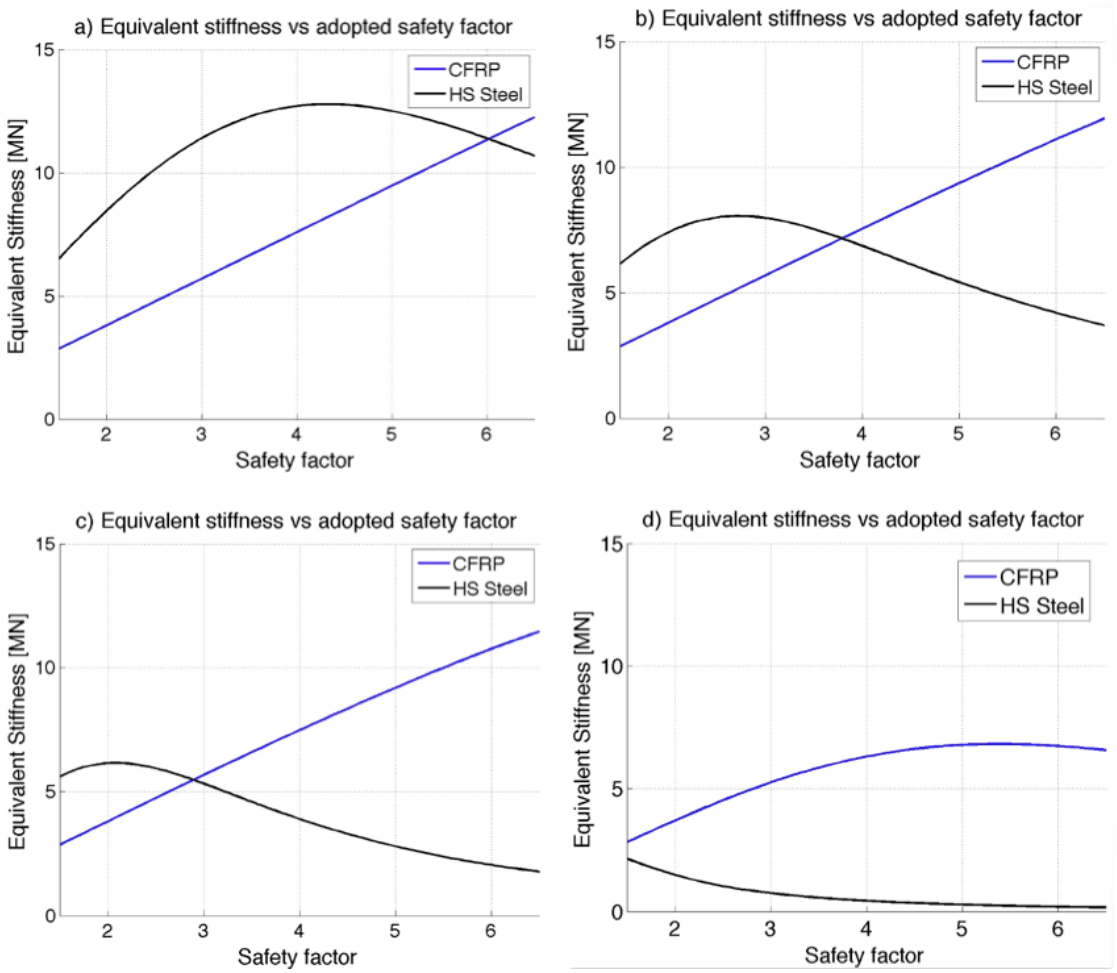

Figure 22. Relation between equivalent stiffness and safety factors for a) 500 meters, b) 1 000 meters, c) 1 500 meters and d) 5 000 meters.

Several important mechanical characteristics of HS steel and CFRP stay cables can be observed in Figure 21 and Figure 22. Firstly, it is apparent that steel exhibits a highly nonlinear relation between equivalent modulus and adopted safety factors, already for cable lengths ≈ 500 meters. For CFRP, on the other hand, the reduction is very limited with increasing safety factors for cable lengths up to ≈ 1 500 meters. This implies that CFRP will have an almost linear relation between increments in equivalent stiffness and increasing sectional area for cable lengths within 1 500 meters, whereas the early nonlinearity in stiffness efficiency of steel yields a premature nonlinear relation between equivalent stiffness and safety factors. This behaviour is clearly seen in Figure 22 a) - c).

It should also be mentioned that the stiffness efficiency, referred to above, corresponds to the equivalent modulus while the equivalent stiffness ($E_{sec}A$) corresponds to the actual deformation resistance of the stay cables. It can therefore be concluded that steel has a higher static performance (equivalent stiffness) than CFRP for shorter spans (when adopting equal safety factors), but the static performance of CFRP is increasing in relation to the static performance of steel for increasing span lengths. This is partly due to the deficiency in initial modulus, and partly due to the higher ultimate strength of CFRP. However, under further increase in cable length, the CFRP cable ultimately exhibits higher equivalent stiffness for the same value of safety factor.

In the next section, these tendencies of decreasing stiffness efficiency and corresponding nonlinearity in equivalent stiffness are further discussed, together with a discussion of appropriate safety factors when estimating applicable cable lengths.

Estimates of applicable cable lengths

As previously mentioned, the lower limit of applicable safety factors for steel is related to the long-term strength, and lies in the range between 2.2 - 2.5. For CFRP on the other hand, the lower limit cannot be specified with the same certainty, and values in the range of 3.0 – 5.0 have been suggested. Furthermore, in applications of super long span bridges, the mentioned safety factors are plausible to be insufficient, due the apparent reduction in stiffness efficiency.

Nevertheless, despite the difficulties regarding the determination of appropriate safety factors, it can still be concluded that an absolute upper limit of applicable span lengths relates to the point where the safety factor, corresponding to the maximum stiffness, falls below the lowest applicable safety factor. For HS steel stay cables, this point roughly corresponds to a horizontal cable length of 1 500 meters, at which the stiffness maximum is reached for a corresponding safety factor of ≈ 2.1. Utilizing the same criterion for CFRP, and adopting the stiffness equivalency principle, it can be concluded that the maximum applicable cable length is related to the point where the stiffness maximum is reached for a safety factor of ≈ 5, which corresponds to a cable length of approximately 5 000 meters.

In concluding remarks, regarding the estimated maximum cable lengths, it can be settled that the obtained values merely should be seen as rough estimates of the upper limit of applicable cable lengths. Since no consideration is taken to axial forces in the deck in the calculation, the results are not analogous with applicable span lengths. A more accurate prediction of the applicable span lengths, with respect to statics, requires designs of the complete bridge structure and analyses of the static response under loading to determine the actual deflections in service state.

5 Dynamic Performance

The dynamic performance of CFRP cables in super long span bridges is analysed in the following chapter. The great flexibility and high propensity for aerodynamic instability makes the aerodynamic performance of cable supported bridges one of the most crucial design aspects for span lengths exceeding 2 000 meters (Larsen & Esdahl, 1998). Furthermore, as the susceptibility for wind induced instability increases with increasing span lengths, bridge aerodynamics becomes increasingly important and ultimately a key issue in the development of future super long span bridges. Thus, in order to evaluate the feasibility of super long span bridges with CFRP cables, it is of outermost importance to analyse their dynamic performance.

As a basis for further analyses, the beginning of the chapter aims to provide sufficient insight into some of the most important instability problems encountered in the design of modern cable supported bridges. Emphasis will be given to the response of the bridge girder, as this is the most influential aspect in the aeroelastic design. However, as will be seen, the stiffness and weight of the cables also are influential aspects for the dynamic response, as they not only affect the mass and mass moment of inertia of the bridge, but indirect also the natural frequencies. The second part of this chapter consists of an aerodynamic analysis, where an investigation of the aerodynamic response of a 3 700 meters suspension bridge over Sognefjorden is conducted, using both HS steel and CFRP cables. The results from the calculations of the two cable alternatives are analysed and compared in the third part of the chapter, and the alternative with CFRP cables actually proves to have a higher critical flutter wind speed. The last part of the chapter contains previous studies in the field of aerodynamics of bridges using CFRP cables, and aims to briefly retail the state of the art in the field and give a basis for comparison of the results from the analysis.

5.1 Bridge aerodynamics

Bridge aerodynamics is the engineering field concerning the dynamic response of bridge structures under the action of wind loads. It regards aeroelastically safe and adequate design of bridge structures under the combined effect of static time-averaged mean wind loads, fluctuating wind loads induced by turbulence (buffeting) and motion-induced wind loads. The fluctuating forces on a bridge deck in motion (motion-induced wind loads) are especially essential for cable supported bridges due to their large flexibility and strong wind-velocity dependence of the natural frequencies (Dyrbye & Hansen, 1997). Generally, the most critical design aspect of cable supported bridges regards the instability phenomenon of flutter (coupled flutter), in which a strong torsional motion is generated through coupling of the lower eigenfrequencies for torsion and bending. The critical wind speed related to flutter is defined as the point where the input from the motion-induced wind load equals the amount of energy dissipated through structural damping (Dyrbye & Hansen, 1997). Flutter is consequently an instability phenomenon where large deck movements primarily are induced by motion-induced wind forces. Especially large movements can be expected in cases where the antinodes of the different modes coincide in the longitudinal direction of the bridge.

In addition to the fierce instability phenomenon of flutter, several other instability phenomena such as buffeting, vortex shedding and galloping have been found to induce oscillations in the bridge deck, pylons, and cables of cable supported bridges.

Although these problems generally are of less catastrophic nature, they are important in the aeroelastic design as well, as they may impede the serviceability of the bridge and often occurs for relatively low wind velocities. Furthermore, the cumulative damage of these oscillations may also significantly reduce the fatigue life of certain vulnerable components of the bridge, and thus increase the cost for maintenance (Gimsing & Georgakis, 2012). However, since the coupled flutter is the governing instability phenomenon for super long span bridges, it is the only one that is further treated in this thesis (besides the related phenomenon of static divergence).

5.1.1 Bridge deck

The aerodynamic response of cable supported bridges is primarily attributed to aerodynamic response of the bridge girder. For this reason the response of the bridge girder has been the primary subject for research within the discipline of bridge aerodynamics. Extensive research and advancements in the field of computational methods, such as finite element modelling (FEM) and computational fluid dynamics (CFD), has led to a deepened understanding of several instability phenomena that long puzzled the engineers. Late developments in the field of computational tools have, for example, helped researchers to establish the full mechanisms responsible for the failure of the Tacoma Narrows Bridge, somewhat 60 years after the collapse (Larsen, Larose, & Livesey, 1999). Furthermore, progressions in the field of aerodynamics have also led to the contemporary design of the shallow twin-box girders, used in the design of several recently constructed long span cable supported bridges, to ensure high critical wind speeds.

Although the general availability of FEM analyses have helped facilitate the assessment of natural frequencies and associated mode shapes, full-scale aerodynamic analyses are still rather cumbersome and costly, as it generally warrants elaborate wind tunnel testing of alternative cross-section designs in combination with 3D non-linear aeroelastic analyses. It is therefore advantageous to get insight into the governing parameters, by idealizing the bridge girder as a flat plate and the structural system by a simple Rayleigh-Ritz cable/beam model, making it possible to assess the natural frequencies and aerodynamic derivatives (describing the self-excited aeroelastic forces). With these idealizations, the airflow around the girder is considered 2-dimensional, and the natural frequencies can be readily evaluated based on the tension and stiffness of the cables together with the cross-sectional constants of the girder.

In the following, the flat plate analogy is used for evaluating the critical wind speed with respect to coupled flutter, based on the static divergence velocity. A similar approach is later also used in the comparative aerodynamic study of the proposed suspension bridge over Sognefjorden. In order to get a better understanding of the important instability mechanisms of static divergence and coupled flutter, both phenomena are treated separately in the following sub-chapters.

Static divergence

Before discussing the mechanisms of flutter it is helpful to start by looking at another instability phenomenon, called static divergence. Static divergence refers to the point at which the torsional resistance of the bridge deck, or the "flat plate", is exceeded by the torsional moment, induced by aerostatic pressure. The aerostatic pressure can be decomposed into a lifting force, L, and a torsional moment, M. For a flat plate of

width b, infinitesimal thickness and infinite length, these driving forces can, under the assumption of small rotational angles, be expressed as (Dyrbye & Hansen, 1997)

$$L = -\frac{1}{2}\rho b U^2 \theta \frac{dC_L}{d\theta} \qquad \frac{dC_L}{d\theta} = 2\pi \ \ (flat\ plate) \qquad (5.1)$$

$$M = \frac{1}{2}\pi\rho b^2 U^2 \theta \frac{dC_M}{d\theta} \qquad \frac{dC_M}{d\theta} = \frac{\pi}{2} \ \ (flat\ plate) \qquad (5.2)$$

where U is the wind velocity, ρ the density of air, and $dC_L/d\theta$ and $dC_M/d\theta$ are the slope of lift and moment, respectively. Figure 23 shows the aerostatic resultant acting on the quarter point of the deflected thin plate.

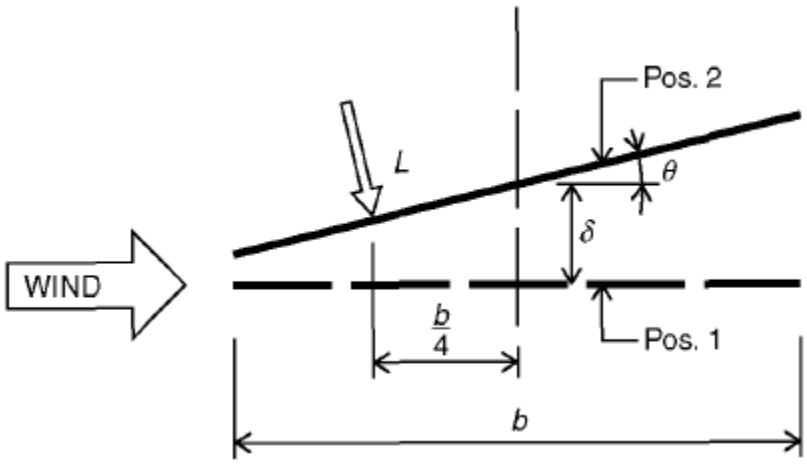

Figure 23. The aerostatic resultant acting on the quarter point of the deflected thin plate (Gimsing & Georgakis, 2012).

If assuming a constant mean wind velocity, U, and constant slope of moment, $dC_M/d\theta$, along the bridge deck it is apparent that the moment increases with increasing angle, or conversely, an increased moment will increase the angle of incidence. As the structural modal torsional stiffness, k_θ, also decreases with increasing angle of incidence, it can be shown that for a certain wind velocity, U_{div}, the modal torsional stiffness, k_θ, equals the change increase in moment as a function of the angle, $\frac{dM}{d\theta}$. Thus, the divergence wind velocity can be expressed as

$$U_{div} = \sqrt{\frac{2k_\theta}{\frac{dC_M}{d\theta}\rho b^2}} \qquad (5.3)$$

where U_{div} is the divergence wind velocity and k_θ is the structural modal torsional stiffness in still air. A considerable safety margin against static divergence must be ensured, as it corresponds to the excessive twist and collapse of the bridge deck for any angle $\theta \neq 0$ (Dyrbye & Hansen, 1997). The structural modal stiffness is defined as

$$k_\theta = (2\pi f_\theta)^2 I \qquad (5.4)$$

Since the structural modal torsional stiffness depends both on the natural torsional frequency, f_θ, and the mass moment of inertia (including cables), I, it becomes apparent that the cable weight also affects the static divergence velocity. However, although a decreased cable weight will lead to a decreased mass moment of inertia, it is not as straightforward to deem the cables effect on the divergence velocity since

they also affect the torsional natural frequency of the bridge, as will be seen later in the chapter.

Coupled flutter

Cable supported bridges are generally susceptible to flutter induced oscillations, as these flexible structures exhibits high propensity of coupling between the torsional and bending modes (Dyrbye & Hansen, 1997). The critical wind speed related to the instability phenomenon of flutter, U_{cr}, is therefore generally of higher interest than the static divergence velocity, U_{div}, as it occurs for lower wind speeds (Gimsing & Georgakis, 2012). Although flutter is a dynamic instability phenomenon, expressions for the flutter velocity, based on the expression for static divergence, has shown to agree fairly well with empirical results. Gimsing & Georgakis (2012) presented an expression for the flutter velocity of a thin flat plate according to

$$U_{cr} = U_{div}\sqrt{1 - (\frac{f_v}{f_\theta})^2} \qquad (5.5)$$

where f_v and f_θ are the natural frequencies with respect to bending and torsion, respectively. From the equation above, it can be seen that the propensity for flutter instability of a cable supported bridge is largely dependent on the ratio between the vertical natural frequency and the torsional natural frequency. If the torsional natural frequency in still air is only slightly higher than the vertical natural frequency in still air, the propensity for flutter instability is significant. For this reason it is desirable to ensure a large frequency separation between the natural frequencies for torsion and bending. Thus, in long span cable supported bridges, it is generally preferable to have a natural torsional frequency twice that for vertical bending (Gimsing & Georgakis, 2012).

Although the expression is not valid for all ratios of $\frac{f_v}{f_\theta}$, as will be seen later, semi-empirical expressions based on the flat plate approximation, adjusted for test results such as the Selberg's formula, have proved to give adequate results for a wide range of frequency ratios. Gimsing & Georgakis (2012) presented the following expression for the critical wind speed, derived by Selberg

$$U_{cr} = 0.52U_{div}\sqrt{\left(1 - \left(\frac{f_v}{f_\theta}\right)^2\right) b\sqrt{\frac{m}{I}}} \qquad (5.6)$$

where m is the mass per unit length of the bridge, b the width, and I the torsional mass moment of inertia. Despite the fact that the bridge decks in cable supported bridges have a much more elaborate geometry than that of the flat plate, contemporary girders of shallow streamlined design are characterized by having critical wind speeds close to that determined using the flat plate analogy (Gimsing & Georgakis, 2012). In a comparative study, the modified Selberg formula was shown to give adequate results of the critical wind speed for frequency ratios f_θ/f_v exceeding 1.5 (Gimsing & Georgakis, 2012). In the comparative aeroelastic study of the suspension bridge over Sognefjorden, where two alternative cables systems (CFRP and HS steel) in combination with a twin-box girder concept are compared, a modified version of the Selberg formula is used.

In Figure 24, four different girder sections are shown, subjected to wind tunnel testing during the design of the Little Belt Bridge in Denmark. The critical flutter velocity, normalized by the theoretical flutter velocity of a flat plate, is presented in conjunction with the corresponding girder. Results from the wind tunnel tests showed that the aerodynamic performance of the streamlined box girder (c) was superior to the others with a critical wind speed corresponding to 91 % of the theoretical flutter velocity, whereas the non-streamlined box girder with no cantilevers (a) only reached 43 % of the theoretical flutter velocity. Noteworthy is also the relatively large influence from the cantilevered deck on the critical wind velocity of cross-section b, showing that small changes in the aerodynamic design may have a considerable effect on the aerodynamic response.

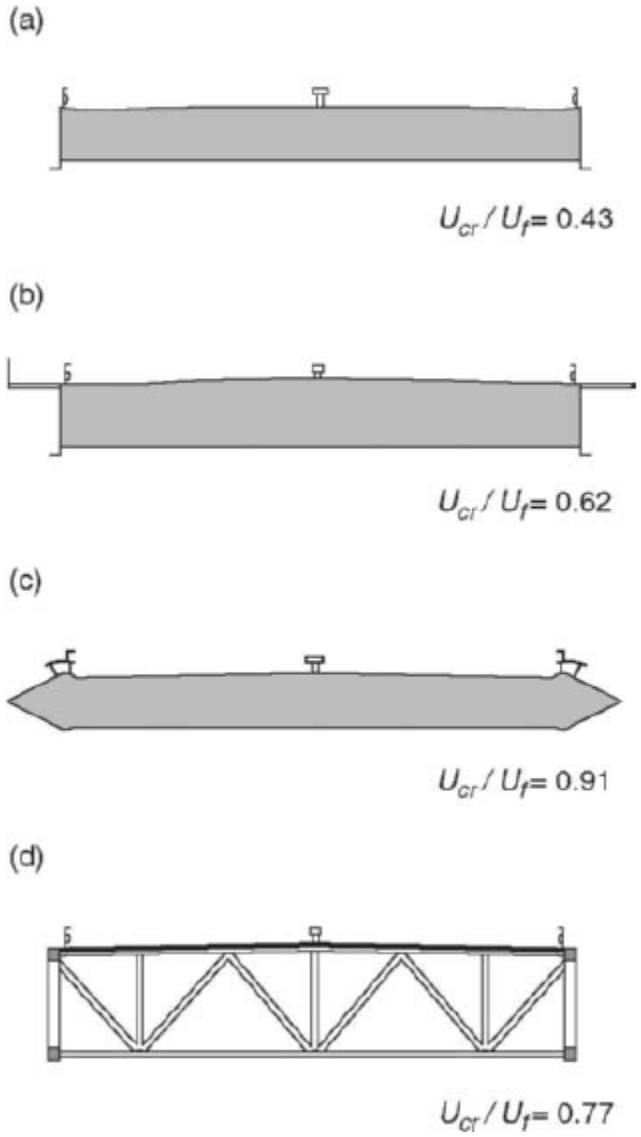

Figure 24. Relation between the critical flutter velocity of the corresponding girder and the theoretical flutter velocity of a flat plate. The results are based on wind tunnel tests (Gimsing & Georgakis, 2012).

Although the expression for the critical wind speed presented by Selberg gives adequate values for a wide range of frequency ratios, it should be emphasized that the formula represents a highly idealized situation where the flow pattern is considered 2-dimensional, and both the structural damping and velocity dependence of the natural frequencies are neglected. In fact, the natural frequencies of cable supported bridges

are not stationary, but depend on the exerted wind velocity. The in-wind frequency separation is therefore not equal to the frequency separation exhibited in still air. Instead, the frequency separation tends to decrease with increasing wind speed, as a result of increasing vertical stiffness and a reduction in torsional stiffness under the action of wind loads (Dyrbye & Hansen, 1997). Flutter consequently occurs at a wind speed where the motion-induced wind loads induce vertical and torsional frequencies of the same magnitude.

Before leaving the subject of flutter instability, some concluding remarks on the influence of the governing parameters with respect to critical wind velocities are given. Dyrbye & Hansen (1997) investigated the influence of the frequency ratio, γ_f, damping ratios in still air for bending, ζ_v, and torsion, ζ_θ, along with the ratios for mass moment, γ_m, and mass moment of inertia, γ_I, in a parametrical study of the reduced critical wind speed for a flat plate. The parameters were defined as

$$\gamma_\omega = f_\theta / f_v \qquad \gamma_m = m/(\rho b^2) \qquad \gamma_I = I/(\rho b^4) \qquad (5.7)$$

where the mass, m, is normalized by the density of air times the squared width of the plate, and the moment of inertia, I, is normalized by the density times the width of the plate raised to the power of four. The results from the parametric study are shown in Figure 25 where the reduced critical wind velocity, defined as $U_{red} = U_{cr}/(n_v b)$, is displayed as a function of the frequency ratio, γ_ω, for four different ratios of mass moment, γ_m, and mass moment of inertia, γ_I.

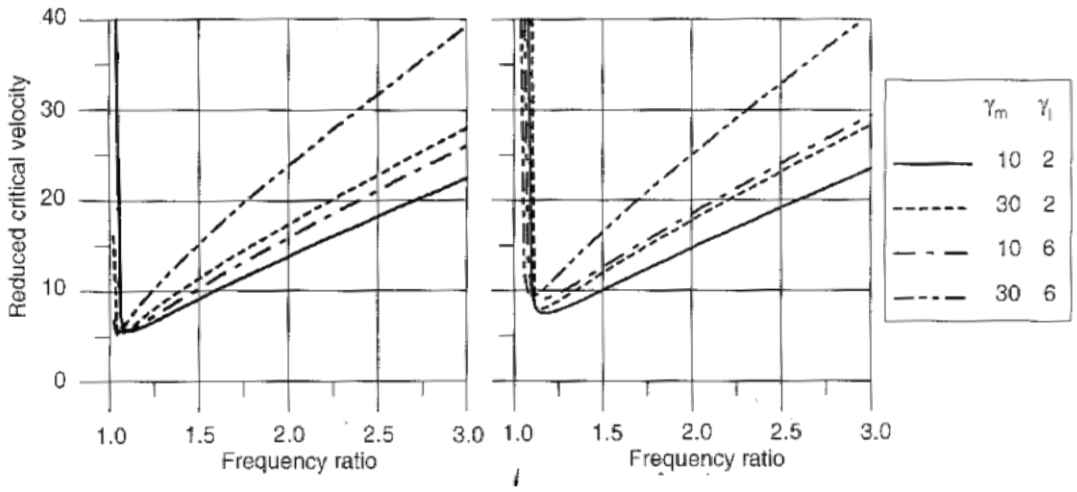

Figure 25. The left side corresponds to a structural damping ratio of 0 % in both torsion and bending, while the right side corresponds to a damping ratio of 1 % (Dyrbye & Hansen, 1997).

From the figure it can be seen that the critical flutter wind velocity increases with increasing mass and mass moment of inertia. It is also apparent that the flutter response is fairly insensitive to structural damping for higher frequency ratios. The most distinguishing characteristic, however, is the influence of frequency ratio, where an increased difference in frequency will lead to a significantly increased flutter velocity. It is, therefore, not straightforward to give a general statement of the influence of the cable weight on the critical flutter wind velocity based on these results, and a more detailed analysis has to be conducted to evaluate the aerodynamic performance of CFRP cables.

Natural frequencies

In order to evaluate the critical wind speed, the natural frequencies for both torsion and bending must be determined. As previously mentioned this may be done through FEM analyses, or by means of a simplified Rayleigh/Ritz cable/beam model, emulating the natural frequencies of the bridge. The latter method has shown to give adequate results (Larsen, Larose, & Livesey, 1999), and is used herein due to its simplicity. The basic assumptions of the Rayleigh/Ritz cable/beam model are; the mode shapes of the bridge are described by harmonic functions in the longitudinal direction of the bridge, horizontal symmetry of the cross-section, and constant cross-sectional properties along the span (Larsen, Larose, & Livesey, 1999). These assumptions are generally fairly well fulfilled in a symmetrical suspension bridge exposed to flutter.

The Rayleigh/Ritz cable/beam model of a suspension bridge is described using the basic parameters H, P_v, and P_θ, expressing the horizontal cable tension, the cable stiffness for the vertical modes, and the cable stiffness for the torsional modes, according to

$$H = \frac{mg{l_m}^2}{8d} \qquad P_v = \frac{32d^2EA_{mc}}{Hl_m l_c} \qquad P_\theta = \frac{P_v}{1+GK/Ha^2} \tag{5.8}$$

where l_m is the main span length, l_c is the length of the cable, d is the sag of the main span, A_{mc} is the main cable area, a is half the distance between the main cables, K is the cross-section torsion constant, E is the modulus of elasticity of the cable, and G is the shear modulus of the cross-section.

Except for the cross-section torsion constant K, all parameters above are readily obtained from geometry, evaluated from design loads, or found as material properties in literature. The geometrical torsional constant, expressing the angle of twist as a function of the applied torque, is a laborious constant to calculate for a complicated geometry such as the twin-box section and will not be explicitly calculated in the aerodynamic analysis in the next part of the chapter. The constant will instead be developed based on the results of a previous study, and this procedure is explained in more detail under Section 5.2.4.

In order to find the bending and torsional frequencies that correspond to the lowest symmetrical mode shapes, the transcendental function, shown below, must be solved for $q_{v/\theta}$

$$P_{v/\theta} = \frac{{q_{v/\theta}}^2}{1 + 2\lambda - \dfrac{\tan(q_{v/\theta}) + \tan(\lambda q_{v/\theta})}{q_{v/\theta}}} \tag{5.9}$$

where λ is the main-to-side span ratio. Once $q_{v/\theta}$ is determined, it is possible to evaluate the natural frequencies that corresponds to the symmetrical mode shapes of half a sine period along the main span (lowest symmetrical mode shapes), according to

$$f_{v1/2} = \frac{q_v}{2\pi}\sqrt{\frac{g}{2d}} \qquad f_{\theta 1/2} = \frac{q_\theta}{\pi l_m}\sqrt{\frac{GK+Ha^2}{I}} \tag{5.10}$$

The natural frequencies corresponding to the asymmetrical mode shapes with one period along the main span (lowest asymmetrical mode shapes), are described according to

$$f_{v1} = \frac{1}{l_m}\sqrt{\frac{H}{m}} \qquad f_{\theta 1} = \frac{1}{l_m}\sqrt{\frac{GK + Ha^2}{I}} \qquad (5.11)$$

Finding the critical wind speed includes finding the worst combination of eigenmodes. By adopting the described method of Selberg's formula in combination with the Rayleigh-Ritz cable beam model, it is assumed that the lowest symmetrical bending mode may couple with the lowest symmetrical torsional mode, or conversely, and that the lowest asymmetrical bending mode may couple with the lowest asymmetrical mode for torsion.

Future trends

The results of significantly increased critical wind speed with increased frequency difference, shown in the parametrical study, is the main reason for the development of the shallow streamlined box girders, where high torsional stiffness in relation to bending stiffness is achieved. The torsional stiffness of the shallow streamlined box girders may, however, prove insufficient in super long span bridge applications. For this reason the concept of split girder sections has been adopted in the design of several recently constructed cable supported bridges at the 1 000 meter scale, where the Stonecutters Bridge (1 018 meters) in Hong Kong is one example. The twin-box girder section has both theoretically, and experimentally, been proved superior to the conventional mono-box girder section (Larsen & Esdahl, 1998). Essentially, the improved aeroelastic stability of the twin-box girder can be explained as an effect of the increased aerodynamic damping, resulting from increased torsional angular velocity (Larsen, Larose, & Livesey, 1999).

However, applications of the twin-box girder concept also require increased material quantities, due to increased lateral moment with increased slot opening. Moreover, the increased deck width requires increased pylon width, which can prove very costly in deep-water foundations (Larsen, Larose, & Livesey, 1999). This has, as a result, intensified the research within the field of active flutter control, where active control forces are induced by active control surfaces attached to the outer sides of the bridge deck, see Figure 26. The idea is to enhance the aerodynamic damping by means of generating a lag between the aerodynamic moment and forced motion of the cross-section (Larsen, Larose, & Livesey, 1999). These systems have, however, not yet been implemented in actual applications due to their high cost and inherent complexity. Contemporary feasibility studies of super long span cable supported bridges therefore generally suggests the design of shallow box girders split into two or more longitudinal girders, to provide sufficient torsional rigidity. One such example is the potential future crossing over Sognefjorden, where a twin-box girder concept was suggested as a result of an aerodynamic feasibility study, see Figure 27. This particular girder section is also subject for the aerodynamic flutter analysis conducted in Section 5.2, where the critical wind speed of the girder section, in combination with both CFRP and HS steel cables, are evaluated.

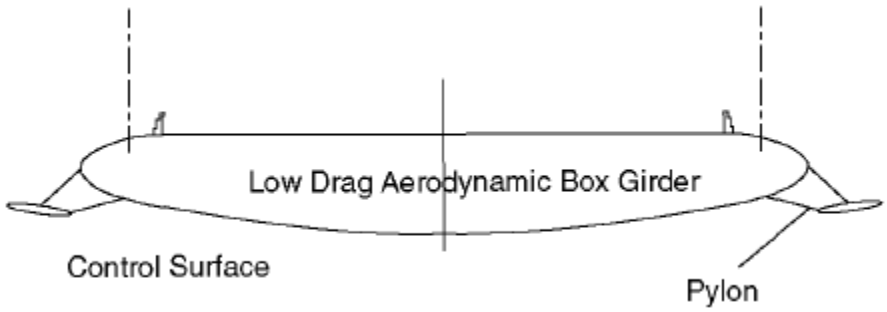

Figure 26. Active control surfaces attached to the outer sides of the bridge deck (Gimsing & Georgakis, 2012).

5.2 Aerodynamic analysis of bridge over Sognefjorden with CFRP cables

The objective for this part of the feasibility study is to investigate and assess the aerodynamic response of a 3 700 meter single span suspension bridge, using a twin-box girder concept in combination with both CFRP and HS steel cables. The aerodynamic analysis is limited to the response of coupled flutter, as this generally is the critical design parameter for spans exceeding lengths of ≈ 2000 meters, and its significance increases with even further growth in span length (Larsen & Esdahl, 1998).

5.2.1 Background

A single span suspension bridge with HS steel cables was suggested as part of a feasibility study for the Coastal Highway Route E39, where the possibility of making a ferry-free connection along the western corridor of Norway is investigated. With a width of 3 700 meters and a depth of 1 250 meters, Sognefjorden is considered one of the most challenging fjords to cross in the project. The bathymetry of the fjord limits the possibilities in design, as deep-water foundations on these extreme depths would be extremely costly and is not considered an option. The contemporary feasibility study, led by the Norwegian Public Roads administration, mainly contains three fundamentally different designs as their prime alternatives; a submerged floating tunnel, a floating bridge, and a super long single span suspension bridge. Irrespective of the adopted design methodology, the crossing of Sognefjorden requires implementation of new groundbreaking technologies, never before used in design.

The aeroelastic stability was considered a key issue in the feasibility study carried out for the single span suspension bridge (HS steel cable system considered only) over Sognefjorden. One especially essential step in the initial phase of the study was to find a feasible structural aerodynamic concept for super long span suspension bridges with low volumes of traffic (Isaksen et al., 2013). To this end it was concluded that the most efficient design was achieved through the use of a twin-box girder section, and the suggested cross-section is presented in Figure 27. Each box has one-way traffic in the design, consisting of one traffic lane and one walkway for pedestrians/bicycles. The elevation of the bridge is also presented below, see Figure 28, and the corresponding dimensions are shown in Table 5, based on the feasibility study from The Norwegian Roads administration, conducted by Berntsen & Lotherington (2013).

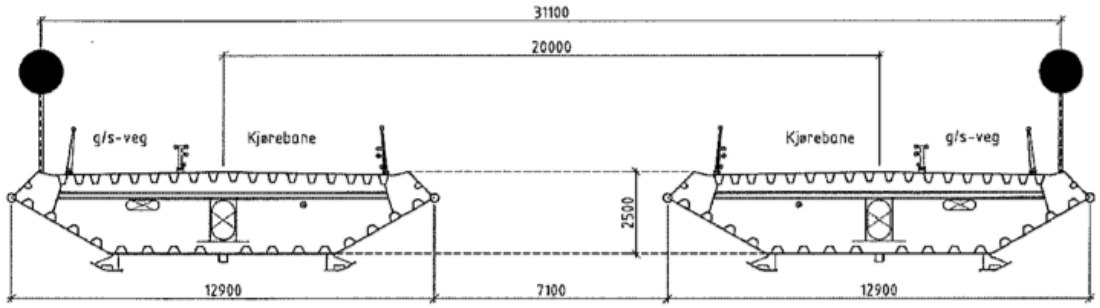

Figure 27. Cross-section of the bridge deck used in the calculations of Sognefjorden (Berntsen & Lotherington, 2013).

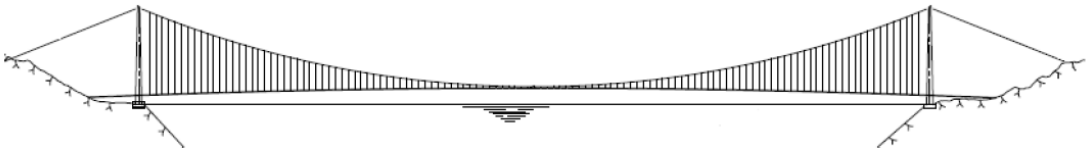

Figure 28. Elevation of the investigated future suspension bridge over Sognefjorden. The corresponding dimensions are listed in Table 5 below (Isaksen et al., 2013).

Table 5. General geometrical input data for the Sognefjorden Bridge.

Main span ($\boldsymbol{l_m}$)	3 700 m
Side span ($\boldsymbol{l_s}$)	0 m
Cable dip/sag ($\boldsymbol{d}$)	370 m

It should be emphasized that the results gained from the aerodynamic analysis by Berntsen & Lotherington (2013), which will be used as a reference in the current study, were based on aerodynamic derivatives extrapolated from wind tunnel testing on a similar cross-section. Furthermore, it is concluded that their final results of the critical wind speed with respect to flutter may be inaccurate, as the results show that the static divergence occurs for a lower wind speed than flutter.

Nevertheless, for the purpose of investigating the influence on the aerodynamic response of using CFRP cables instead of HS steel cables in super long span suspension bridges, the cross-section is deemed adequate, as the exact magnitude of the critical wind speeds are of less importance.

5.2.2 Method

The model outlined in this section is a semi-empirical model for evaluating the critical flutter velocity of a twin-box girder as a function of the slot-to-solid width ratio of the girder. The method was developed by Larsen & Esdahl (1998) as part of a feasibility study carried out for a proposed suspension bridge over the strait of Gibraltar. The objective with the new method was to develop a less elaborate way of evaluating the response of flutter for different twin-box girder concepts. Wind tunnel tests were therefore conducted on two different twin-box girder concepts with variable slot

widths, in order to find a relation between geometry and critical wind speed. The two girder sections, tested in the wind tunnel, are shown in Figure 29.

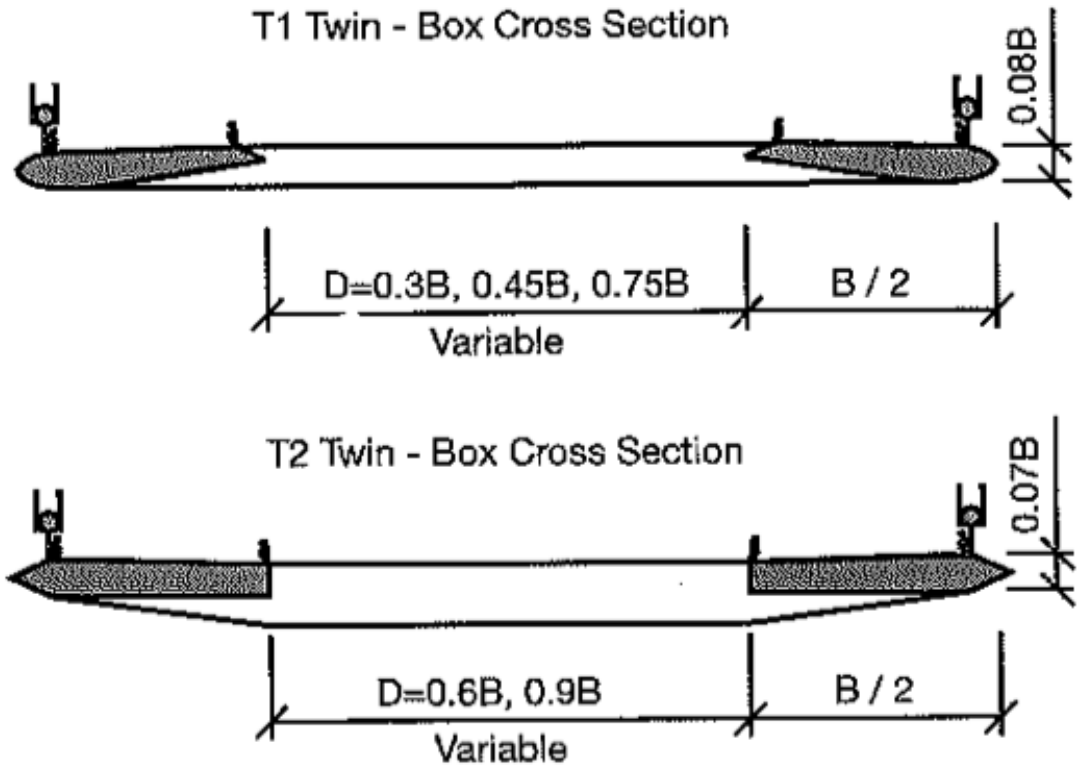

Figure 29. The two girder sections that was tested in the wind tunnel. The second girder section, T2, was selected for further tests (Larsen & Esdahl, 1998).

The second girder section, T2 in Figure 29, proved to be aeroelastically superior, and was selected for more elaborate wind tunnel testing. The most general and important outcome from these tests were the results shown in Figure 30, that links the deck slot opening width to the critical wind speed. In the figure, the results of the critical wind speed for seven different girder configurations are shown together with empirically relations, fitted from the results. The different girder configurations consisted of various slot-to-solid width ratios, in combination with either no wind-screens or 50% porous wind-screens.

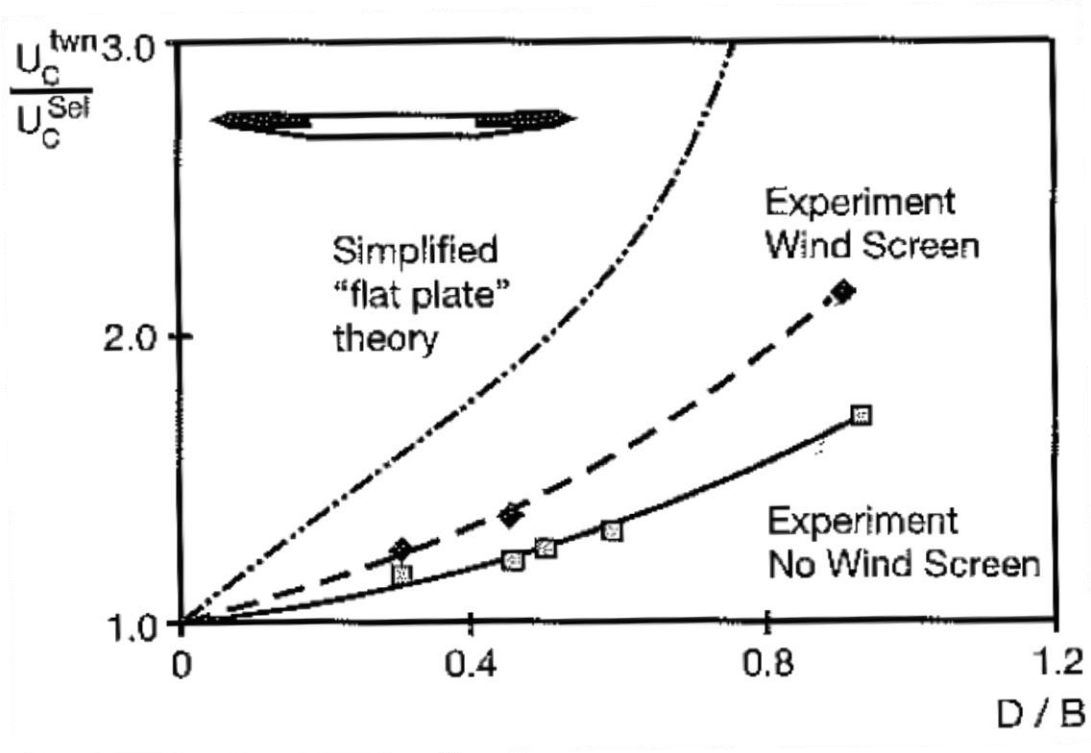

Figure 30. Results from aerodynamic analysis and experiments, demonstrating the relation between the critical wind speed and the slot-to-solid width ratio (Larsen & Esdahl, 1998).

The theoretical value of the critical wind speed as a function of the slot-to-solid width, using the approximation of a flat plate, is also included in Figure 30 for comparison. Although the theoretical relation predicts the trend of increasing critical wind speeds with increasing slot opening, it clearly overestimate its effect. One plausible explanation for the overestimated values of the flat plate, is that the lift on both the up-wind and down-wind side are interrelated, and thus imposing a coupling effect which is not accounted for (Larsen & Esdahl, 1998). Nevertheless, the test results show that increasing slot-to-solid width ratio has a significant positive effect on the critical wind speed with respect to flutter, even though it is smaller than predicted by the flat plate assumption.

The wind tunnel tests were materialized in two empirically fitted expressions for estimating the critical wind velocities of twin-box girders, according to

$$\frac{{U_c}^{twn}}{{U_c}^{Sel}} = C_{D/B} = 1 + 0.7332\left(\frac{D}{B}\right)^{1.4211} \quad \text{(without wind-screens)} \quad (5.12)$$

$$\frac{{U_c}^{twn}}{{U_c}^{Sel}} = C_{D/B} = 1 + 1.2438\left(\frac{D}{B}\right)^{1.4211} \quad \text{(with wind-screens of 50\% open area)} \quad (5.13)$$

where D/B is the slot-to-solid width ratio and the ${U_c}^{twn}/{U_c}^{Sel}$ is the critical wind speed of the twin-box section normalized by the critical wind speed of a flat plate obtained from Selberg's formula. Hence, the critical wind speed of the twin-box section, ${U_c}^{twn}$, can now be found from the modified Selberg formula, according to

$${U_c}^{twn} = K_{twn} * C_{D/B} * f_\theta \sqrt{\frac{\sqrt{m_{c-s}I}}{\rho B}\left(1 - \left(\frac{f_v}{f_\theta}\right)^2\right)} \quad (5.14)$$

where K_{twn} is a cross-sectional constant depending on the geometry of the cross-section, ρ is the density of air, m_{c-s} and I are the cross-sectional mass and mass moment of inertia, respectively, and $f_{\theta/v}$ are the frequencies with respect to torsion and bending.

The above-presented method will be used in the following calculations of the critical wind speed of the bridge. However, since the dimensions and design of the bridge are required prior to the determination of the critical wind speed, a preliminary sizing is conducted as a first step of the calculations.

5.2.3 Calculations

The calculations in this section are conducted for two different cable systems, one with CFRP cables and one with HS steel cables. In order to make an explicit comparison of the materials in the cables, all parameters of the bridge are kept the same in both calculations, except for the cable material. The calculations are divided into two main steps; preliminary sizing and aerodynamic analysis.

The mechanical properties of the CFRP and the HS steel used in the calculations are listed in Table 6 below.

Table 6. Mechanical properties of the CFRP and HS steel used in the calculations.

Mechanical property	**CFRP**	**HS steel**
Density (ρ)	1 600 $\frac{kg}{m^3}$	7 850 $\frac{kg}{m^3}$
Tensile strength $(\sigma_{ultimate})$	3 300 MPa	1 770 MPa
Modulus of elasticity (E)	165 GPa	210 GPa
Shear modulus (G)	Not used	80 GPa

The calculations are all performed as functions of safety factors, mainly due to the difficulties of setting a proper safety factor for CFRP. The safety factor of CFRP varies between $1-7$ in the calculations, while the safety factor of steel varies between $1-3.75*0.95$. The variation of steel will not take higher values since the area of the main cables approaches infinity for values ≥ 3.75 for the actual bridge (see the MATLAB-code in Appendix D for the calculation of this value). However, a more narrow variation of the safety factors might be sufficient, especially for steel. The high variation of the safety factor is rather a way of getting a better understanding of the influence of the two different materials, and to be able to control the calculated span limit of HS steel cables from Chapter 4.

Most of the results will be presented in table form, and particular interesting safety factors are therefore selected. For steel, the calculation for the safety factor 1.8 is presented. This value corresponds to the one used by Berntsen & Lotherington (2013) in their study, and is plausible for steel. Since the estimation of safety factors for CFRP is more uncertain, results from three different safety factors are presented,

where one value is related to the equivalent stiffness, one to strength, and one is chosen between these two.

Relating the safety factor of CFRP to the equivalent stiffness is quite common, and has been proposed by Zhang & Ying (2006) for example. The safety factor for CFRP can be estimated based on the following expression

$$E_{steel}A_{steel\ 1.8} = E_{CFRP}A_{CFRP\ X} \qquad (5.15)$$

where E_{steel} and E_{CFRP} are the modulus of elasticity of steel and CFRP, respectively, $A_{steel\ 1.8}$ is the dimensioning area of the main cables when using steel with the safety factor 1.8, and $A_{CFRP\ X}$ is the dimensioning area of the main cables of CFRP with respect to a safety factor based on the equivalent stiffness. The area was solved as $A_{CFRP\ X} = 1.27\ m^2$, corresponding to a safety factor of 6.5, and the results for this value will be presented in the tables.

The value related to the strength is set to 2.2. This value is close to the adopted value for steel, but slightly higher due to the scarce applications of CFRP as a structural material. The third safety factor is set to a value between the one related to the strength and the one related to the equivalent stiffness. This value will be 4.4 since it fits well with the values from the MATLAB-file.

The results from the calculations are presented throughout this section and analysed in Section 5.2.4.

5.2.3.1 Preliminary sizing

Since the aerodynamic behaviour is the main focus of this section, the detailed steps of the preliminary sizing are not to be presented here. The detailed procedure of the preliminary sizing is, instead, to be found in Appendix A. However, the results of the area of the main cables, the weight of the main cables, the weight of the cross-section, and the total weight of the suspended structure are presented in this section as well.

The results from the calculations of the area are both presented as a function of the safety factors in Figure 31, and in table from for the selected safety factors in Table 7. The values for the distributed main cable load, q_{mc}, are calculated as the sum from both main cables, and are presented in Table 8. The cross-sectional mass, m_{c-s}, which is assumed to include the mass from the main cables and the bridge deck only, is presented in Table 9. The total applied load from the suspended structure (including traffic load and load factors, 1.2 for dead load and 1.3 for traffic load, values according to Berntsen & Lotherington (2013)), q_{tot}, is presented in Table 10.

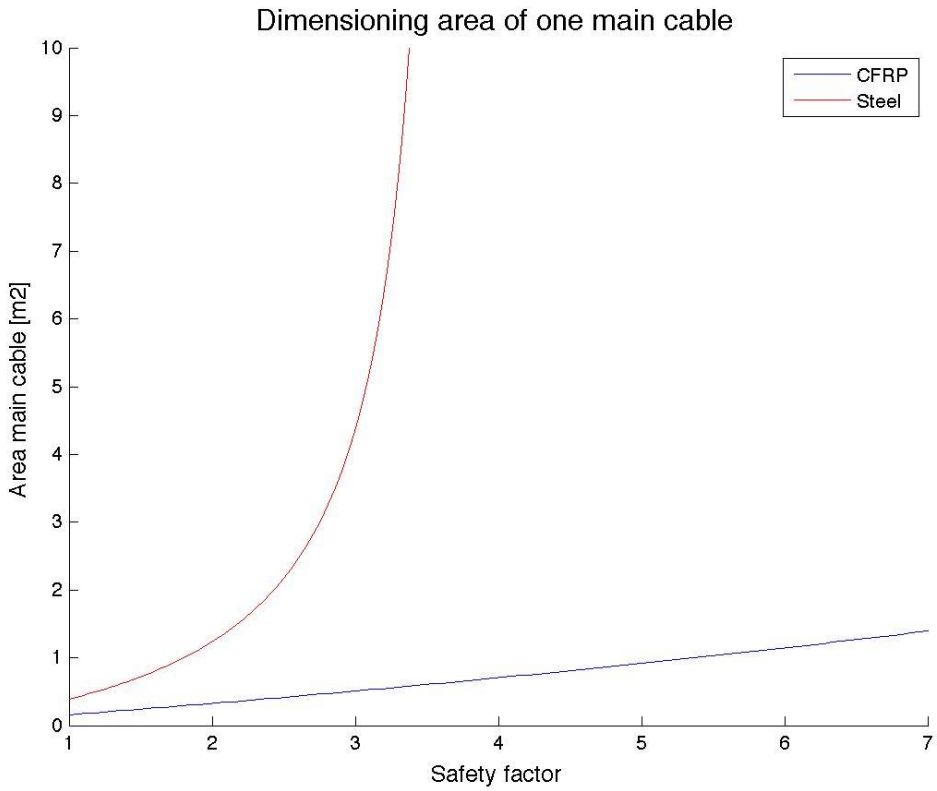

Figure 31. Dimensioning area of one main cable as a function of the safety factors. The blue line represents CFRP and the red line HS steel.

Table 7. Dimensioning area of one main cable.

Material	Safety factor	**Area one main cable** $[\boldsymbol{m^2}]$
CFRP	2.2	0.365
	4.4	0.786
	6.5	1.272
Steel	1.8	0.999

Table 8. Distributed load from both main cables.

Material	Safety factor	**Distributed load main cables** $[\boldsymbol{kN/m}]$
CFRP	2.2	13.2
	4.4	28.5
	6.5	46.1
Steel	1.8	158.0

Table 9. Cross-sectional mass.

Material	Safety factor	**Cross-sectional mass** $[\boldsymbol{kg/m}]$
CFRP	2.2	15 800
	4.4	17 400
	6.5	19 200
Steel	1.8	30 600

Table 10. Total load from suspended structure and traffic load, load factors included.

Material	Safety factor	**Total load suspended structure** $[\boldsymbol{kN/m}]$
CFRP	2.2	218.4
	4.4	237.1
	6.5	258.6
Steel	1.8	394.2

From the plot of the dimensioning area of the main cables, it can be seen that the area is increasing rapidly for a safety factor >3 for steel. At the point of 3.75, the area will approach infinity due to the high density in relation to the allowable stress. The variation of the main cable area of CFRP is almost linear in the analysed interval, due to the high specific strength.

Concerning the loads of the main cables in Table 8, the weight of the steel cables is much higher than the CFRP cables. The load exerted by the steel cables is almost 12

times higher than the CFRP cables with safety factor 2.2. Even with a safety factor of 6.5 for CFRP, which results in a higher cable are than for steel, the steel cables are more than three times heavier. If looking at the total weight of the suspended structure in Table 10, with all parameters equal except for the cable system, the differences are still high. The steel bridge is almost twice as heavy as the CFRP bridge with safety factor 2.2, and 1.5 times heavier than the CFRP bridge with safety factor 6.5.

The results from this preliminary sizing will be input data for the aerodynamic analysis in the next section, and the whole calculation is, as mentioned, to be found in Appendix A.

5.2.3.2 Aerodynamic Analysis

The calculations in the following chapter are conducted according to the method described above. The calculations and the section are both divided into the following four parts; *Mass moment of inertia, Eigenvalues for fundamental bending and torsion modes, Natural frequencies* and *Critical wind speeds.*

Mass moment of inertia

The critical wind speed of the bridge is both directly dependent on the mass moment of inertia of the cross-section, see Equation 5.14, but also indirectly dependent through the natural frequencies of the symmetrical and asymmetrical torsion modes, see Equation 5.10 and 5.11. The mass moment of inertia of the cross-section has therefore been calculated, and the contributions from the bridge deck, hangers, and main cables are taken into account. Since the bridge deck is similar to the one used by Berntsen & Lotherington (2013), their value for the deck is directly taken as

$$I_{bd} = 1.60 * 10^6 \frac{kgm^2}{m}$$

The total mass moment of inertia of the cross-section is the sum of the mass moment of inertia of the deck, hangers and main cables. The mass moment of inertia of the main cables and the hangers are calculated according to

$$I_{mc} = a^2 * \frac{A_{mc}}{2} * \rho * \beta \tag{5.17}$$

$$I_h = \frac{a^2 * V_h * \rho}{2 * l_m} \tag{5.18}$$

where $a = \frac{31.1}{2}$ meters is the distance from the mass center of one main cable (or hanger) to the horizontal neutral axis. The mass moment of inertia of the cross-section then becomes

$$I_{tot} = I_{bd} + 2 * I_{mc} + 2 * I_h \tag{5.19}$$

and the values from the calculation are found in Table 11.

Table 11. Total mass moment of inertia.

Material	Safety factor	**Total mass moment of inertia** $[\boldsymbol{kgm^2/m}]$
CFRP	2.2	$1.93 * 10^6$
	4.4	$2.32 * 10^6$
	6.5	$2.76 * 10^6$
Steel	1.8	$5.55 * 10^6$

Eigenvalues for fundamental bending and torsion modes

The eigenvalues for the fundamental bending and torsion modes are input parameters in the calculation of the natural frequencies in the next part of the section. In order to find the eigenvalues, the three basic parameters of the cable/beam model, presented in Equation 5.8, has to be calculated. As mentioned above under Section 5.1.1, all input parameters in the expressions for the basic parameters are readily obtained from geometry, except for the cross-section torsion constant K. The value of K is here set equal to 2, and this estimation is further explained under Section 5.2.4. The values for the basic parameters are not presented here, but can be calculated from the MATLAB-code (Appendix D). After calculating the basic parameters, the eigenvalues, $q_{v,\theta}$, can be solved from Equation 5.9, which is restated below

$$P_{v,\theta} = \frac{{q_{v,\theta}}^2}{1 + 2\lambda - \frac{\tan(q_{v,\theta}) + 2\tan(\lambda q_{v,\theta})}{q_{v,\theta}}}$$

where

$$\lambda = \frac{l_s}{l_m} = 0$$

since the actual bridge consists of one main span only. The eigenvalues for fundamental bending modes, q_v, and torsion modes, q_θ, were solved numerically in MATLAB with both HS steel and CFRP cables as functions of the safety factors. The values for q_v and q_θ are not presented here, but can be calculated from the MATLAB-code (Appendix D).

Natural frequencies

The natural frequencies are calculated for symmetric and asymmetric bending and torsion. The natural frequencies for symmetric bending and torsion are calculated based on the eigenvalues for fundamental bending modes, q_v, and torsion modes, q_θ, according to Equations 5.10, and are presented for the selected safety factors in Table 12 and Table 13, respectively. The natural frequencies for asymmetric bending and torsion are calculated based on Equations 5.11, and are presented for the selected safety factors in Table 14 and Table 15, respectively.

Table 12. Natural frequency in symmetric bending.

Material	Safety factor	**Natural frequency symmetric bending** [$\boldsymbol{Hz}$]
CFRP	2.2	0.080
	4.4	0.081
	6.5	0.082
Steel	1.8	0.081

Table 13. Natural frequency in symmetric torsion.

Material	Safety factor	**Natural frequency symmetric torsion** [$\boldsymbol{Hz}$]
CFRP	2.2	0.125
	4.4	0.139
	6.5	0.136
Steel	1.8	0.109

Table 14. Natural frequency in asymmetric bending.

Material	Safety factor	**Natural frequency asymmetric bending** [$\boldsymbol{Hz}$]
CFRP	2.2	0.058
	4.4	0.058
	6.5	0.058
Steel	1.8	0.058

Table 15. Natural frequency in asymmetric torsion.

Material	Safety factor	**Natural frequency asymmetric torsion** $[\boldsymbol{Hz}]$
CFRP	2.2	0.112
	4.4	0.105
	6.5	0.099
Steel	1.8	0.081

Critical wind speeds

The estimation of the critical wind speed is based on the method developed by Larsen & Esdahl (1998), presented under Section 5.2.2. The critical wind speed is here calculated for the interactivity between the natural frequencies in bending and torsion, both for the symmetrical and the asymmetrical modes. The formula for the critical wind speed was presented in Equation 5.14, and is restated below

$$U_c = K_{twn} * C_{D/B} * f_\theta \sqrt{\frac{\sqrt{m_{c-s} I_{tot}}}{\rho_{air} B}\left(1 - \left(\frac{f_v}{f_\theta}\right)^2\right)}$$

with the parameters defined in the method. f_θ, f_v, m_{c-s}, and I_{tot} has already been calculated for the different materials and safety factors, $\rho_{air} = 1.25\, kg/m^3$, and $K_{twn} = 3.72$ (constant from twin-box girder). Since B is the width of the solid parts of the cross-section of the deck, it is the sum of the width of the two boxes, see Figure 27

$$B = 12.9 * 2 = 25.8\, m$$

For a twin-box section without wind-screens (assuming no wind-screens, giving a conservative value), the parameter $C_{D/B}$, presented in Equation 5.12, is calculated according to

$$C_{D/B} = 1 + 0.7332\left(\frac{D}{B}\right)^{1.4211} = 1.12$$

where the spacing between the boxes, D, is equal to 7.1 meters, see Figure 27. The critical wind speeds for the interaction of symmetrical modes are presented in Table 16, and the critical wind speeds for the interaction of asymmetrical modes in Table 17. The results from these two tables are mixed together in Table 18, which presents the most critical wind speeds (both symmetrical and asymmetrical) for the selected safety factors.

Table 16. Critical flutter wind speed (symmetric).

Material	Safety factor	**Critical wind speed (symmetric)** $[m/s]$
CFRP	2.2	29.3
	4.4	36.9
	6.5	38.3
Steel	1.8	33.8

Table 17. Critical flutter wind speed (asymmetric).

Material	Safety factor	**Critical wind speed (asymmetric)** $[m/s]$
CFRP	2.2	29.5
	4.4	28.9
	6.5	28.3
Steel	1.8	26.6

Table 18. Final critical flutter wind speed (most critical from symmetric and asymmetric).

Material	Safety factor	**Final critical wind speed** $[m/s]$
CFRP	2.2	29.3
	4.4	28.9
	6.5	28.3
Steel	1.8	26.6

5.2.4 Interpretation of results

Independent of the choice of cable material, the critical wind speeds for the actual bridge are far too low compared to the requirements (reasonably around 65 m/s for the Sognefjorden bridge). However, the most interesting result is still the comparison between CFRP and HS steel cables, and the CFRP cables seems to have a slightly better aerodynamic behaviour, see Table 18.

When interpreting the results of this analysis, it should first be mentioned that they deviate strongly from the reference calculation by Berntsen & Lotherington (2013). In their coupled flutter calculation for steel cables with safety factor 1.8, the critical wind speed was calculated to 125 m/s (Isaksen et al., 2013), which can be compared to 26.6 m/s in this analysis. The calculation from Berntsen & Lotherington (2013) has, however, some uncertainties. Berntsen & Lotherington (2013) states in their discussion that their aerodynamic derivatives, which are essential in the calculation of the coupled flutter, have a great uncertainty. Another indication of an error is that their critical wind speed of the static divergence is lower than the critical wind speed of coupled flutter, something they also comment.

The calculation conducted in this thesis also contains some error sources that might influence the final results. It should be emphasized that the adopted model of the critical wind speed is tailor-made for a cross-section similar to that of the Gibraltar Bridge, see Figure 29. The bridge deck used in this calculation is, however, quite similar to the one of the Gibraltar Bridge, see Figure 27, but there are some differences that might influence the magnitude of the critical wind speeds. Another uncertainty in the calculation conducted by the authors is the value of the cross-section torsion constant, K. The exact value of K has not been calculated, but the adopted value is instead based on the natural torsional frequencies calculated by Berntsen & Lotherington (2013). The procedure for the estimation of K is briefly described below.

The natural torsional frequencies calculated by the authors should be quite similar to the frequencies obtained by Berntsen & Lotherington (2013), due to the similarities in preliminary sizing and material properties between the two studies. The natural torsional frequencies from Berntsen & Lotherington (2013) are evaluated based on a FEM-model, and are therefore assumed to be accurate. In the calculation from the authors, the natural torsional frequencies are dependent of the cross-section torsion constant, and can consequently not be calculated without knowing its value. However, since the frequencies should be quite similar to the frequencies obtained by Berntsen & Lotherington (2013), a suitable value for K can be solved by comapring the frequencies between the two studies for different values of K. Using this method, the value of $K = 2\,m^4$ was found to give sufficiently small differences in frequencies between the studies, see Table 19. The order of magnitude of K also seems reasonable in comparison with other studies. Larsen[3] for example, proposed $K = 2.5\,m^4$ for a twin-box girder over the Strait of Messina (3 300 meters), which should be quite similar to the adopted value due to the twin-box design. After the compilation of the results, Larsen[3] suggested that a value of $K = 1.9\,m^4$ would be accurate for the analysed twin-box girder section. It should be emphasized that the lower the value of K, the more conservative are the calculations. However, the differences in the results

[3] Allan Larsen (Chief Specialist, Aero and Structural Dynamics, Cowi Lyngby), E-mail conversation with the authors, 15th of April and 27th of May 2014.

of the critical wind speed with $K = 1.9\,m^4$ instead of $K = 2\,m^4$ are less than 2 %, and the adopted value of K is assumed to be sufficiently accurate.

Table 19. Comparison of the natural torsional frequencies for steel between the two studies, K=2.

	Symmetric torsion $[Hz]$	**Asymmetric torsion** $[Hz]$
Berntsen & Lotherington (2013)	0.099	0.082
Calculation by the authors	0.109	0.081

Nevertheless, as already mentioned, the most interesting result in this analysis is not the exact magnitude of the critical wind speed but rather the differences between CFRP and steel cables. The alternative with CFRP cables proves to have an aerodynamic behaviour in the same range as steel, perhaps even somewhat better, see Table 18. To understand this, the formula for the critical flutter wind speed has to be studied in more detail

$$U_c = K_{twn} * C_{D/B} * f_\theta \sqrt{\frac{\sqrt{m_{c-s} I_{tot}}}{\rho_{air} B}\left(1 - \left(\frac{f_v}{f_\theta}\right)^2\right)}$$

Due to the higher specific strength of CFRP compared to steel, both mass and area of the cables are reduced. The mass, especially, has a great influence on the critical flutter wind speed. The reduced mass directly decreases the cross-sectional mass, m_{c-s}, and the mass moment of inertia, I_{tot}, which at first glance seems to decrease the critical wind speed. However, the influence of the mass and the mass moment of inertia on the critical wind speed is of a more complex nature, since they also influence the frequencies of the bridge. In the parametric study by Dyrbye & Hansen (1997), briefly presented in Section 5.1.1, the influence on the critical wind speed of frequency ratio, damping in still air for bending and torsion, mass moment, and mass moment of inertia were analysed. It was concluded that the frequency ratio, defined as $\gamma_\omega = f_\theta / f_v$, was the single most important parameter of the critical wind speed. It can be seen in the formulas of torsional frequency, see Equation 5.10 and 5.11, that a reduced mass moment of inertia increases the torsional frequency and thereby the frequency ratio. This will, in turn, lead to an increased critical wind speed.

The results in this analysis comport well with the conclusions from Dyrbye & Hansen (1997), which can be seen when comparing CFRP and HS steel in terms of critical wind speeds and asymmetric frequencies. The values for CFRP with safety factor 4.4 is here compared with the corresponding values for steel with safety factor 1.8, according to

$$f_{\theta 1_{CFRP\ 4.4}} / f_{\theta 1_{Steel}} = 0.111/0.084 = 1.32$$

$$f_{v1_{CFRP\ 4.4}} / f_{v1_{Steel}} = 0.058/0.058 = 1.00$$

$$U_{C_{CFRP\ 4.4}} / U_{C_{Steel}} = 31.1/28.7 = 1.08$$

where it can be seen that the torsional frequency is 32 % higher with CFRP, the bending frequency is equal, and the critical wind speed is 8 % higher for CFRP. Even though the direct consequence of reduced mass and mass moment of inertia in the cables is decreased critical wind speed, the important indirect increase in torsional frequency result in a higher critical flutter wind speed when using CFRP cables instead of steel cables.

Although the cables are the centre of this analysis, the bridge deck has to be mentioned as well due to its importance on the aerodynamic behaviour. In a twin-box girder, the spacing between the boxes is a very important parameter for the aerodynamic behaviour of the deck. A higher spacing generally results in a higher critical wind speed, and since the adopted deck in this analysis has a relatively low slot-to-solid width ratio, an increased spacing might increase the critical wind speed radically. However, since the torsional frequency decreases with a higher spacing (due to increased mass moment of inertia), it is not straightforward to find an optimal design of the bridge deck, and analyses beyond the scope of this thesis are necessary for this purpose.

5.2.5 Results from other aerodynamic investigations

In this section, results from two comparative studies of the aerodynamic response in cable supported bridges with steel and CFRP cables are reviewed. In the first presented study, Zhang & Ying (2006) investigated the aerodynamic response with respect to flutter in two existing long span cable supported bridges (one suspension and one cable-stayed bridge), using both HS steel and CFRP cables. Zhang & Ying (2006) found that the critical wind speed could be increased with the use CFRP cables when implemented in long span suspension bridges, while the aerodynamic stability was basically unaffected in cable-stayed bridges. In the second comparative study, conducted by Xiong et al. (2011), both the static and dynamic response of 1 400 meter long composite cable-stayed bridges with various CFRP componens was investigated and compared with the response of a homengous steel bridge with the same design. The results regardning the aerodynamic performance of the homogenous steel bridge and the composite structure with CFRP stay-cables in combination with a steel bridge deck are the only ones included in the following. A slight increase in critical wind speed was herein achieved when using CFRP instead of HS steel in the cables.

However, it should be emphasized that the research on aerodynamic stability of cable supported bridges with lightweight cable materials still are scarce, especially within the field of super long span bridges.

Suspension bridges

In the study conducted by Zhang & Ying (2006) the second largest suspension bridge in China, the Runyang Bridge, was chosen as reference for the comparative aerodynamic analysis of suspension bridges. The bridge has a main span of 1490 meters and two equally large side spans of 479 meters, see Figure 32. The rise-to-main span ratio is 1/10 (same ratio as for Sognefjorden) and the spacing between the main cables is 34.3 meters. In contrast to the proposed single span supension bridge over Sognefjorden, this bridge has a mono-streamlined box girder of 3.0 meters height and 35.9 meters width, see Figure 32. The cross-sectional constants and material properties of both the existing bridge (HS steel cables) and the "fictional" bridge (CFRP cables), are shown in Table 20. The cross-sectional area of both main cables and hangers of the fictional bridge were determined based on the assumption of equivalent axial stiffness, thus resulting in a bridge of equal stiffness, but with decreased mass and mass moment of inertia.

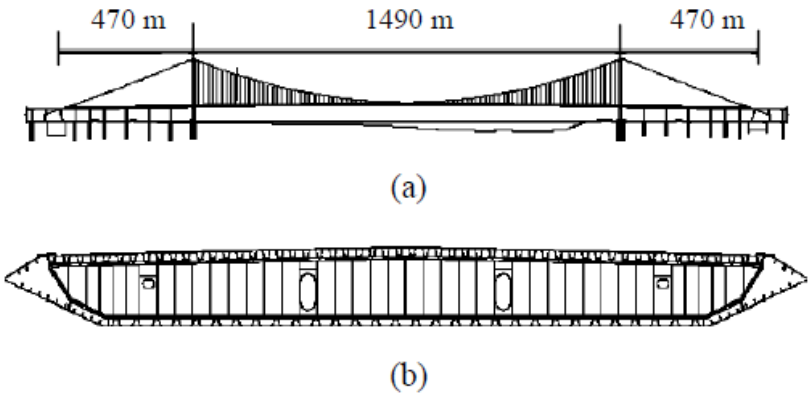

Figure 32. The Runyang Bridge, elevation of the bridge is presented in a), and the cross-section of the girder is presented in b) (Zhang & Ying, 2006).

The results from the analysis showed that the implementation of CFRP cables resulted in an increase in critical wind speed with approximaterly 15 %. As for the analysis for Sognefjorden, the increaesed critical wind speed with CFRP cables was primarily attributed to the significant increase in torsional frequency. In Table 20, the reduction in mass and mass moment of inertia is shown together with the increase in fundamental frequencies, both for the suspension bridge over Sognefjorden and the Runyang Bridge. The values chosen from the aerodynamic analysis of the suspension bridge over Sognefjorden corresponds to the higher safety factor of 6.5, as this roughly corresponds to the adopted design of equivalent stiffness.

Table 20. Comparison of steel and CFRP cables in terms of aerodynamic behavior. The results for the Runyang Bridge (based on the calculation of Zhang & Ying (2006)) are shown to the right and the results of Sognefjorden to the left (based on the calculations from the authors).

	Sognefjorden			**The Runyang Bridge**		
	Steel	**CFRP**	**Diff. [%]**	**Steel**	**CFRP**	**Diff. [%]**
Safety factor $[-]$	1.8	6.5		-	-	
Mass $[kg/m]$	30593	19188	-37.3	26020	20180	-22.4
Mass moment of inertia $[kgm^2/m]$	$5.55 \cdot 10^6$	$2.76 \cdot 10^6$	-50.3	$2.97 \cdot 10^6$	$2.12 \cdot 10^6$	-28.6
Natural frequency vertical bending $[Hz]$	0.0576 1-AS	0.0576 1-AS	0	0.1260 1-S	0.1305 1-S	3.6
Natural frequency lateral bending $[Hz]$	-	-	-	0.0498 1-S	0.0508 1-S	2.0
Natural frequency torsion $[Hz]$	0.0840 1-AS	0.1043 1-AS	24.2	0.2410 1-S	0.3123 1-S	29.6
Critical wind speed $[m/s]$	26.6	28.3	1.7	60.6	79.9	14.8

From Table 20, it can be seen that the trend of significantly increased torsional frequency, due to decreased mass and mass moment of inertia, is valid also when evaluating the frequencies using a 3-dimensional finite element model. In the aerodynamic analysis of the Runyang Bridge, it can also be seen that the impact of the cable material on both the vertical and the lateral bending frequency is quite small. From the results of the aerodynamic analysis for the Runyang suspension bridge, Zhang & Ying (2006) concluded that, viewed from the aspect of aerodynamic stability, the use of CFRP cables is feasible in long span suspension bridges.

Cable-stayed bridges

Zhang & Ying (2006) conducted a similar aerodynamic analysis for cable-stayed bridges as for suspension bridges. The analysed bridge was the three-span Jingsha Bridge in China, with a main span of 500 meters and side spans of 200 meter each, see Figure 33. The stiffening girder has a width of 27 meters and a height of 2.0

meters. In resemblance with the aerodynamic analysis of the suspension bridge, a "fictional" cable-stayed bridge was designed using a 3-dimensional finite element model, where beam elements were used to model the pylons and girder, and the stay cables were modeled using bar elements.

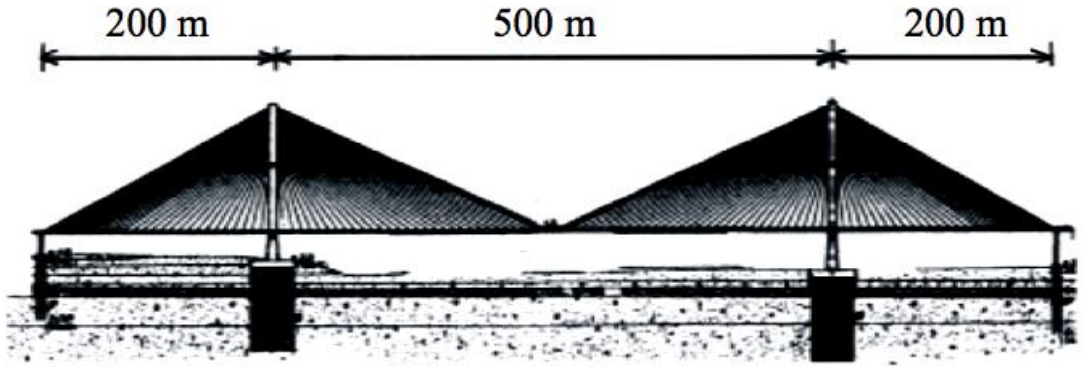

Figure 33. Elevation of the Jingsha Bridge in China (Zhang & Ying, 2006).

The results from the aerodynamic analysis showed that the critical wind speed with respect to flutter for the cable-stayed bridge was almost unaffected by the decrease in mass and mass moment of inertia. Although the decrease in structural mass led to a slight increase of the fundamental frequencies, the critical wind speed remained unaffected, as the effect was counteracted by the direct negative effects of decreased structural mass. In Table 21, the slight increase of the natural frequencies is shown together with the resulting critical wind speeds. Based on these results, Zhang & Ying (2006) concluded that the use of CFRP cables is feasible from an aerodynamic point of view also in cable-stayed bridges under current span lengths.

Table 21. Comparison of steel and CFRP cables in terms of aerodynamic behaviour for the Jingsha Bridge (based on the calculation by Zhang & Ying (2006)).

	Steel	**CFRP**	**Diff. [%]**
Natural frequency vertical bending $[Hz]$ 1-S	0.1841	0.1870	1.6
Natural frequency vertical bending $[Hz]$ 1-AS	0.2472	0.2510	1.5
Natural frequency lateral bending $[Hz]$ 1-S	0.3520	0.3576	1.6
Natural frequency torsion $[Hz]$ 1-S	0.3951	0.4065	2.9
Natural frequency torsion $[Hz]$ 1-AS	0.5202	0.5332	2.5
Critical wind speed $[m/s]$	87.4	87.0	-0.5

Another interesting study in the field, mentioned above, was conducted by Xiong et al. (2011). Xiong et al. (2011) designed a model for a super long span cable-stayed

bridge in their analysis, with main and side span of 1 400 meters and 636 meters, respectively. Within the side span three intermediate piers were placed to increase the vertical flexural stiffness, see Figure 34. A streamlined mono-box girder was used for the calculations, with a width of 32.5 meters and a depth of 4.5 meters. The natural frequencies and corresponding mode shapes were obtained from the 3-dimensional finite element model, and the critical wind speed with respect to flutter were calculated based on the simplified flat plate analogy, described under Section 5.1.1. In the flutter calculations, only the lowest symmetrical or assymmetrical frequencies with respect to vertical bending and torsion were assumed to couple in flutter. The obtained natural frequencies are shown together with the critical wind speeds in Table 22.

Somewhat surprisingly, the natural frequencies with respect to vertical bending is lowered with the use of CFRP. This can be explained by the decrease in axial stiffness of the CFRP stay cables, which consequently decreaseses the supporting stiffness of the girder (Xiong et al., 2011). Although a decreased equivalent stiffness might seem contradictory, it may be explained by the fact that a relatively low safety factor was adopted in design (γ=2.5) in combination with the low initial modulus (137 GPa) of the CFCC-brand type of stay cables. However, Xiong et al. (2011) concluded that this realtion could be the opposite if the span was extended beyond 1 400 meters, as the non-linear behaviour of steel becomes more pronounced with increasing span lengths.

Table 22. Comparison of steel and CFRP cables in terms of aerodynamic behaviour for the imaginary super long span cable-stayed bridge modeled by Xiong et al. (2011) (the table is based on the results from their study).

	Steel	**CFRP**	**Diff. [%]**
Natural frequency vertical bending $[Hz]$ 1-S	0.1986	0.1771	-10.8
Natural frequency vertical bending $[Hz]$ 1-AS	0.2312	0.2160	-6.6
Natural frequency torsion $[Hz]$ 1-S	0.4626	0.4727	2.2
Natural frequency torsion $[Hz]$ 1-AS	0.4635	0.4737	2.2
Critical wind speed $[m/s]$	96.7	100.1	3.5

Nevertheless, in analogy with previous results, the torsional frequncies were found to be increased due to the decrease in mass and mass mass moment of inertia. Hence, with an increase of the ratio between torsional and vertical frequencies, the aerodynamic performance was found to be slighly enhanced. The results from the aerodynamic instability analysis of the 1 400 meter cable-stayed bridge indicates that from an aerodynamic point of view, the use of CFRP cables are feasible also in super long span cable stayed-bridges.

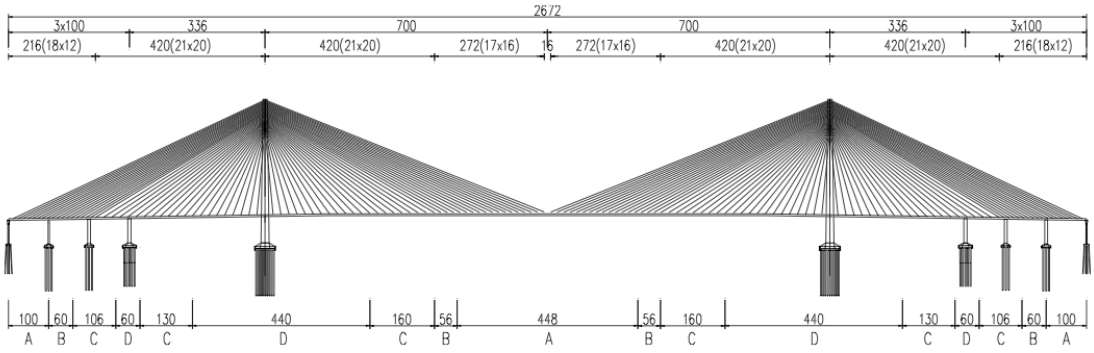

Figure 34. The model of a super long span cable-stayed bridge developed by Xiong et al. (2011).

6 Structural Problems related to Poor Shear Capacity and Transverse Weakness

The poor shear capacity and transverse weakness of CFRP was discussed already in Chapter 3. The inherent weakness with respect to transverse loading and shear of the isotropic composites poses great challenges in applications of CFRP cables in suspended structures. In the following chapter, two important structural problems related to these properties are treated; the anchorage of the cables and the fixation of the cables on top of the pylons (suspension bridges).

The problem related to the anchorage is known as an impediment for the widespread application of CFRP cables, and research has already been done on the subject. Due to lack of time and equipment, no further investigations or calculations are conducted for the anchorage problem within this thesis, but the state of the art is presented. The second problem, related to the fixation of the cables to the pylon top, rather represents a gap of research in the field. Problems may arise in the connection between cable and saddle where large radial stresses are induced, and a simplified calculation is therefore performed for the suspension bridge over Sognefjorden in the end of the chapter.

6.1 Anchorage of cables

Conventional mechanical anchorage systems are developed for use of conventional yieldable isotropic structural materials, and rely on friction induced by transverse compressive forces. The mechanical anchorage solutions are therefore not suitable for CFRP cables, and the anisotropic structure of CFRP calls for new anchorage techniques where the peak transverse stresses and peak shear stresses are reduced.

Although the experimental optimization of new anchoring systems for CFRP cables is restricted due to insufficient testing and measuring methods, a couple of new anchorage systems have still been developed (Noisternig, 2000). The new anchorage systems for CFRP cables and tendons are instead developed and optimized by the use of computerized FEM-analyses, which evaluate deformation and stresses for different design. In principle, there exist two different types of anchorage system for CFRP cables. The first type is the bonded anchorage where, normally, an outer sleeve surrounds a cohesive bonding material, e.g. epoxy resin, inside which the cable or tendon is anchored (Schmidt et al., 2012), see Figure 35. The second type is the mechanical anchorage mentioned above, where the mechanical bond is generated through an inner sleeve, clamped by a cone-shaped interface between a barrel and a wedge (Schmidt et al., 2012), see Figure 37. These two principal anchorage systems are treated in more detail in the following.

Bonded anchorage

The Swiss Federal Laboratories for Materials Science and Technology, EMPA, was first to develop an anchorage system for CFRP cables in suspension and cable-stayed bridges, using computer-aided material design. The bonded anchorage system utilizes an advanced gradient load transfer media (LTM), consisting of ceramics and polymers to anchor the CFRP cables inside a conical termination. The key issue was found to lie in the development of a LTM that could transfer the load from the wires without reducing the long-term static performance of the cables, and also prevent galvanic corrosion between the wires and the metallic cone (Meier, 2000). The conical shape of

the termination was adopted to increase the radial pressure on the wires, and thereby enhance the in-plane shear strength of the CFRP wires.

When evaluating different LTM it was concluded that an unfilled resin would also decrease the shear peak at loaded end of the termination. This solution was, however, abandoned due to increased risk of creep and early stress rupture. Instead, it was found that the most suitable way to reduce the shear peak was through the use of a gradient LTM, with decreasing elastic modulus towards the loaded end, see Figure 35. Figure 36 shows the stress distribution for a termination with homogenous LTM (left), and a termination with a gradient LTM (right). To manufacture a gradient load transfer media EMPA developed a manufacturing process, where aluminum oxide ceramic granules were coated with varying thickness of epoxy resin. By adopting this method EMPA could manufacture LTMs with tailor-made elastic modulus. A low elastic modulus was achieved by surrounding the granules of aluminum with a thick layer of epoxy resin coating and, conversely, a gradual increase of the elastic modulus was achieved using thinner coating, see Figure 35. To avoid shrinkage, the granules also had to be cured during manufacturing and, in the last step, vacuum-assisted resin transfer molding with epoxy resin were used to fill the holes between the granules (Meier, 2012).

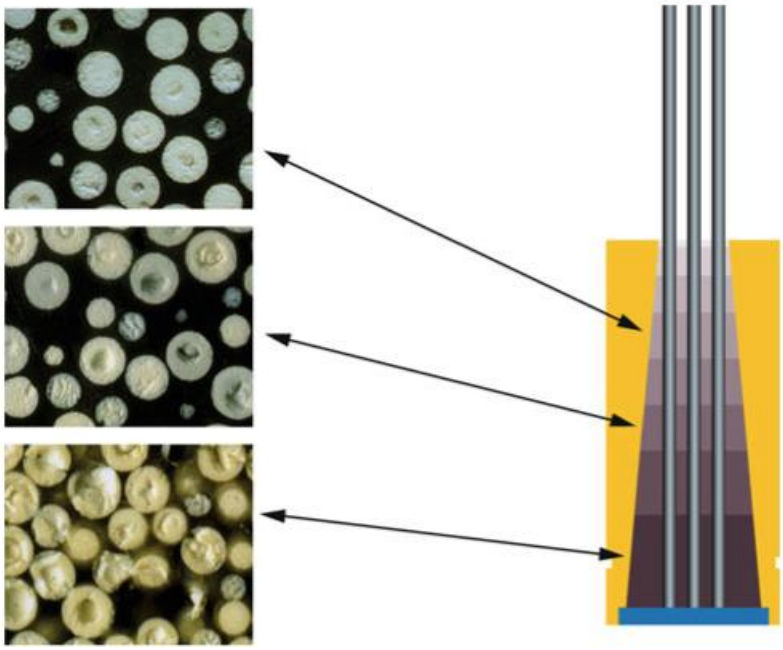

Figure 35. CFRP cables anchored to conical termination. The layers with different modulus of elasticity can be distinguished, and their composition is shown in more detail to the left. The solution is developed by EMPA (Meier, 2012).

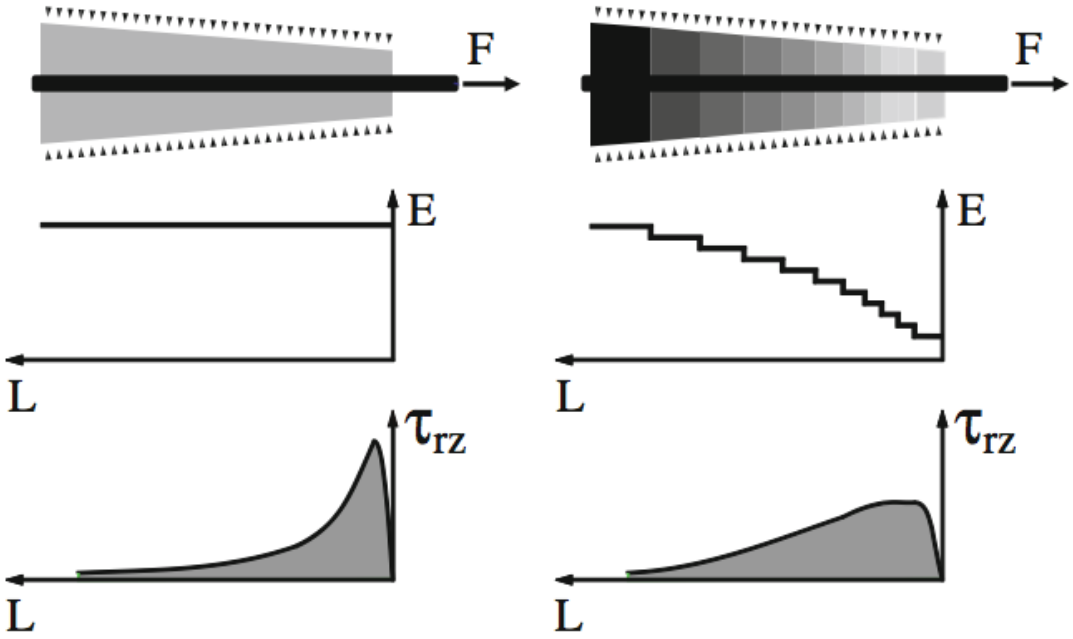

Figure 36. Elastic modulus and shear stress variations in two different cones, one with equal LTM over the whole length and one with gradient elastic modulus (Meier, 2012).

Tests carried out on the static and fatigue performance of the anchorage of a 19-wire bundle showed satisfactory results. The test results showed that the anchorage system was reliable for small wire bundles, and that static load capacity generally reached about 92 % of the ultimate strength (Meier, 2000). This was very close to the theoretically determined value of 94 %. Moreover, the results from the fatigue tests showed that the termination could withstand amplitudes of 450 MPa for over 2 million cycles (Meier, 2000). However, tests conducted on similar bonded anchorage systems for CFRP cables have showed that it becomes increasingly problematic to ensure a pore free filling of the potting material with increased number of wires (Noisternig, 2000).

Prior to the implementation of the new anchorage system, fatigue tests were conducted, showing that the cable could withstand more than 10 million load cycles when subjected to a load three times the allowable load of the bridge (Meier, 2000). This is equivalent to at least five times the number of cycles predicted during the entire life of the bridge (Meier, 2000). Furthermore, upon installation the cables were equipped with optical sensors that continuously measures stresses and deformations in the cables, and up to date, these measurements are satisfactory and match the predicted values (Meier, 2012).

Mechanical anchorage

An alternative to the epoxy resin bonded anchorage system is the mechanical anchorage system. As mentioned in the beginning of this chapter, conventional mechanical anchorage techniques are not applicable for anchoring of CFRP cables, due to large stress concentrations. The mechanical anchorage utilizes large compressive forces to grip the cable and this induces stress concentrations at the loaded end of the termination, just as for bonded anchorage. To relieve this problem, Sayed-Ahmed (2002) proposed a solution for the anchoring of tendons and stay cables using differential angle design at the interface between the barrel and the wedge, see Figure 37.

The anchorage system proposed by Sayed-Ahmed (2002) consists of a four-pieced wedge inside a conical barrel and an internal sleeve, see Figure 37. The surfaces at the interface between the barrel and the wedge are smooth and greased to facilitate movement, and the purpose of using an inner sleeve is merely to distribute the stresses around the wire more uniformly (Schmidt et al., 2012). Through numerical analysis, Sayed-Ahmed (2002) found that a differential angle between 0.05˚ and 0.15˚ was the most beneficial for reducing the radial stresses.

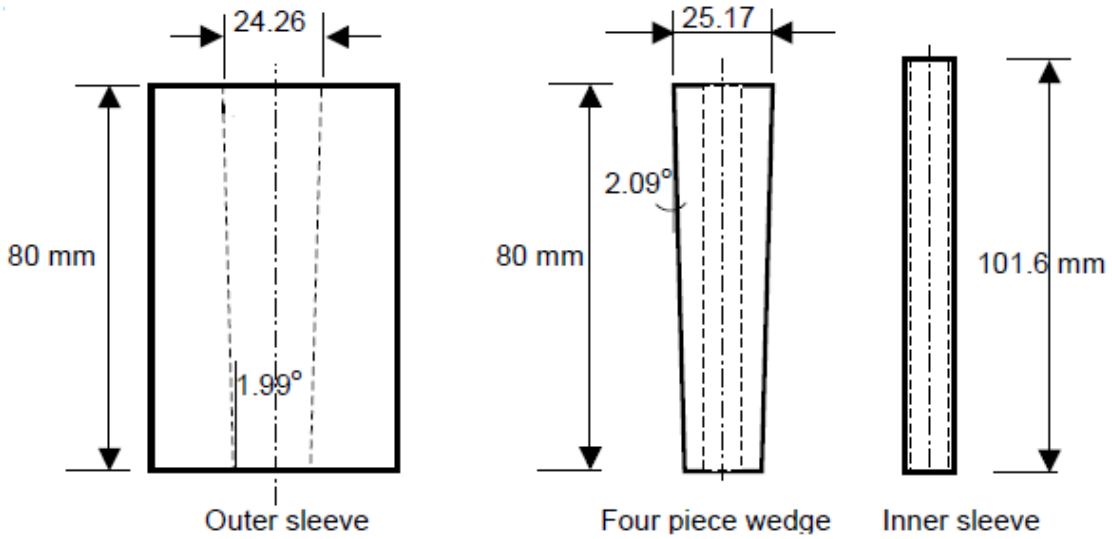

Figure 37. Schematic picture of the single strand anchorage system (Sayed-Ahmed, 2002).

Several tests were conducted on the final design, where a differential angle of 0.1˚ was adopted, all of which passed the requirements from the Post Tensioned Institute (PTI). However, it should be emphasized that the test were carried out on a single wire anchorage system, designed to anchor one CFRP wire with a diameter of 8 mm.

A mechanical anchorage of this sort is beneficial due to its simplicity, and requires no advanced technology for manufacturing or mounting. However, the long-term reliability of these systems is not yet fully verified, and test results from similar mechanical anchorage system (used for anchoring tendons) suggest that small differences in the mounting procedure may greatly affect the performance (Schmidt et al., 2012).

For the reasons mentioned above, mechanical anchorage systems are not yet ready for applications, and the only viable solution today for anchoring the tensile forces of large CFRP cables is the bonded anchorage solution developed by EMPA. However, due to its advanced gradient technology and, thus, relative high manufacturing cost, further research in the field of new anchorage systems for CFRP cables is of outermost importance. In addition, there exist uncertainties of how the system from EMPA will behave when the dimensions are increased, due to the lack of field applications in longer spans.

6.2 Fixation of cables on top of pylons

The magnitude of the contact stresses developed at the interface between the main cable and the saddle of a suspension bridge depends on the design of the saddle as well as the geometry and total weight of the suspended structure. This section focuses on evaluating the interfacial stresses between cable and saddle, and assesses the applicability of conventional saddle design methodologies in connection with CFRP cables. To this end, expressions for evaluating the contact forces between cable and saddle, based on a simplified analytical model by Zheng, Jiang, & Lu (2011), are utilized.

6.2.1 Cable-saddle interaction

The interfacial stresses between the main cable and the saddle is, as mentioned previously, dependent on the saddle design, geometrical configuration of the bridge and total dead load of the suspended structure. The two latter parameters determines the loading condition at the two end sections of the cable segment located within the saddle, whereas the design of the saddle determines the contact area and the bending radius of the cable. Thus, the loading condition at the ends of the segment are predestined, and determined by prevailing loading conditions and cost-efficient main-to-side span and rise-to-main span ratios. Therefore, in order to develop an apt design with respect to the mechanical characteristics of CFRP, it is essential to study the stress state of the cable-saddle interaction as a function of the two saddle design parameters, contact area and radius of curvature (Zheng, Jiang, & Lu, 2011).

Contact forces

Adopting the simplified analytical method, presented by Zheng, Jiang, & Lu (2011), it is assumed that the cable-saddle interaction is equivalent to superposition of three simple load cases as shown in Figure 38. The first load case corresponds to the condition of an unloaded cable segment exerted only by its self-weight. In the second case, the smaller of the two tensile forces, T_m and T_s, are applied to both ends of the segment. Since the horizontal component in the cable, H, is constant along the bridge, the relationship between T_m and T_s can be expressed as

$$T_s \cos(\varphi_s) = T_m \cos(\varphi_m) = H \qquad (6.1)$$

In the third load case, the difference in tensile force between the main span and side span, ΔT, is applied to the side where the largest cable force is acting. Figure 38 shows the three load cases in a polar coordinate system, expressed in the variables θ and r, and with the radius of curvature denoted as R_s, self-weight of the cable denoted q_c, and the angle of the cable ends towards the main and side span denoted φ_m and φ_s, respectively.

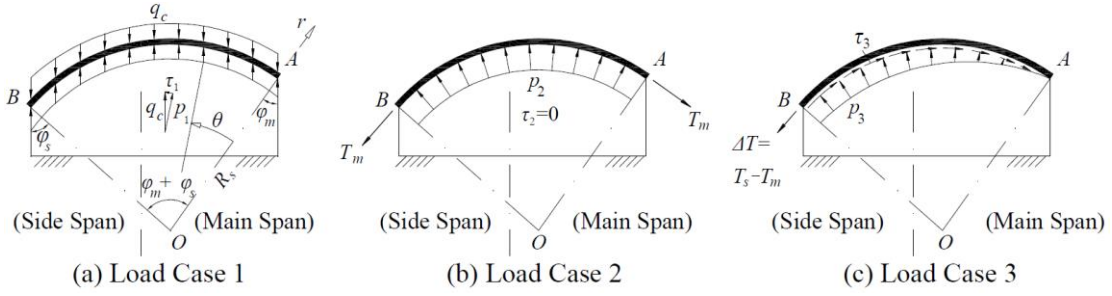

Figure 38. Three load cases with different cable forces (Zheng, Jiang, & Lu, 2011).

The interfacial contact resultants, corresponding to each load case, can be expressed in terms of a radial force component p_i and a tangential friction component τ_i, where $i = 1, 2\ or\ 3$. Both components are expressed in the units $[force/length]$. The contact forces are evaluated under the assumption that the design requirement of full cable fixation relative to the saddle (to prevent abrasion of the cable and stabilizing the cable shape) is fulfilled and thus, all parts of the system are in balance. Furthermore, it is assumed that the curvature of the saddle has the shape of a circular arc.

Based on the assumptions above, expressions for the two contact force components can be derived from equilibrium condition for an infinitesimal cable segment, in any part of the cable segment within the saddle. In the first two load cases it is straightforward to derive the force components from radial and tangential equilibrium. In the third case it is also assumed that the cable force ΔT decays linearly along the arc segment, and that the tangential friction follows the same distribution, see Figure 38c). The radial pressure components and tangential friction components, corresponding to load cases 1-3, are as follows (Zheng, Jiang, & Lu, 2011)

Equilibrium load case 1:

$radial\ equillibrium$: $p_1 = q_c \cos(\varphi_m + \theta)$

$tangential\ equillibrium$: $\tau_1 = q_c \sin(\varphi_m + \theta)$

Equilibrium load case 2:

$radial\ equillibrium$: $p_2 ds = T_m d\theta \Longrightarrow p_2 = T_m \frac{d\theta}{ds} = \frac{T_m}{R_s}$

$tangential\ equillibrium$: $\tau_2 = 0$

Equilibrium load case 3:

$radial\ equillibrium$: $p_3 = \frac{\Delta T}{R_s} \frac{\theta^2}{(\varphi_m + \varphi_s)^2}$

$tangential\ equillibrium$: $\tau_3 = -\frac{2\Delta T}{R_s} \frac{\theta}{(\varphi_m + \varphi_s)^2}$

The resultants of both the radial compressive components and the tangential friction components can now be expressed by combining the three load cases according to

$$p = q_c \cos(\varphi_m + \theta) + \frac{T_m}{R_s} + \frac{\Delta T}{R_s} \frac{\theta^2}{(\varphi_m + \varphi_s)^2} \tag{6.2}$$

$$\tau = q_c \sin(\varphi_m + \theta) - \frac{2\Delta T}{R_s} \frac{\theta}{(\varphi_m + \varphi_s)^2} \tag{6.3}$$

In addition to the design criteria of $\sigma_{2cd} > p_{eff}$ and $\tau_{12d} > \tau_{eff}$ (p_{eff} and τ_{eff} are the effective contact stresses, i.e. contact forces adjusted with respect to effective contact area per meter length of the cable), the condition of full fixation of the cable relative to the saddle implies that the total critical frictional force, F_r, must exceed or equal ΔT at all times (Zheng, Jiang, & Lu, 2011). Adopting Coulombs' law, the

critical friction force is a function of radial force component, p, multiplied by the frictional constant, μ, expressing the sliding resistance of the two materials according to (Zheng, Jiang, & Lu, 2011)

$$F_r = \int_0^{\varphi_m+\varphi_s} \mu p R_s d\theta \quad (6.4)$$

In the following calculations the latter requirement is assumed to be fulfilled at all times. However, in actual design this criterion must be met and the friction coefficient between cable and saddle must be evaluated.

Assessment of conventional saddle design

In this section a parametrical investigation, based on the previously defined design criteria, is performed to assess the applicability of conventional saddle design in combination with the use of CFRP cables. The bridge that is subject for the parametrical study is the proposed suspension bridge over Sognefjorden (3 700 meters). The preliminary sizing of the structural system of the bridge has already been performed in Section 5.2, based on the feasibility study by the Norwegian Public Roads administration. For the purpose of conceptually evaluating the saddle design for implementation of CFRP cables, only the gross geometry of the bridge and the horizontal cable force are of interest. Furthermore, the parametrical investigation should merely be seen as a rough estimate of the required design parameters for the saddle design with CFRP cables in super long span suspension bridges in general, and not as the detailed design of the saddle for the described bridge project.

The gross geometry of the single span suspension bridge was shown in Figure 28, and the pertinent data, relevant for evaluating the saddle design, are summarized in Table 23.

Table 23. Input data based on the calculations on Sognefjorden in Section 5.2.

Geometrical input data for Sognefjorden (safety factor 4.4)		
$\boldsymbol{H}$	$\frac{(q_c + q_d + q_l)l^2}{8d}$	$1.092 * 10^6\ kN$
$\boldsymbol{\varphi_m}$	$tan^{-1}\frac{4d}{l}$	21.8°
$\boldsymbol{\varphi_s}$	$tan^{-1}\frac{d}{0.3l}$	18.4°
$\boldsymbol{A_{cable}}$	–	$0.786\ m^2$

The expression for evaluating the horizontal force is valid for distributed loads and parabolic shaped main cables. The distributed loads are self-weight of the main cable, q_c, other distributed dead loads of the suspended structure, q_d, and live loads from traffic etc., q_l. When estimating the angles, the idealized conditions of a perfectly parabolic shaped cable in main span and no cable sag in the side span are adopted. For

more detailed description of the single span suspension bridge over Sognefjorden and assumptions regarding loading conditions, see Section 5.2 and Appendix A.

6.2.2 Method

Due to large uncertainties regarding both the distribution of the contact stresses within the saddle and the effective contact area (see Figure 39 for definition of effective contact area), a parametrical study is conducted to evaluate the applicability of conventional saddle design in combination with CFRP cables. In addition to the assumptions of full fixation of the cable and circular shape of the saddle, it is also assumed that the contact forces are evenly spread over the contact area. In reality, such a design would generate larger stresses in the bottom than in the top of the cross-section. Although the differences in contact area might be large, this can be counteracted by choosing a smaller value for the contact area. The largest uncertainties in the simplified analysis are thus related to accurately determining the effective contact area, accounting for both the actual contact area between cable and saddle and the uneven stress distribution over the cross-section. To overcome this problem the contact stresses are evaluated for a wide range of effective contact areas (ranging from 25 % in effective contact area to complete contact, i.e. 100 %, see Figure 39). The second design parameter is the radius of curvature for the saddle. This parameter is governed by the size of the saddle and, thus, by the practical limitations of assembling and attaching large structures on the pylon top. In the calculations the maximum length of the saddle is set to the length of the pylon top (in the preliminary sizing the pylon top length is 15 meters ➔ $R_s \approx 22$ meters).

Furthermore, as previously discussed, there are also large uncertainties related to the design strengths with respect to transverse and shear loading of composites. For this reason, both the conservative estimates $\sigma_{2cu} = \sigma_{2mcu}$ / $\tau_{12u} = \tau_{12mu}$ and experimentally obtained values for CFRP with similar properties, as presented in Table 1 under Chapter 3, are included and compared with the calculated interfacial stresses. It should, however, also be emphasized that under the prevailing conditions, where both transverse compressive stresses and shear stresses are present, the in-plane shear strength is significantly increased due to the confining compressive stresses. This relation is, however, very difficult to assess and is not accounted for in the following calculations. Moreover, it should also be emphasized that only contact stresses are evaluated in the following calculations, and no consideration is therefore taken to the stress-state within the cable.

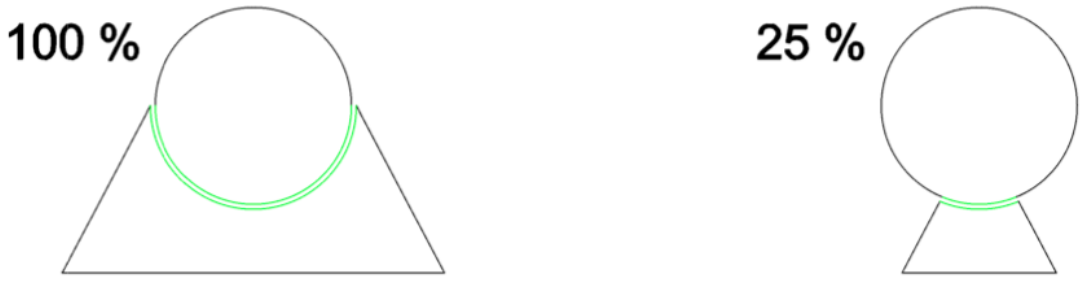

Figure 39. Definition of the effective contact area between cable and saddle. Complete contact, 100 %, is shown to the left, and the lowest contact area in the calculations, 25 %, is shown to the right.

6.2.3 Results from parametrical study

In Figure 40 and Figure 41 the radial compressive stresses and tangential frictional stresses are shown as functions of the radius of the saddle for three different ratios of effective area. The corresponding strengths for the CFRP cables are plotted as additional horizontal lines, based on the values from Table 1.

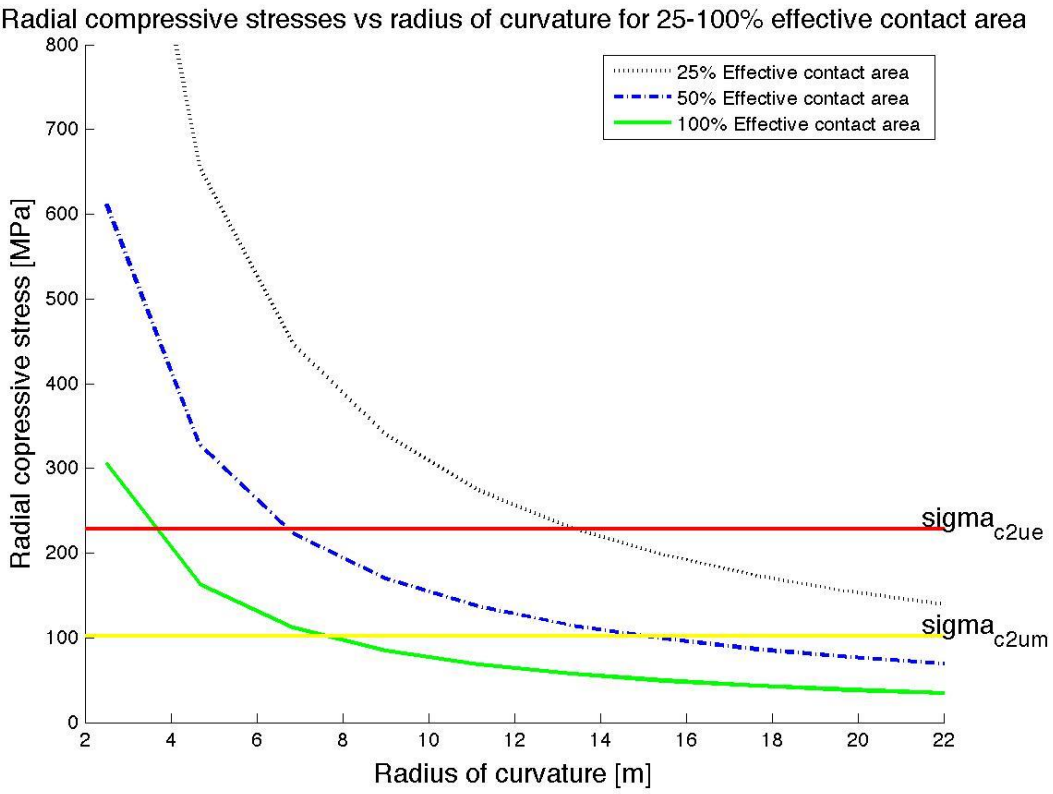

Figure 40. Radial compressive stresses vs. radius of curvature for 25 %, 50 %, and 100 % effective contact area. The yellow horizontal line represents the transverse compressive strength of the matrix, and the red line represents the corresponding empirical value (based on Table 1).

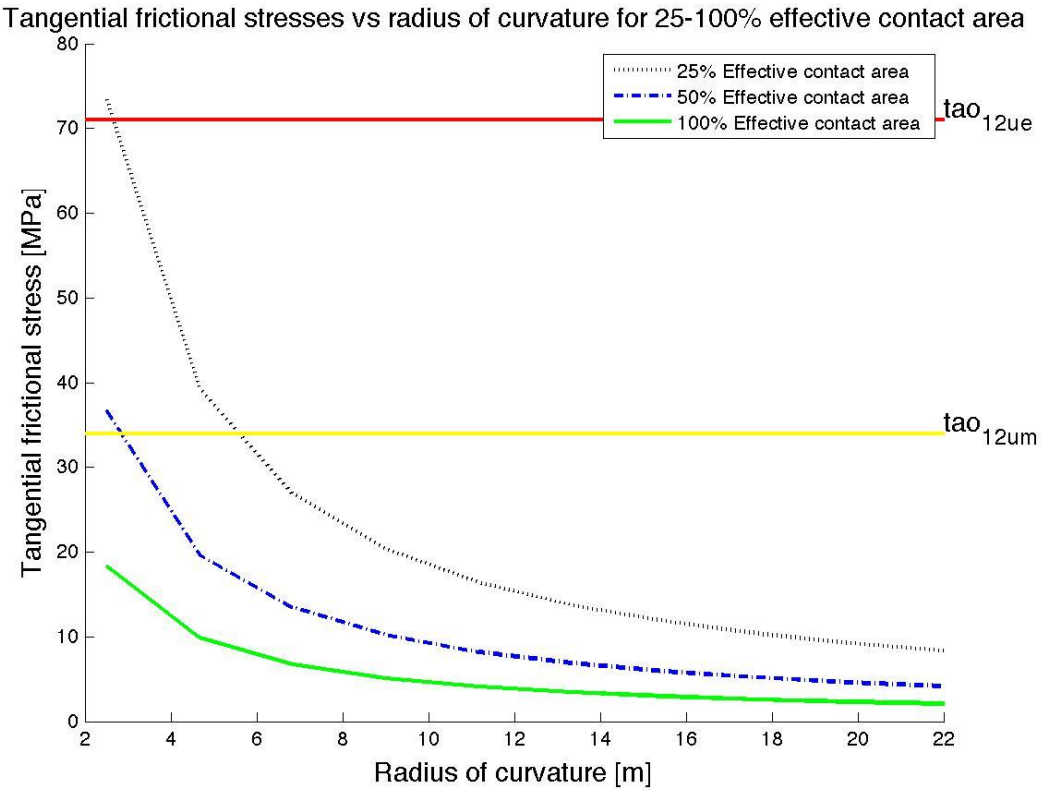

Figure 41. Tangential frictional stresses vs. radius of curvature for 25 %, 50 %, and 100 % effective contact area. The yellow horizontal line represents the in-plane shear of the matrix, and the red line represents the corresponding empirical value (based on Table 1).

6.2.4 Interpretation of results

It becomes apparent that both the radius of curvature of the saddle and effective area has a large influence on the magnitude of the developed contact stresses. Considering that the stresses are not evenly distributed over the contact area and that the contact ratio will be considerably below 100 %, it can be seen that large radius of curvature are needed to accommodate for the high radial stresses. However, due to large uncertainties regarding stress concentrations and contact area it is difficult to draw any conclusions, apart from

- The developed tangential frictional forces are quite small and are not likely to impede with the structural performance of the cable.
- Conventional saddle design in combination with CFRP requires large saddle radiuses.

At first glance, it seems feasible to fixate CFRP main cables on top of the pylons in super long span suspension bridges using conventional design methods. However, it is probably more economically efficient to adopt new design methodologies to increase the contact area, and thereby reduce the required radius of the saddle.

7 Case Studies

The pilot projects for the applications of CFRP cables in the cable system of cable supported bridges are scarce. The single most relevant and interesting project up until today is probably the Stork Bridge (Storchenbrücke) in Winterthur, Switzerland, see Figure 42. The Stork Bridge was finished in 1996 and is a cable-stayed bridge for both vehicles and pedestrians (Meier, 2012). The bridge has two spans of 63 and 61 meters on each side of a central pylon, see Figure 43 (Meier, 2012). The cable system consists of 24 stay cables and two of these cables are made of CFRP, while the other 22 cables are conventional steel cables (Meier, 2012).

Figure 42. The Stork Bridge in Winterthur, Switzerland (decentlab.com, 2014).

The CFRP cables used in the bridge have 241 wires each and a diameter of 5 mm. To be on the safe side before the erection, the cables were tested for more than 10 million cycles with a load of three times the magnitude for the permissible load. Once the cables were erected, advices for measuring stresses, deformations etc. were installed. The results from the measurements have been analysed ever since in order to control if the theoretical expectations on the CFRP cables are in accordance with the behaviour of the practical application. The most fundamental measurements are regarding the relative displacement in the critical detail of the anchorage. The results show that there has been a relative displacement between the cones and the LTM at the anchorage caused by creep. On the other hand, the results also show an apparent tendency that the displacement curves are levelling out. However, both the result of the relative displacements and the levelling out of the displacement curves are in great accordance to the theoretical expectations. (Meier, 2012)

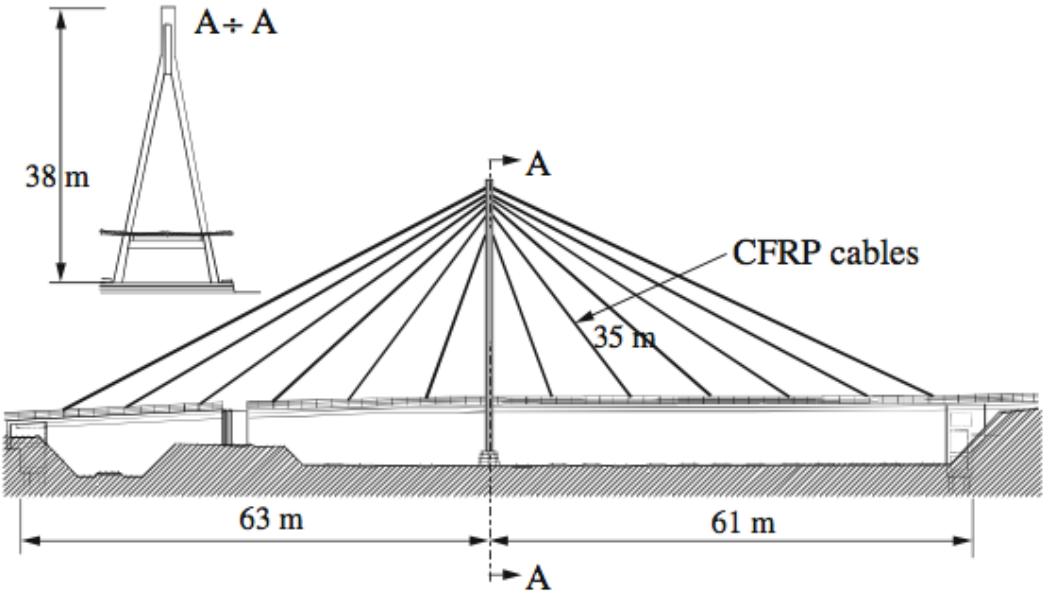

Figure 43. Elevation of the Stork Bridge in Winterthur, Switzerland (Meier, 2012).

Besides the Stork Bridge, the applications of CFRP cables are mainly found in pedestrian bridges. Worth mentioning is the Laroin footbridge in France, finished in 2002, see Figure 44. This bridge has a main span of 110 meters that is solely supported by CFRP cables, 16 in total, eight connected to each pylon (Dehmous & Welemane, 2011). The bridge has no side spans but is anchored at each side with a steel cable (Dehmous & Welemane, 2011). Even though the CFRP cables plays a greater role in the structural system of the Laroin footbridge compared to the Stork Bridge, it has to be taken into account that the bridges differ substantially in terms of loads and dimensions since the Laroin footbridge is dimensioned for pedestrians only.

Since there exists no applications of CFRP cables in bridges with longer spans, their feasibility in super long spans cannot be validated based on the applications of today. Nevertheless, the applications have still proved that the performance of CFRP cables is satisfying in minor scale (for cable-stayed bridges), which is fundamental for their feasibility in longer spans.

Figure 44. The Laroin footbridge in France. The CFRP cables that are supporting the span can clearly be seen together with one of the steel cables that anchor the bridge on the sides (geocaching.com, 2014).

8 Summary of Results and Discussion

In this section, the results obtained from the static and dynamic analysis are recaptured and evaluated from a feasibility and applicability point of view. The validity of the results is also assessed, based on the limitations of the adopted methods and by comparison with results from previous work within the field. Finally, the last part of this section, is devoted to a discussion of the prospects of CFRP cables in future super long span bridge applications, including a discussion of the most important, and as of yet, unresolved related structural issues.

Static span limits suspension bridge

In Section 4.1, it was shown that there, for suspension bridges, exists a limiting span beyond which the stresses induced by the load of the suspended structure exceed the allowable stress in the cables. It was also shown, as the spans become longer, an increasing part of the cable stress will be related to the cable's own self-weight. The shown behaviour indicates that the limiting span is closely related to the characteristics of the cable material, and that the feasibility of future super long span bridges, exceeding ≈ 4 000 - 5 000 meters, is feasible only with the implementation of new lightweight and high-strength materials such as CFRP.

In the calculations of the limiting span, a highly simplified linear analysis was adopted, considering only vertical static loads and the strength of the cables. In terms of the objective, of evaluating the span limits with respect to statics, the limitations of the expression primarily lie in its inability to assess the deflections of the bridge. However, as a previous study have shown that the behaviour of a suspension bridge tends to the behaviour of a free hanging main cable under increasing spans, and that the deformational characteristics improves for span lengths exceeding ≈ 2 500 - 3 000 (Clemente, Nicolosi, & Raitel, 2000), evaluation of the limiting span purely based on the strength of the cables is justified. Nevertheless, it should be emphasized that the calculations are highly simplified and does not account for the induced second order effects under live loads. Furthermore, both the calculation of the limiting span, presented herein, and Clemente, Nicolosi, & Raitels (2000) investigations of the deformability of long span suspension bridges, considered only vertical loads. In actual design, the horizontal deflections under static wind loads must be considered as well, but for the purpose of estimating the limiting span the method is considered sufficiently accurate.

In terms of feasibility considerations the results are more difficult to assess. The uncertainties are foremost related to the practical limitations of the non-dimensional load parameter β, representing the ratio between additional loads and the cable-weight itself. In general, no specific limit with respect to this ratio can be specified, since the maximum allowable cable force ultimately is governed by the capacity of the connections (saddle, and anchor blocks) and practical limitations related to increasing cable area. Furthermore, as the relation between additional loads, supported by the cables, and the cable-weight itself determines the required cable area, lower β-values are feasible in bridges with light girders and low levels of traffic volume. Nevertheless, despite the difficulties of assessing an upper practical span limit for suspension bridges, it can still be concluded that the use of conventional HS steel seems feasible, from a static viewpoint, even up to span lengths of 4 000 or 5 000 meters.

The static capacity of CFRP in real applications is even more difficult to assess, since the connection detailing require new solutions. Therefore, it is difficult to assess not only the limitations with respect to ultimate applicable span lengths, but also the beneficial aspects in terms of decreasing structural dead load. However, even upon stipulation that the structural issues, related to the connections, will not constituent impediments in future super long span bridge applications, full utilization of the static potential of CFRP seem implausible due to the large propensity of aerodynamic instability of extremely long span bridges. Hence, irrespective of the lower applicable limits of the β-values, it can be concluded that, due to its superior static properties, neither the static strength nor the static performance, will be governing with respect to ultimate span length, in suspension bridges with CFRP cables.

Applicable cable lengths in cable stayed bridges

Due to differences in structural behaviour, a similar evaluation criterion as used for suspension bridges cannot be used for evaluating the static span limits of cable-stayed bridges. The most essential difference lies in the deformational characteristics where cable-stayed bridges, as opposed to suspension bridges, suffer from a considerable decrease in vertical stiffness under increasing span length, due to the decreased stiffness of the stay cables. Therefore, with an equivalent stiffness which can only increase a certain extent, under increasing cable area (due to decreasing equivalent modulus under decreasing levels of stress), a suitable criterion for evaluating applicable cable lengths can be deduced to the point of maximum equivalent stiffness and the lowest applicable safety factor. From this evaluation criterion, the maximum applicable cable lengths were found to be around 1 500 meters for steel and about 5 000 meters for CFRP.

It should however be mentioned, that the evaluated ultimate cable lengths are not equivalent with half the limiting span, since no consideration is taken to the axial forces in the deck. The main reasons for not considering the axial stresses in the deck is due to the lack of generalizability of such results, as the magnitude of the stresses primarily is related to the weight of the bridge girder and also since the compressive forces are independent of the choice of cable material. Nevertheless, in super long cable-stayed bridges the axial forces might become governing, with respect to ultimate span limits, and it might become necessary to reduce the weight of the suspended structure or by other means alleviate the compressive stresses in the girder. Moreover, it should also be emphasized that the assumption that the safety factors used for conventional cable-stayed bridges within 1 000 meters can be adopted also for super long span cable supported bridges presumably leads to slight overestimates of the applicable cable lengths. This is because the conventional safety factor, based on the long term strength of the material, presumably becomes insufficient with respect to stiffness in super long span bridge applications.

As reference to the obtained results, it can be mentioned that from a static analysis performed by Wang & Wu (2010), of a tentatively designed 2 000 meter long steel cable-stayed bridge, the maximum permitted mid-span deflection, of $l_m/400$, was obtained for an adopted safety factor of 2.5. From the results, Wang & Wu (2010) concluded that, for longer spans, a safety factor of 2.5 will be insufficient to fulfil the stiffness requirements of the bridge. These results indicate that the evaluated maximum applicable cable lengths in fact are slightly overestimated. However, more accurate evaluations of appropriate safety factors for different span lengths require

evaluation of the deformability of the bridge and thus, also preliminary sizing, which is considered beyond the scope of this thesis.

Nevertheless, based on applicability considerations, it can be concluded just as for suspension bridges, the limiting cable length of CFRP widely exceeds the applicable cable length of steel. In this case, the superior static capacity of CFRP is owed not only to the superior specific strength but also the outstanding specific stiffness of the material. However, it should be emphasized that, even for cable-stayed bridges, real span lengths are likely to be limited with respect to the aerodynamic instability, or due to compressive stresses in the deck, prior to full utilization of the static capacity of the CFRP cables.

Flutter instability

As described in Section 5.1, cable supported bridges are very vulnerable to wind-induced instability, with wind stability generally becoming a key aspect in the design of any long span cable supported bridge. Furthermore, with the susceptibility for wind action increasing with decreasing structural mass and increasing span lengths, the use of CFRP in super long span bridges seem unfeasible. Somewhat surprisingly though, the aerodynamic investigation presented herein, showed slight enhancements of the critical flutter velocities with the use of CFRP cables. Although, the results may seem inconsistent with the negative effects of decreased structural mass, it was found when analysing the results that the negative effects related to decreased mass was counteracted by the positive effects related to increased torsional frequencies. The relative increase in critical wind speed was found to lie in the range between 6.4% - 10.2%, depending on the choice of safety factor.

The obtained results, of slightly increased critical wind velocities, due to increased torsional frequencies with decreasing peripheral mass, are however not unique. Similar trends have been shown in previous aerodynamic studies, investigating the aerodynamic response of both steel and CFRP. One example where this trend showed to be even more emphatic, was in the comparative aerodynamic analysis, conducted by Zhang & Ying (2006), where the response of both steel and CFRP was investigated for the already existing long span Runyang Bridge in China. Similar to the present study, Zhang & Ying (2006) found an increased critical flutter velocity of 14.8% - 17.2% with CFRP cables, primarily was owed to the significant increase in natural torsional frequency.

Another important outcome of the aerodynamic investigations is that, irrespective of the choice of cable material, far too low critical wind-speeds were obtained for the proposed girder section. Even in the most favorable combination, the evaluated critical wind speed, 29.3 m/s, falls considerably short of the required critical wind speed of approximately 65 m/s. As previously also mentioned, in Section 5.2.4, the results of the present study deviates considerably from the previous flutter calculations, performed by Berntsen & Lotherington (2013) on the same girder section. Furthermore, it was mentioned that both calculations are afflicted with large uncertainties. For this reason, with great discrepainces in results and large uncertainties regardning aerodynamic derivatives employed in the flutter calculations conducted by Berntsen & Lotherington (2013), the coupled flutter velocity was also evaluated using discrete vortex simulations to extract the aerodynamic derivatives.

These calculations showed very good agreement with the simplified analysis adopted in this study, only differing with differing with approximately 1% [4].

Furthermore, as reference to the low critical wind-speed obtained in this study, it can be mentioned that during the feasibility study of a continuous steel cable suspension bridge proposal for crossing of the Gibraltar Strait, an aeroelastic stability study revealed the feasibility of spanning the required 3 550 meters using a slot-to-solid width ratio of approximately 1 (Larsen & Esdahl, 1998). Even though, the results are not equivalent with the single span suspension bridge and the aerodynamic results are very sensitive with respect to differences in the girder design, the mentioned results still indicates that the adopted slot-to-solid width of about 0.3 is insufficient for the proposed single span suspension bridge over Sognefjorden.

Nevertheless, once again referring to the mentioned aeroelastic stability study of the continuous suspension bridge proposal for the Strait of Gibraltar (Larsen & Esdahl, 1998), it was shown aerodynamically feasible to span even up to 5 000 meters, adopting the twin-box girder design with considerable slot-to-solid-width. For this reason, even though the proposed girder section for the single span suspension bridge failed to comply with the aerodynamic stability requirements, it can be concluded that with an adequate bridge girder design, it is feasible to span the 3 700 meter long fjord using either steel or CFRP.

Connections

As discussed in Chapter 6, the inherent transverse weakness and poor shear capacity of the CFRP wires poses great challenges in bridge applications. The key problems are primarily related to connecting the cables to bridge deck, pylons and anchorage devices without inducing too high shear and transverse compressive stresses. For this reason, even stay cables, which have been considered prime candidates for replacement with CFRP due to their simplicity in terms of required mechanical properties, are faced with the structural issue of how to securely anchoring the CFRP cables without reducing the long term strength.

As described in Section 6.1, conventional mechanical anchorage system are not suitable for anchoring the CFRP cables, due to the high peak shear and compressive stresses, arising towards the loaded end of the termination. Instead, the as of today only application of CFRP cables in a vehicular bridge, utilizes an advanced bonded anchorage solution where the peak stresses are alleviated and the in-plane shear strength enhanced, through the use of a conical termination and a gradient load transfer media. Due to the uncertainties, regarding this state of the art anchorage technology and the deficiency in long-term health monitoring of CFRP cables, monitoring of the structural response is a key-aspect in the pilot, Stork Bridge project. As previously also mentioned, these measurements have all been found to match the high set expectations (Meier, 2012).

However, despite the success of the pilot Stork Bridge project, large impediments still remain unresolved. Especially, with the superior static potential and the relative high cost of CFRP, great uncertainties are related to the systems applicability in super long span applications. Furthermore, with already reluctant investment prospects for CFRP partly due to the materials high manufacturing cost, the presumed high cost of the advanced gradient anchorage technology is likely to represent another impediment.

[4] Allan Larsen (Chief Specialist, Aero and Structural Dynamics, Cowi Lyngby), E-mail conversation with the authors, 27th of May 2014.

Besides the anchorage problem, the transverse weakness and poor shear capacity of CFRP is probable to pose challenges in the connections between main cables and hangers and also when fixating the main cable on top of pylons, when used in suspension bridges. For this reason, with the stress field deviating from the pure axial direction and with larger concentrated tensile forces which need to be anchored, compared to cable-stayed bridges, CFRP cables have been considered unsuited for use in suspension bridges. Nevertheless, due to their greater potential with respect to span lengths, it is highly interesting also to investigate the feasibility of implementing CFRP in super long span suspension bridges.

Simplified calculations were performed in this thesis to evaluate the stresses developed at the interface between the main cable and the saddle, for the reference single span suspension bridge over Sognefjorden. The calculations suggest that, even though very large saddle radiuses are required, it seems possible to fixate the main cable within the saddle without exceeding the radial strength of the material. However, from an economical viewpoint it might be advisable to adopt new designs methodologies and increase the contact area rather than using the conventional design and increase the saddle radius, to apt with the lower transverse capacity of CFRP. As mentioned in Section 6.2, it should also be highlighted that the performed calculations represents a highly idealized situation, where the interfacial stresses are assumed to be uniformly distributed over the contact area, and the results are merely to be seen as rough estimates rather than actual design requirements.

Prospects of CFRP cables in future super long span bridge applications

Unquestionably, the use of CFRP cables in cable supported bridges opens up new possibilities of vastly increasing span lengths. However, realization of the huge static potential requires new ground-breaking technology, especially within the field of aerodynamics. Moreover, under prevailing conditions, of high manufacturing cost for CFRP and with construction cost often being the decisive parameter in bridge design, the future of CFRP cables in suspended bridge applications primarily lies beyond the range of conventional HS steel cables. For this reason, the largest impediments, besides those related to the anisotropic structure of the material, preventing widespread use of CFRP in super long span bridges are related to the inherent characteristics of cable supported bridges.

The first and by far the largest issue, is related to the large flexibility of cable supported high propensity for wind-induced instability. As mentioned previously, numerous solutions have been proposed to enhance the aerodynamic stability of super long span cable supported bridges. Modern aeroelastic design with passive systems for mitigation of flutter generally utilizes a twin-box girder design with large slot-to-solid width to increase of the aerodynamic damping. However, even though twin-box girder sections with large slot-to-solid width ratio have been shown theoretically feasible for span lengths approaching the 5 000 meter scale, their potential is likely to be limited, as further increase in span length will increase the use of materials and cost even more. Therefore, one of the most important aspects, related to the future prospects of CFRP, is related to the development of new and reliable active control systems for flutter mitigation. Especially this is true for suspension bridges where the static potential exceeds that of cable-stayed bridges.

Although the static span limits of cable-stayed bridges are considerable lower compared to suspension bridges, it is difficult to assess whether this might lead to higher utilization of the static potential of CFRP. This uncertainty regards both

aerodynamic response of super long cable-stayed bridges exceeding, say ≈ 2 000 meters, and also the problem of increasing axial forces.

Finally, there are a number of unresolved issues related to connecting and fixating the cables to other structural elements, facing the implementation of CFRP cables in suspension bridges. Perhaps the largest structural impediment, aside from the limiting factor related to the aerodynamic response, is to find a technically feasible and economically viable solution for anchoring the huge tensile forces of the main cables, in super long span suspension bridges.

9 Conclusion

With the purpose of evaluating the feasibility of CFRP in super long span cable supported bridges, the static span limits, aerodynamic stability, and connection detailing has been investigated and compared with steel. With the underlying purpose of investing the applicability of CFRP in the future single span suspension bridge over Sognefjorden, this particular case has been used as reference in the analyses for suspension bridges. Both suspension and cable-stayed bridges has been analysed in this thesis, and the two bridge types are treated separately in this conclusion.

Suspension bridges

- The static potential with CFRP cables, based on the static strength of the cables, is radically higher compared to steel cables. Using steel cables, the static span limits seems to be approximately 4 000- 5000 meters while it seems possible to span > 10 000 meters with CFRP cables.
- The aerodynamic performance of CFRP is good, and proves to be slightly better compared to steel cables. However, the aerodynamic performance is still the factor that will govern the span lengths of suspension bridges. Based on previous studies of steel cables, it seems feasible to span up to 5 000 meters from an aerodynamically point of view with a twin-box girder design. The slot-to-solid width ratio already has to be quite high for these span lengths, and further increase in span lengths with the current design will increase the use of materials and the costs even more. Therefore, new aerodynamic designs are probably necessary for increasing the spans further. An approximately similar aerodynamic span limit will apply for CFRP as well.
- With the current aerodynamic design of the bridge girder, HS steel and CFRP cables are probably applicable in the same range of spans with respect to full-scale response of static and dynamics. Further development in the aerodynamic design of suspension bridge is therefore the key in order to utilize the static potential of CFRP cables.
- Concerning the details, calculations has been conducted on the fixation of the cables to pylons. Based on the results, it seems feasible to transfer the forces with a conventional design of the saddles. However, the economical aspect and alternative solutions should be analysed in future projects. The anchorage of the main cables and the connection between main cable/hangers has not been analysed in this thesis, and are therefore interesting in future projects.
- Assuming that the details are feasible in super long spans, CFRP seems possible in the crossing of Sognefjorden. However, since steel cables seem feasible up to these span lengths as well, an economical comparison between the two materials is necessary. Since such a comparison is quite complex due to differences in cable costs, maintenance costs (excellent corrosion resistance and fatigue behaviour of CFRP), pylon dimensions, etc. it is a subject for future projects.

Cable-stayed bridges

- Due to the difference in structural behaviour from suspension bridges, limiting cable lengths has been analysed instead of span limits. This approach

highlights the potential of CFRP compared to steel, and the potential cable lengths of CFRP are 5 000 meters compared to 1 500 meters for steel. The results are slightly overestimated since the conventional safety factor are likely to be insufficient due to decreased stiffness with increasing cable lengths, but gives a good indication of potential cable lengths.

- It should be emphasized that the static span limits for cable-stayed bridges cannot be evaluated solely on the potential cable lengths. The induced axial forces in the bridge deck might govern the span limits, and analyses of these forces are necessary for each particular bridge project when evaluating static span limits. These calculations were beyond the scope of this thesis, but are interesting in future studies of potential span limits.
- No calculations of the dynamic behaviour for cable-stayed bridges were conducted in this thesis, but CFRP and steel show similar critical flutter velocity based on previous studies in the field.
- It can be conducted that CFRP are as good as steel from an aerodynamic point of view, but no exact span limit based on the aerodynamics is here evaluated. Consequently, it cannot be stated how much of the static potential that can be utilized in a cable-stayed bridge. It is therefore interesting to, in a future study, analyse the span limits based on the optimal aerodynamic design for a general cable-stayed bridge.
- Concerning the details, no analyses have been conducted for cable-stayed bridges. The anchorage system from EMPA has been proved feasible for shorter spans (spans of approximately 60 meters), but there are no applications in longer spans. In a future project, it would be interesting to look at the possibilities of applying this detail in a larger scale, based on the forces in a super long span bridge. The economical aspect of this particular detail in super long span bridges and possible alternatives would also be essential parts of such a project.
- Further research of the dynamics and the axial forces has to be conducted before setting an upper span limit for cable-stayed bridges with CFRP cables. However, based on the static calculations, it is clear that CFRP has raised the potential in terms of span lengths compared to steel cables.
- Since the static limitations seem to be lower with steel cables in cable-stayed bridges compared to in suspension bridges, the capacity of CFRP cables can probably be more utilized in the cable-stayed bridges. However, as mentioned, the axial forces and dynamics have to be evaluated in more detail first.

Appendix

A - Preliminary sizing

The focus of this preliminary sizing mainly lies on the dimensions of the cable system. Dimensioning and design of other elements are beyond the scope of this thesis, and are therefore based on the model from Berntsen & Lotherington (2013). The conditions at the site for the bridge were presented briefly under Section Background, where Table 5 showed some of the essential geometrical parameters for the bridge, which will be input data in the calculations.

The preliminary sizing will be calculated in three main steps. The first step is the estimation of the load from the bridge deck, the traffic and the connection devices between deck and hangers. These loads are then assumed as equally distributed over the length of the bridge, and the hangers are dimensioned to carry these loads together with their own self-weights (second step). The dimensions of the main cables are finally calculated in a similar way as the hangers (third step).

Distributed loads

Bridge deck

The bridge deck was presented and described under Section 5.2.1 and illustrated in Figure 27. The deck is built up by steel in all calculations. The mass per meter in the longitudinal direction of each box girder is equal to

$$m_{box} = 6\,542\ kg/m$$

which is taken from Berntsen & Lotherington (2013). Since the adopted bridge deck has cross-beams connecting the box-girders, their mass has to be taken into account as well. The distributed mass of the cross-beams (longitudinal direction of the bridge) is

$$m_{c-b} = 1\,405\ kg/m$$

which is taken from Berntsen & Lotherington (2013). The total load per meter of the bridge deck (longitudinal direction) is now calculated as

$$q_{bd} = (2 * m_{box} + m_{c-b}) * g = 142\ kN/m$$

and this value is used throughout the calculations for the distributed load from the deck.

Traffic load

The traffic load is, in accordance with the limitations of this analysis, not be thoroughly analysed. In Berntsen & Lotheringtons (2013) study of a suspension bridge over Sognefjorden, the distributed traffic load was set to 9 *kN/m* for each traffic

lane and 2 *kN/m* for each walkway, making the total distributed traffic load equal to (two traffic lanes and two walkways)

$$q_t = 2 * 9 + 2 * 2 = 22\ kN/m$$

The same distributed traffic load is adopted in this analysis, and no point loads are considered. The only load case studied is an equally distributed traffic load in the longitudinal direction of the bridge. The simplification of using one load case only saves time and still gives a good estimation in a preliminary design. However, in a more detailed analysis, all load cases should be taken into account.

Connection devices (deck/hangers)

The weights from the connection devices between deck and hangers are already partly accounted for in the self-weight of the deck, but an additional weight of 439 kg (m_{cbdh}) are added at each connection. This weight corresponds to the one used by Berntsen & Lotherington (2013), and is therefore not customized for a CFRP connection. It is difficult to find a suitable weight of the connection devices of CFRP cables due to scarce applications. On the one hand, the reduced dimensions of the cable system with CFRP might lead to a reduced weight of the devices. On the other hand, the connections of CFRP cables are a problematic issue that might lead to heavier devices. The distributed loads of the connections between deck and hangers, q_{cbdh}, are calculated according to

$$q_{cbdh} = \frac{m_{cbdh} * amt_h * g}{l_m} = 0.28\ kN/m$$

where $amt_h = 121 * 2$, is the total amount of hangers (value taken from Berntsen & Lotherington (2013)).

Dimensions of hangers

The dimensions of the hangers are calculated based on the ultimate limit state (ULS). The load factors are set to 1.2 for dead load (γ_{dead}) and 1.3 for the traffic load ($\gamma_{traffic}$), which is in accordance with Berntsen & Lotherington (2013). It should be noticed that Berntsen & Lotherington (2013) used steel only in the cable system and a different load factor might therefore be adopted when using CFRP. However, since it is difficult to set a proper load factor for a new structural material applied in a super long span bridge, and in order to compare CFRP to steel, the authors have adopted the same values.

In the dimensioning of the hangers, the weight from the deck, connection devices, traffic and the hangers themselves are taken into account. When calculating the self-weight of the hangers, all hangers are simplified as having equal lengths, based on an average value. The effect of this simplification on the dimensions of the cable system is negligible. The hangers are modelled with a spacing, S_h, of 30 meters, giving an amount of 121 hangers at each side and a total hanger length, l_h, of 32 594 meters

(Berntsen & Lotherington, 2013). The dimensions of the hangers are calculated for both CFRP and steel, with the mechanical properties showed in Table 6. The allowable stress in the cables, $\sigma_{allowable}$, is calculated as

$$\sigma_{allowable} = \frac{\sigma_{ultimate}}{\gamma_{safe}}$$

where γ_{safe} contains all safety factors in the intervals presented above for CFRP and steel. In order to find the dimensioning area of the hangers, an expression for the area is developed from equilibrium between the resistance of the hangers and the applied load, according to

$$\sigma_{allowable} * A_h = \left(\left(q_{bd} + q_{cbdh} + (A_h * l_h * \rho * \frac{g}{l_m})\right) * \gamma_{dead} + q_t * \gamma_{traffic}\right) * S_h * \frac{1}{2}$$

$$\rightarrow$$

$$A_h = \frac{\left(\left((q_{bd} + q_{cbdh}) * \gamma_{dead} + q_t * \gamma_{traffic}\right) * S_h * \frac{1}{2}\right)}{\sigma_{allowable} - l_h * \rho * \frac{g}{l_m} * \gamma_{dead} * S_h * \frac{1}{2}}$$

where A_h is the area of one hanger. The results of the dimensioning area of one hanger for the selected safety factors are shown in Table 24. The total amount of material for all hangers can now be calculated as

$$V_h = A_h * l_h$$

see Table 25 for the results.

Table 24. Dimensioning area of one hanger.

Material	Safety factor	**Area of one hanger A_h [m^2]**
CFRP	2.2	0.002
	4.4	0.004
	6.5	0.006
Steel	1.8	0.003

Table 25. Total volume of hangers.

Material	Safety factor	**Total volume hangers V_h $[m^3]$**
CFRP	2.2	65.5
	4.4	130
	6.5	194
Steel	1.8	100

Dimensions of main cables

To find the dimensioning area of the main cables, the same procedure as for the hangers is adopted. The resistance of the main cables is set equal to the applied load, and the area is then solved from the expression.

The distributed weight from deck, traffic and connection devices between hangers/deck have already been calculated prior to the dimensioning of the hangers. However, the main cables also have to support the weight from hangers, connection devices between main cables/hangers, and its own self-weight. The weight of the hangers per meter can be expressed as

$$q_h = \frac{V_h * \rho * g}{l_m}$$

and the results from the calculations are shown in Table 26 below.

Table 26. Distributed load from hangers.

Material	Safety factor	**Distributed load hangers $[kN/m]$**
CFRP	2.2	0.31
	4.4	0.62
	6.5	0.92
Steel	1.8	2.09

For the connection devices between the hangers and the main cables, a weight of 439+3000 kg is added at each connection. This is the same as used in Berntsen & Lotherington (2013), with the same motivation as for the connection between deck/hangers above. The distributed weight from these connection devices, q_{chmc}, is calculated as

$$q_{chmc} = \frac{(439 + 3\,000) * amt_h * g}{l_m} = 2.21\ kN/m$$

The load from the main cables themselves is calculated as a function of their area, A_{mc}. Due to the parabolic shape of the cables, their actual cable length is longer than the span length, leading to a higher weight per meter along their horizontal projection. The actual length of one main cable is calculated according to

$$l_{mc} = l_m * \left(1 + \frac{8}{3}\left(\frac{d}{l_m}\right)^2\right) = 3\,798\ m$$

The weight of the cables are assumed to be uniformly distributed along the horizontal projections in this calculation, and the additional weight per meter is taken into account by the factor

$$\beta = \frac{l_{mc}}{l_m} = 1.027$$

giving a distributed main cable load according to

$$q_{mc} = A_{mc} * \rho * \beta * g$$

which is a function of the area of the main cables. However, even though the additional weight of the main cables has been taken into account, the modelling of the cable weight is still simplified since it is assumed to be evenly distributed. The parabolic shape of the cables result in a variation of the cable slope over the main span, which in turn leads to a more concentrated cable weight closer to the pylons. This simplification will not, however, affect the results since the distributed load only affects the horizontal component of the axial force, which can be assumed as constant throughout the main span, and therefore independent of the slope of the cables. The axial force at a certain point of the cable is calculated by multiplying the constant horizontal component with the factor $\frac{1}{\cos\alpha}$, which takes the slope into account. The expression for the axial force in the cables becomes

$$F_{Applied} = \frac{1}{\cos\alpha} * \frac{q_{tot}{l_m}^2}{8d}$$

where $\frac{q_{tot}{l_m}^2}{8d}$ is the constant horizontal component of the cable force. To find the dimensioning area, the most critical section of the main cables is controlled, which is adjacent to the pylons. The highest slope is found here, and therefore also the largest

vertical component and the highest axial force in the cables. The angle here, α, is calculated as

$$\alpha = \arctan\left(\frac{4d}{l_m}\right) = 21.8°$$

The total applied load on the main cables, q_{tot}, is calculated with the same load factors as for the hangers, $\gamma_{dead} = 1.2$ and $\gamma_{traffic} = 1.3$. The expression for q_{tot} becomes

$$q_{tot} = (q_{mc} + q_{bd} + q_h + q_{cbdh} + q_{chmc}) * \gamma_{dead} + q_t * \gamma_{traffic}$$

which is a function of the main cable area.

The allowable stress of the main cables, $\sigma_{allowable}$, is the same as for the hangers (equal mechanical properties of the materials and equal safety factors), and the resistance of the main cables can be written as

$$F_{Rd} = \sigma_{allowable} * A_{mc}$$

which also is a function of the area of the main cables. The expressions of the resistance of the main cables and the applied stress at the section adjacent to the pylons are finally set equal, and the dimensioning area is solved according to

$$F_{Rd} = F_{Applied}$$

$$\rightarrow$$

$$\sigma_{allowable} * A_{mc} = \frac{1}{\cos\alpha} * \frac{q_{tot} {l_m}^2}{8d}$$

$$\rightarrow$$

$$\sigma_{allowable} * A_{mc} =$$

$$= \frac{1}{\cos\alpha} * \frac{\left((q_{mc} + q_{bd} + q_h + q_{cbdh} + q_{chmc}) * \gamma_{dead} + q_t * \gamma_{traffic}\right) * {l_m}^2}{8d}$$

when inserting the expression for q_{mc}, the area can be solved according to

$$A_{mc} = \left(\frac{\left(\frac{1}{\cos\alpha} * \frac{\left((q_{bd} + q_h + q_{cbdh} + q_{chmc}) * \gamma_{dead} + q_t * \gamma_{traffic}\right) * {l_m}^2}{8d} \right)}{\sigma_{allowable} - \frac{1}{\cos\alpha} * \frac{\rho * \beta * g * \gamma_{dead} * {l_m}^2}{8d}} \right)$$

which is the sum of the area of both main cables. In the presentation of the dimensioning area, this value is divided by two in order to get the area of one main

cable only. The results from the calculations of the area are both presented as a function of the safety factors in Figure 45, and in table form for the selected safety factors in Table 27. The values for the distributed main cable load, q_{mc}, are calculated as the sum from both main cables, and are presented in Table 28. The cross-sectional mass, m_{c-s}, which is assumed to include the mass from the main cables and the bridge deck only, are found in Table 29. The cross-sectional mass was calculated according to

$$m_{c-s} = 2 * m_{box} + m_{c-b} + A_{mc} * \rho * \beta$$

The total applied load from the suspended structure (including traffic), q_{tot}, is finally calculated with load factors included and the results are presented in Table 30.

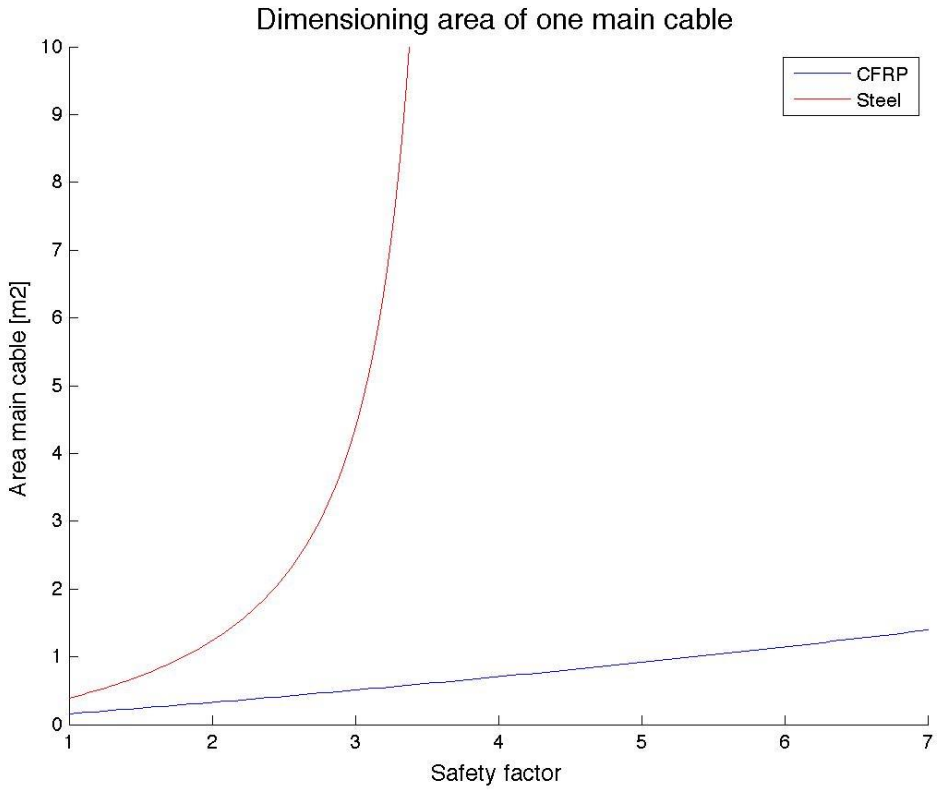

Figure 45. Dimensioning area of one main cable as a function of the safety factors. The blue line represents CFRP and the red line HS steel.

Table 27. Dimensioning area of one main cable.

Material	Safety factor	**Area one main cable** $[\boldsymbol{m^2}]$
CFRP	2.2	0.365
	4.4	0.786
	6.5	1.272
Steel	1.8	0.999

Table 28. Distributed load from main cables.

Material	Safety factor	**Distributed load main cables** $[\boldsymbol{kN/m}]$
CFRP	2.2	13.2
	4.4	28.5
	6.5	46.1
Steel	1.8	158.0

Table 29. Cross-sectional mass.

Material	Safety factor	**Cross-sectional mass** $[\boldsymbol{kg/m}]$
CFRP	2.2	15 800
	4.4	17 400
	6.5	19 200
Steel	1.8	30 600

Table 30. Total load from suspended structure and traffic load, load factors included.

Material	Safety factor	**Total load suspended structure** $[\boldsymbol{kN/m}]$
CFRP	2.2	218.4
	4.4	237.1
	6.5	258.6
Steel	1.8	394.2

B - MATLAB-code for calculation of static span limit (suspension bridges)

Limiting span length suspension bridges (simplified static)

```
% Filiph Banck
% Oskar Rosen Almberg

% Gothenburg 9/4 2014


clc
clear all
close all

%
for l=1:2
r=[0.1 0.35]; %ratio height pylon over deck/span length (d/l)

sigma_allow=[1770e6/1.8 3300e6/4.4];
pc=[7850 1600];
g=9.8;

l_lim_1=ones(100,1000,2);%linspace(1,10000,10000);

beta=linspace(0,10);

% Input data Sognefjorden
q_tot=[394.2e3 237.1e3];    % Total load incl. distr. traffic load
A_c=[0.999 0.786];

for j=1:2
for k=1:100


tol=1000;
i=1;
while tol>1e-3
    i=i+1;

    alpha_pylon=atan(4*r(l));

l_lim_1(k,i+1,j)=r(l)*l_lim_1(k,i,j)*8*cos(alpha_pylon)*sigma_allow(j)/(pc(j)*g*(l
tol=l_lim_1(k,i+1,j)-l_lim_1(k,i,j);

end

l_lim(k,l,j)=l_lim_1(k,i,j);

end

end
% Beta values Sognefjordem
```

```
Beta_sognefjord(l)=(q_tot(l)-1.2*pc(l)*2*A_c(l)*(1+8/3*r(l)^2)*g)/(1.2*pc(l)*2*A_c

end
figure(1)
axis([0 10 0 50000])
xlabel('Beta','FontSize',12)
ylabel('Theoretical span limit [m]','FontSize',12)
title('Theoretical span limit - Static strength ','FontSize',15)
hold on

plot(beta,l_lim(:,1,1),'k','linewidth',2)
plot(beta,l_lim(:,1,2),'b','linewidth',2)
plot(beta,l_lim(:,2,1),'--k','linewidth',2)
plot(beta,l_lim(:,2,2),'--b','linewidth',2)
legend('Steel (d/l=0.1)','CFRP(d/l=0.1)','Steel (d/l=0.35)','Steel (d/l=0.35)')

Beta_steel_x1=[Beta_sognefjord(1),Beta_sognefjord(1)];
Beta_steel_y1=[0,3700];
plot(Beta_steel_x1,Beta_steel_y1,'k','linewidth',2)
Beta_steel_x2=[0,Beta_sognefjord(1)];
Beta_steel_y2=[3700,3700];
plot(Beta_steel_x2,Beta_steel_y2,'k','linewidth',1)

Beta_CFRP_x=[Beta_sognefjord(2),Beta_sognefjord(2)];
Beta_CFRP_y=[0,3700];
plot(Beta_CFRP_x,Beta_CFRP_y,'k','linewidth',2)
Beta_CFRP_x2=[0,Beta_sognefjord(2)];
Beta_CFRP_y2=[3700,3700];
plot(Beta_CFRP_x2,Beta_CFRP_y2,'k','linewidth',1)

text(Beta_sognefjord(1)-0.3,-4000 , 'Beta_s_t_e_e_l', 'Color', 'k','FontSize',14);
text(Beta_sognefjord(2)-0.3,-4000, 'Beta_C_F_R_P', 'Color', 'k','FontSize',14);
saveas(figure(1),'Static performance','jpeg')
```

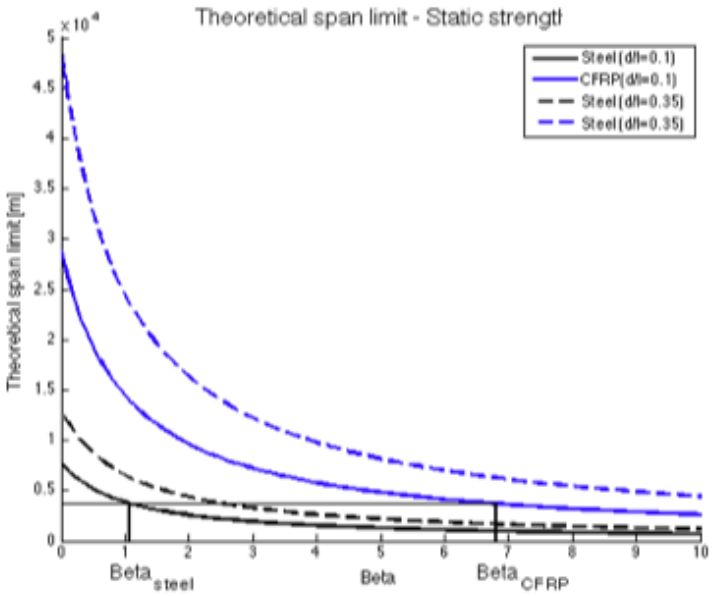

Published with MATLAB® R2013b

C - MATLAB-code for calculation of static cable length limit (cable-stayed bridges)

Limiting span length cable-stayed (simplified static)

```
% Filiph Banck
% Oskar Rosen Almberg

% Gothenburg 9/4 2014


clc
clear all
close all


% Input
sigma_ult=[1770e6 3300e6];
pc=[7800 1600];
g=9.8;
psf=linspace(1.5,6.5);
E_ini=[200e9 160e9];
L_c=[500 1000 1500 5000];

% Allowable stress
sigma_all_Steel=sigma_ult(1)./psf;
sigma_all_CFRP=sigma_ult(2)./psf;

% Area cable
A_CFRP=sigma_all_CFRP(50)/sigma_all_Steel(50);
%A_steel=linspace(8,);
% weight per meter length
w_Steel=pc(1)*g;
w_CFRP=pc(2)*g;

for i=1:length(L_c)
E_sec_Steel(i,:)=1./(1/E_ini(1)+w_Steel.^2*L_c(i)^2/24.*(sigma_all_Steel.*0.8+sigm
E_sec_CFRP(i,:)=1./(1/E_ini(2)+w_CFRP.^2*L_c(i)^2/24.*(sigma_all_CFRP.*0.8+sigma_a
EA_sec_Steel(i,:)=A_CFRP*pi*0.0615^2.*psf.*E_sec_Steel(i,:);
EA_sec_CFRP(i,:)=pi*0.0615^2.*psf.*E_sec_CFRP(i,:);
end


figure(1)
axis([1.5 6.5 0 250])
set(gca,'FontSize',18);
xlabel('Safety factor','FontSize',20)
ylabel('Equivalent modulus [GPa]','FontSize',20)
title('a) Equivalent modulus vs. adopted safety factor','FontSize',20)
hold on
grid on

plot(psf,E_sec_CFRP(1,:)/(10^9),'b','linewidth',2)
```

1

```
plot(psf,E_sec_Steel(1,:)/(10^9),'k','linewidth',2)
legend('CFRP ','HS Steel','Location','Best','FontSize',16)
hold off
saveas(figure(1),'Equivalent modulus 500 meters','jpeg')

figure(2)
axis([1.5 6.5 0 250])
set(gca,'FontSize',18);
xlabel('Safety factor','FontSize',20)
ylabel('Equivalent modulus [GPa]','FontSize',20)
title('b) Equivalent modulus vs. adopted safety factor','FontSize',20)
hold on
grid on

plot(psf,E_sec_CFRP(2,:)/(10^9),'b','linewidth',2)
plot(psf,E_sec_Steel(2,:)/(10^9),'k','linewidth',2)
legend('CFRP ','HS Steel','Location','Best','FontSize',16)
hold off
saveas(figure(2),'Equivalent modulus 1 000 meters','jpeg')

figure(3)
axis([1.5 6.5 0 250])
set(gca,'FontSize',18);
xlabel('Safety factor','FontSize',20)
ylabel('Equivalent modulus [GPa]','FontSize',20)
title('c) Equivalent modulus vs. adopted safety factor','FontSize',20)
hold on
grid on
plot(psf,E_sec_CFRP(3,:)/(10^9),'b','linewidth',2)
plot(psf,E_sec_Steel(3,:)/(10^9),'k','linewidth',2)
legend('CFRP ','HS Steel','Location','Best','FontSize',16)
hold off
saveas(figure(3),'Equivalent modulus 2 000 meters','jpeg')

figure(4)
axis([1.5 6.5 0 250])
set(gca,'FontSize',18);
xlabel('Safety factor','FontSize',20)
ylabel('Equivalent modulus [GPa]','FontSize',20)
title('d) Equivalent modulus vs. adopted safety factor','FontSize',20)
hold on
grid on
plot(psf,E_sec_CFRP(4,:)/(10^9),'b','linewidth',2)
plot(psf,E_sec_Steel(4,:)/(10^9),'k','linewidth',2)
legend('CFRP ','HS Steel','Location','Best')
hold off
saveas(figure(4),'Equivalent modulus 5 000 meters','jpeg')

figure(5)
axis([1.5 6.5 0 15])
set(gca,'FontSize',18);
xlabel('Safety factor','FontSize',20)
ylabel('Equivalent Stiffness [MN]','FontSize',20)
title('a) Equivalent stiffness vs adopted safety factor','FontSize',20)
```

```
hold on
grid on

plot(psf,EA_sec_CFRP(1,:)/(10^9),'b','linewidth',2)
plot(psf,EA_sec_Steel(1,:)/(10^9),'k','linewidth',2)
legend('CFRP ','HS Steel','Location','Best','FontSize',16)
hold off
saveas(figure(5),'Equivalent stiffness 500 meters','jpeg')

figure(6)
axis([1.5 6.5 0 15])
set(gca,'FontSize',18);
xlabel('Safety factor','FontSize',20)
ylabel('Equivalent Stiffness [MN]','FontSize',20)
title('b) Equivalent stiffness vs adopted safety factor','FontSize',20)
hold on
grid on

plot(psf,EA_sec_CFRP(2,:)/(10^9),'b','linewidth',2)
plot(psf,EA_sec_Steel(2,:)/(10^9),'k','linewidth',2)
legend('CFRP ','HS Steel','Location','Best','FontSize',16)
hold off
saveas(figure(6),'Equivalent stiffness 1 000 meters','jpeg')

figure(7)
axis([1.5 6.5 0 15])
set(gca,'FontSize',18);
xlabel('Safety factor','FontSize',20)
ylabel('Equivalent Stiffness [MN]','FontSize',20)
title('c) Equivalent stiffness vs adopted safety factor','FontSize',20)
hold on
grid on
plot(psf,EA_sec_CFRP(3,:)/(10^9),'b','linewidth',2)
plot(psf,EA_sec_Steel(3,:)/(10^9),'k','linewidth',2)
legend('CFRP ','HS Steel','Location','Best','FontSize',16)
hold off
saveas(figure(7),'Equivalent stiffness 2 000 meters','jpeg')

figure(8)
axis([1.5 6.5 0 15])
set(gca,'FontSize',20);
xlabel('Safety factor','FontSize',20)
ylabel('Equivalent Stiffness [MN]','FontSize',20)
title('d) Equivalent stiffness vs adopted safety factor','FontSize',20)
hold on
grid on
plot(psf,EA_sec_CFRP(4,:)/(10^9),'b','linewidth',2)
plot(psf,EA_sec_Steel(4,:)/(10^9),'k','linewidth',2)
legend('CFRP ','HS Steel','Location','Best')
hold off
saveas(figure(8),'Equivalent stiffness 5 000 meters','jpeg')
```

D - MATLAB-code for preliminary sizing and aerodynamic analysis of the Sognefjorden Bridge

Some of the longest equations could not fit in the format for the publishing and they are therefore not complete.

Table of Contents


```
% Aerodynamic analysis and preliminary sizing of cable system
%    - Suspension bridge over Sognefjorden

% Filiph Banck
% Oskar Rosen Almberg

% Gothenburg 9/4 2014


clc
clear all
close all
```

Preliminary sizing

```
% In the first part of this code, the dimensions  of the cable system is
% calculated for the bridge. The dimensions of hangers and main cables are
% calculated as a function of the safety factors. A calculation is made for
% both steel and CFRP, with different ranges for the safety factors. For
% steel, the safety factors goes from 1 to the value at which the area of
% the main cables are going towards infinity. The corresponding safety
% factor for CFRP (where the area of main cables goes towards infinty) is a
% quite high value and unrealistic in real applications. Since it is hard
% to say which safety factor that is the most suitable for CFRP, the range
% will go from 1 to 5.

l=3700;                 % [m] Length of main span
l_s=0;                  % [m] Length of side span
lambda=l_s/l;            % Ratio side to main span
d=370;                  % [m] Cable dip (sag)
l_c=l*(1+8/3*(d/l)^2);  % [m] Length of each cable in main span
g=9.81;                 % [m/s^2] Gravitational acceleration
sigma_ultimate=[3300 1770]*1e6;  % [MPa] Ultimate tensile strength of cables
p=[1600 7850];              % [kg/m3] Density of main cables and hangers
E=[165 210]*1e9;  % [GPa] Elasticity modulus of cables
G=80*1e9; % [GPa] Shear modulus of cross-section (using the value for steel in bot



% - Deck load

m_box=6542;             % [kg/m] Mass per meter of each box girder
```

```
m_cb=1405;              % [kg/m] Mass per meter of cross-beams
                        % (longitudinal direction of bridge)


% Calculating the weight of the deck per meter in the longitudinal
% direction of the bridge

q_bd=(2*m_box+m_cb)*g; % [N/m]



% - Traffic load


% Setting the traffic load to a fixed value, one load case only (evenly
% distributed load)
q_traffic=22*1e3;  % [N/m]



% - Connections deck/hangers load


% An additional weight due to connection devices between hangers and deck
% is added.
amount_h=121*2;  % Amount of hangers (both sides)

m_con_bd_h=439;  % [kg/device]

% Calculating the weight of the devices per meter

q_con_bd_h=(m_con_bd_h*amount_h*g/l);  % [N/m]



% - Dimensions hangers and main cables


s_h=30;  % [m] spacing between hangers
l_h=32594; % [m] Total length of all hangers

y_dead=1.2;  % Load factor dead load
y_traffic=1.3;  % Load factor traffic load

% Two seprated for-loops are now made for CFRP and steel, respectively. The
% safety factors for CFRP goes from 1-5, but for steel its decided by the
% safety factor for which the area of the main cables goes towards infinity
% This value is found when the nominator for the expression of the area of
% the main cables is approaching zero. This nominator is according to:

% sigma_allowable-(1/cos(a))*p*b*g*y_dead*l^2/(8*d)
```

```
% where b is
b=l_c/l;

% and a is the slope of the main cable adjacent to the pylons. The
% stress will have its maximum in the cable here. The slope is necesseray
% to know in order to calculate the stress in the direction of the cables
% based on the horizontal component of the stress in the cable, which is
% done further down in the equilibirum calculations.
a=atan(4*d/l);

% We now get the maximum safety factor for steel:
safe_max_steel=sigma_ultimate(2)/((1/cos(a))*p(2)*b*g*y_dead*l^2/(8*d));

% Making a matrix of safety factors, where the first row contains 100
% values for the safety factors of CFRP (between 1-5) and the second row
% contains 100 values of the safety factors for steel (between
% 1-safe_max_steel):
safe=[linspace(1,7); linspace(1,safe_max_steel*0.95)];


% Predimensioning of matrices before the loop:
sigma_allowable=zeros(2,100);    % Allowable tensile strength of cables
A_h=zeros(2,100);                % Total area of hangers
V_h=zeros(2,100);                % Total volume of hangers
q_h=zeros(2,100);                % The distributed weight of the hangers
A_tot_mc=zeros(2,100);           % Total area of main cables (both)
A_mc=zeros(2,100);               % Area of each main cable
q_mc=zeros(2,100);               % The distributed weight of main calbes
q_total=zeros(2,100);            % The total distributed weight


for j=1:2
    for i=1:100

sigma_allowable(j,i)=sigma_ultimate(j)/safe(j,i); % [MPa] Allowable tensile streng


% Finding an expression for the area of the hangers:
% sigma_allowable*A_h=((q_bd+q_connection_bd_h+(A_h*l_h*p*g/l))*y_dead+q_traffic*y

% Solving the equation for the area of the hangers (A_h):
A_h(j,i)=(((q_bd+q_con_bd_h)*y_dead+q_traffic*y_traffic)*s_h/2)/(sigma_allowable(j

% The total volume of material for the hangers
V_h(j,i)=A_h(j,i)*l_h;

% The distributed weight from the hangers
q_h(j,i)=(V_h(j,i)*p(j)*g/l);  % [N/m]

% The distributed load of connection devices between hangers and
% main cable is now calculated. Two devices are taken into account, one
% connected to the hanger (439kg) and one to the main cable (3000kg).
m_con_h_mc=439+3000;  % [kg/device]
```

```
q_con_h_mc=(m_con_h_mc*amount_h*g/l);  % [N/m]

% Equilibrium is now set between the resistance of the cables and the
% applied load. The area is solved from the expression to find the
% dimensioning area of the main cables for the bridge:

%sigma_allowable*A_mc=(1/cos(a))*q*l^2/(8*d)

%sigma_allowable*A_mc=(1/cos(a))*((q_bd+q_con_bd_h+q_con_h_mc+q_h+(A_mc*p*b*g))*y_

% Calculating the area in m2 for each main cable
A_mc(j,i)=(((1/cos(a))*((q_bd+q_con_bd_h+q_con_h_mc+q_h(j,i))*y_dead+q_traffic*y_t

% In order to account for the extra weight per meter in the horizontal
% direction due to the parabolic form of the main cables, the weigth is
% multiplied by b, which is the length of the cable divided by the span, as
% defined above.

% The distributed load from the main cables per meter becomes
q_mc(j,i)=A_mc(j,i)*p(j)*b*g*2;  % [N/m]

% And the total load is
q_total(j,i)=(q_bd+q_con_bd_h+q_con_h_mc+q_h(j,i)+q_mc(j,i))*y_dead+q_traffic*y_tr

end
end

figure(1)
axis([1 7 0 10])
xlabel('Safety factor','FontSize',12)
ylabel('Area main cable [m2]','FontSize',12)
title('Dimensioning area of one main cable ','FontSize',15)
hold on
plot(safe(1,:),A_mc(1,:),'b',safe(2,:),A_mc(2,:),'r')
legend('CFRP','Steel')
saveas(figure(1),'Area plot matlab','jpeg')
```

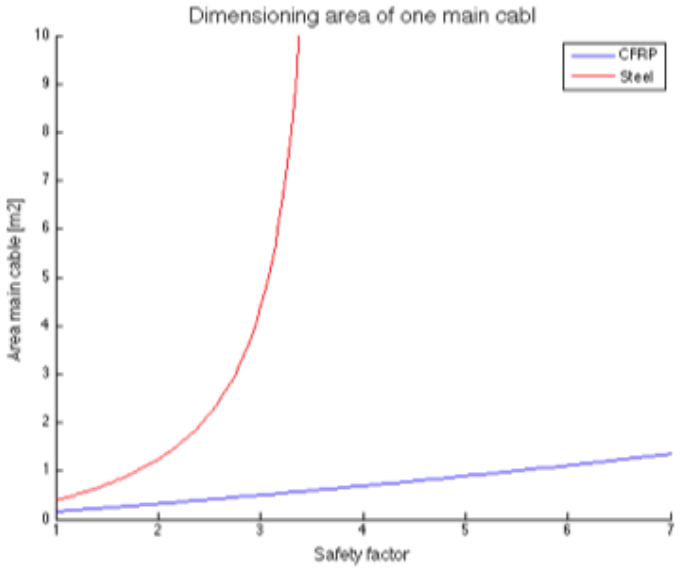

Aerodynamic analysis

```
% The critical wind speed for the bridge is now calculated in a
% simplified way. To calculate the critical wind speed, the moment of
% inertia of the cross section and the natural frequencies are first
% calculated.



% - Moment of inertia of cross-section


% Calculating the moment of inertia for the cross-section, including the
% contribution from the bridge deck, hangers and the main cables.

% The contribution from the deck is already calculated by []:

I_bd=1600000;  % [kgm2/m] Moment of inertia of the bridge deck

% The contribution from the main cables is calculated by their mass per
% meter multiplied by the distance from their mass center to the neutral
% axis in the horizontal direction, raised by 2.

r=31.1/2; % [m] Distance from mass center of main cable to the neutral
```

```
%     axis in the horizontal direction of the cross-section

% Predimensioning of matrices
I_mc=zeros(2,100);   % Moment of inertia for one cable
I_h=zeros(2,100);   % Moment of inertia for hangers (one plane)
I_tot=zeros(2,100);  % Total moment of inerta for cross-section
m_cross_sec=zeros(2,100);  % Total cross-section mass
H=zeros(2,100); % The horizontal cable tension H
P_h=zeros(2,100); % Vertical cable stiffness parameter
P_a=zeros(2,100); % Torsional cable stiffness parameter
qph=zeros(2,100);  % Eignevalues bending
qpa=zeros(2,100);  % Eignevalues torsion

for j=1:2
   for i=1:100

I_mc(j,i)=r^2*A_mc(j,i)*p(j)*b; % [kgm2/m] Moment of inertia of one main cable

I_h(j,i)=r^2*V_h(j,i)*p(j)/(l*2); % [kgm2/m] Moment of inertia of hangers (one pla

I_tot(j,i)=I_bd+I_mc(j,i)*2+I_h(j,i)*2; % [kgm2/m] Moment of inertia of total cros



% - Basic parameters


% Calculating three basic parameters of the cable/beam model:
% The horizontal cable tension H, the vertical cable stiffness parameter
% P_h and the torsional cable stiffness parameter P_a.

% Total cross-section mass (including bridge deck and main cables)
m_cross_sec(j,i)=2*m_box+m_cb+A_mc(j,i)*p(j)*b*2;
% The horizontal cable tension H
H(j,i)=m_cross_sec(j,i)*g*l^2/(8*d);

% Vertical cable stiffness parameter
P_h(j,i)=32*d^2*E(j)*2*A_mc(j,i)/(H(j,i)*l*l_c);

% Cross-section torsion constant
K=1.9;
% Torsional cable stiffness parameter
P_a(j,i)=P_h(j,i)*0.5/(1+G*K/(H(j,i)*r^2));

end
end



% - Eigenvalues fundamental bending and torsion modes
```

```
% The eigenvalues for fundamental bending and torsion modes is solved from
% the following equation. The eigenvalues are q_ph and q_pa in the formula,
% but will be saved in the matrices S(i) and then stored in qph and qpa.

% Predimensioning of matrices
qph=zeros(2,100);  % Eignevalues bending
qpa=zeros(2,100);  % Eignevalues torsion

% Bending
   for i=1:100
syms q_ph
S(i)=vpasolve(P_h(1,i)==q_ph^2/(1+2*lambda-(tan(q_ph)+2*tan(lambda*q_ph))/q_ph),q_
   qph(1,i)=S(i);
   end

      for i=1:100
syms q_ph
S(i)=vpasolve(P_h(2,i)==q_ph^2/(1+2*lambda-(tan(q_ph)+2*tan(lambda*q_ph))/q_ph),q_
   qph(2,i)=S(i);
      end

% Torsion
   for i=1:100
syms q_pa
S(i)=vpasolve(P_a(1,i)==q_pa^2/(1+2*lambda-(tan(q_pa)+2*tan(lambda*q_pa))/q_pa),q_
   qpa(1,i)=S(i);
   end

      for i=1:100
syms q_pa
S(i)=vpasolve(P_a(2,i)==q_pa^2/(1+2*lambda-(tan(q_pa)+2*tan(lambda*q_pa))/q_pa),q_
   qpa(2,i)=S(i);
      end



% - Natural frequencies


% The symmetrical and asymmetrical  natural frequencies is now calculated
% in bending (vertical) and torsion

% Predimensioning of matrices
fsym_h=zeros(2,100);  % Natural frequencies symmetrical bending (vertical)
fsym_a=zeros(2,100);  % Natural frequencies symmetrical torsion
fasym_h=zeros(2,100); % Natural frequencies asymmetrical bending (vertical)
fasym_a=zeros(2,100); % Natural frequencies asymmetrical torsion

for j=1:2
    for i=1:100
```

```
% Symmetric frequencies


% Bending (vertical)
fsym_h(j,i)=(qph(j,i)/(2*pi))*sqrt(g/(2*d));

% Torsion
fsym_a(j,i)=(qpa(j,i)/(pi*l))*sqrt((G*K+H(j,i)*r^2)/I_tot(j,i));




% Asymmetric frequencies


% Bending (vertical)
fasym_h(j,i)=(1/l)*sqrt(H(j,i)/m_cross_sec(j,i));

% Torsion
fasym_a(j,i)=(1/l)*sqrt((G*K+H(j,i)*r^2)/I_tot(j,i));

    end
end



% - Critical wind speed


% The critical wind speed can now finally be calculated with the formula
% from Allan Larsen.

D=7.1; % [m] Slot width of cross-section of deck
B=12.9*2; % [m] Solid part width of cross-section of deck
C_DB=1+0.7332*(D/B)^1.4211;
K_constant=3.72;
p_air=1.25; % [kg/m3] Density of air

% Predimensioning of matrices
U_c_sym=zeros(2,100);
U_c_asym=zeros(2,100);


for j=1:2
    for i=1:100

% Critical windspeeds


% Symmetric
U_c_sym(j,i)=K_constant*C_DB*fsym_a(j,i)*sqrt((sqrt(m_cross_sec(j,i)*I_tot(j,i))/(
```

```
% Asymmetric
U_c_asym(j,i)=K_constant*C_DB*fasym_a(j,i)*sqrt((sqrt(m_cross_sec(j,i)*I_tot(j,i))

    end
end
```

Results to use in tables

```
% The results from this calculation will mainly be presented in table form
% in the thesis. The results for all variations of safety factors is
% therefore to much to present, and only some values will be presented. To
% decide which values that are to be presented, the following has been
% done:

% For steel, the same value will be used as in a previous feasability
% study, that is 1.8. This value is the only value for which the
% calculations is presented for for steel, and corresponds to element
% (2,32) in the calculations. In some articles, the safety factor is based
% on the equivalent stiffness of the cables. A proper safety factor for
% CFRP is therefore calculated based on the expression EA=EA for steel and
% CFRP, where the area for steel is calculated based on
% its proper safety factor (here 1.8). The area for CFRP is solved from the
% expression, and the safety factor that corresponds to that area is the
% safety factor adopted for the CFRP:

A_CFRP_safe_high=A_mc(2,32)*E(2)/E(1);

% In this calculation, this area of the main cables for CFRP corresponds to
% a safety factor of 6.52, which corresponds to element (1,92) in the
% calculations.

% The safety factor can also be based on the strength of the material
% instead of the equivalent stiffness. This value is therefore much closer
% to the adopted value for steel, but slightly hihger due to the scarce
% applications of the material. The safety factor based on the strength is
% set to 2.2, corresponding to element (1,21).

% The third safety factor is a mix of the two above. It will therefore
% be set to a value between them, which will be 4.4 since it fits with the
% values from the linespaceing. The corresponding element is (1,57)

% To easily find the corresponding areas, frecuencies etc. for these
% values, they are collected in vectors. The results for CFRP is the first
% 3 columns and steel is the 4:th column, according to:

% Res = [CFRP 2.2   CFRP 4.4   CFRP 6.5   Steel 1.8]



% Preliminary Sizing:
```

```
% Area hanger
Res_A_h=[A_h(1,21) A_h(1,57) A_h(1,92) A_h(2,32)]

% Volume hangers
Res_V_h=[V_h(1,21) V_h(1,57) V_h(1,92) V_h(2,32)]

% The distributed weight from the hangers
Res_q_h=[q_h(1,21) q_h(1,57) q_h(1,92) q_h(2,32)]

% Area main cable
Res_A_mc=[A_mc(1,21) A_mc(1,57) A_mc(1,92) A_mc(2,32)]

% Distributed load main cables
Res_q_mc=[q_mc(1,21) q_mc(1,57) q_mc(1,92) q_mc(2,32)]

% Total distributed load
Res_q_total=[q_total(1,21) q_total(1,57) q_total(1,92) q_total(2,32)]

% Mass cross-section
Res_m_cross_sec=[m_cross_sec(1,21) m_cross_sec(1,57) m_cross_sec(1,92) m_cross_sec



% Aerodynamic analysis:


% Total moment of intertia
Res_I_tot=[I_tot(1,21) I_tot(1,57) I_tot(1,92) I_tot(2,32)]


% Symmetric frequencies

% Bending (vertical)
Res_fsym_h=[fsym_h(1,21) fsym_h(1,57) fsym_h(1,92) fsym_h(2,32)]
% Torsion
Res_fsym_a=[fsym_a(1,21) fsym_a(1,57) fsym_a(1,92) fsym_a(2,32)]


% Asymmetric frequencies

% Bending (vertical)
Res_fasym_h=[fasym_h(1,21) fasym_h(1,57) fasym_h(1,92) fasym_h(2,32)]
% Torsion
Res_fasym_a=[fasym_a(1,21) fasym_a(1,57) fasym_a(1,92) fasym_a(2,32)]


% Critical windspeeds

% Symmetric
Res_U_c_sym=[U_c_sym(1,21) U_c_sym(1,57) U_c_sym(1,92) U_c_sym(2,32)]

% Asymmetric
```

```
Res_U_c_asym=[U_c_asym(1,21) U_c_asym(1,57) U_c_asym(1,92) U_c_asym(2,32)];
```

Published with MATLAB® R2013b

References

Adanur, S., Mosallam, A., Shinozuka, M., & Gumusel, L. (2011). A comparative study on static and dynamic responses of FRP composites and steel suspension bridges. *Journal of Reinforced Plastics and Composites* , 1265-1279.

Berntsen, K., & Lotherington, H. (2013). MULIGHETSSTUDIE – HENGEBRU OVER SOGNEFJORDEN. Unpublished. Oslo: The Norwegian Public Roads Administration.

bestbridge.net. (March 27, 2011) (Photo). Retrieved February 25, 2014, from bestbridge.net: http://www.bestbridge.net/data/upimages/vladimir/Asia/tur/dsc09153.JPG

Chen, W.-F., & Duan, L. (2000). *Bridge engineering handbook.* Boca Raton: CRC Press.

Clemente, P., Nicolosi, G., & Raitel, A. (2000). Preliminary design of very long-span suspension. *Engineering Structures , 22* (12), 1699-1706.

Cobo del Arco, D., & Aparicio, Á. (2001). Preliminary static analysis of suspension bridges. *Engineering Structures , 23*, 1096-1103.

decentlab.com. (n.d.) (Photo). Retrieved February 26, 2014, from decentlab.com: http://www.decentlab.com/sites/default/files/storchenbruecke.jpg

Dehmous, H., & Welemane, H. (2011). Multi-scale reliability analysis of composite structures – Application to the Laroin footbridge. *Engineering Failure Analysis*, *18*, 988-998.

Dyrbye, C., & Hansen, S. O. (1997). *Wind Loads on Structures.* Chichester: John Wiley & Sons.

geocaching.com. (n.d.) (Photo). Retrieved February 26, 2014, from geocaching.com: http://img.geocaching.com/cache/d418344a-2678-4430-9ae4-5aeb4e99cf86.jpg?rnd=0.0528025

Gimsing, N., & Georgakis, C. (2012). *Cable Supported Bridges - Concept and Design (3:rd edition).* John Wiley & Sons.

Isaksen, B., Berntsen, K., Lotherington, H., & Mrowiec, M. I. (2013). *A 3700 m single span suspension bridge.* Oslo: The Norwegian Public Roads Administration.

Jiang, Y., & Jia, L. (2012). Contrastive Analysis on Limitation Span between Suspension Bridge using steel and CFRP Cable. *Advanced Materials Research , 568*, 57-60.

Larsen, A., & Esdahl, S. (1998). Bridge Aerodynamics. *Advances in Bridge Aerodynamics* (pp. 1-10). Rotterdam: A.A Balkema.

Larsen, A., Larose, G., & Livesey, F. (1999). Wind Engineering into the 21st Century. *Tenth International Conference on Wind Engineering* (pp. 1-10). Rotterdam: A.A Balkema.

Liu, Z., LV, Z.-t., Mei, K.-h., & Zang, H. (2007). Research and Application Review on CFRP Cables for Cable-stayed Bridges. *Journal of Highway and Transportation Research and Development , 2* (1), 29-33.

Mahmoud, Z. I. (1997). *Bond characteristics of fibre reinforced polymers prestressing reinforcement.* Alexandria: Alexandria University.

Mallick, P. K. (2007). *Fibre-reinforced composites Materials, Manufacturing, and Design, Third Edition.* Dearborn, Michigan: CRC Press.

Meier, U. (2012). Carbon Fibre Reinforced Polymer Cables: Why? Why Not? What if? *Arabian journal for science and engineering, Section B, engineering , 37* (2), 399-411.

Meier, U. (2000). Composite Materials in bridge repair. *Applied Composite Materials* , 75-94.

Meier, U. & Mehdi, F. (1996). Connecting high-performance carbon-fibre-reinforced-polymer cables of suspension and cable-stayed bridges through the use of gradient materials. *Journal of Computer-Aided Materials Design* , 379-384.

news.com.au. (n.d.) (Photo). Retrieved February 26, 2014, from news.com.au: http://resources3.news.com.au/images/2012/09/11/1226471/666943-apec-summit-russia-social-vladivostok-putin-files.jpg

Noisternig, J. F. (2000). Carbon fibre composites as Stay Cables for Bridges. *Applied Composite Materials* , 139-150.

Sayed-Ahmed, E. (2002). SINGLE- AND MULTI-STRAND STEEL ANCORAGE SYSTEMS FOR CFRP TENDONS / STAY. *4th structural speciality conference of the canadian society for civil engineering*, (pp. 1381-90). Montreal, Quebeq, Canada .

Schmidt, J. W., Bennitz, A., Täljsten, B., Goltermann, P., & Pedersen, H. (2012). Mechanical anchorage of FRP tendons - A litterature review. *Construction and Building Materials* , 110-121.

Thylén, C. (2009). *Förenklad numerisk analys av hängbroars verkningssätt - Utveckling av programmet SusB med tillämpning ac CalFEM toolbox.* Department of Civil and Architectural Engineering. Stockholm: KTH.

Wang, X., & Wu, Z. (2010). Evaluation of FRP and hybrid FRP cables for super long-span cable-stayed bridges. *Composite Structures , 92* (10), 2582-2590.

Xiong, W., Cai, C., Zhang, Y., & Xiao, R. (2011). Study of super long span cable-stayed bridges with CFRP components. *Enginerering structures* , 330-343.

yokogawa-bridge.co.jp. (n.d.) (Photo). Retrieved May 23, 2014, from *yokogawa-bridge.co.jp*: http://www.yokogawa-bridge.co.jp/english/05_steelbridges/index.html

Zhang, H., Xie, X., & Zhao, J.-L. (2011). Parametric vibration of carbon fibre reinforced plastic cables with damping effects in long span cable-stayed bridges. *Journal of vibration and control* , 20117-2130.

Zhang, X.-j., & Ying, L.-d. (2006). Aerodynamic stability of cable-supported bridges using CFRP cables. *Journal of Zhejiang University SCIENCE A* , 693-698.

Zheng, H., Jiang, H., & Lu, Z. (2011). Design Method of the Cable Saddle for CFRP Main Cable in long-span suspension Bridge. *Advanced Materials Research* , 1557-1560.

Zoghi, M. (2014). *The International Handbook of FRP COMPOSITES IN CIVIL ENGINEERING.* Boca Raton: CRC Press.